High-resolution Holocene record based on detailed tephrochronology from Torfdalsvatn, north Iceland, reveals natural and anthropogenic impacts on terrestrial and aquatic environments

David J. Harning[1,2], Christopher R. Florian[1,2,3], Áslaug Geirsdóttir[2], Thor Thordarson[2], Gifford H. Miller[1], Yarrow Axford[4], Sædís Ólafsdóttir[5]

[1]Institute of Arctic and Alpine Research, University of Colorado, Boulder, CO, USA
[2]Faculty of Earth Sciences, University of Iceland, Reykjavík, Iceland
[3]National Ecological Observatory Network, Battelle, Boulder, CO, USA
[4]Department of Earth and Planetary Sciences, Northwestern University, Evanston, IL, USA
[5]Reykjavík Energy, Reykjavík, Iceland

Correspondence to: David J. Harning (david.harning@colorado.edu)

Abstract. Open questions remain around the Holocene variability of climate in Iceland, including the relative impacts of natural and anthropogenic factors on Late Holocene vegetation change and soil erosion. The lacustrine sediment record from Torfdalsvatn, north Iceland, is the longest known in Iceland (~12000 cal a BP) and along with its high sedimentation rate, provides an opportunity to develop high-resolution quantitative records that address these challenges. In this study, we use two sediment cores from Torfdalsvatn to construct a high-resolution age model derived from marker tephra layers, paleomagnetic secular variation, and radiocarbon. We then apply this robust age constraint to support a complete tephrochronology (>2200 grains analyzed in 33 tephra horizons) and sub-centennial geochemical (MS, TOC, C/N, $\delta^{13}C$, and BSi) and algal pigment records. Along with previously published proxy records from the same lake, these records demonstrate generally stable terrestrial and aquatic conditions during the Early and Middle Holocene, except for punctuated disturbances linked to major tephra fall events. During the Late Holocene, there is strong evidence for naturally driven algal productivity decline beginning around 1800 cal a BP. These changes closely follow regional Late Holocene cooling driven by decreases in Northern Hemisphere summer insolation and the expansion of sea-ice laden Polar Water around Iceland. Then at 880 cal a BP, ~200 years after the presumed time of human settlement, a second shift in the record begins and is characterized by a strong uptick in landscape instability and possibly soil erosion. Collectively, the Torfdalsvatn record highlights the resilience of low-elevation, low-relief catchments to the pre-settlement soil erosion in Iceland, despite a steadily cooling background climate. The precisely dated, high-resolution tephra and paleoenvironmental record from this site can serve as a regional template for lowland regions of north Iceland.

Deleted: ≤

1 Introduction

As the planet continues to warm, paleoclimate information is increasingly more important to constrain Earth system models (Tierney et al., 2020). Within the northern North Atlantic, Iceland serves as an ideal location as the island sits at the confluence of major atmospheric and oceanic circulation patterns integral to global heat distribution (Wunsch, 1980; Marshall et al., 2001). Continuous and high-resolution lake sediment records from Iceland form the backbone of its recent geologic climate history. These empirical records have analyzed physical properties for glacier history (Larsen et al. 2011; Striberger et al., 2012; Harning et al., 2016a, 2016b), pollen, macrofossils, and sedimentary ancient DNA (*sed*aDNA) for plant communities (Rundgren, 1995, 1998; Hallsdóttir and Caseldine, 2005; Gathorne-Hardy et al., 2009; Eddudóttir et al., 2015, 2016; Alsos et al., 2021; Geirsdóttir et al., 2022; Harning et al., 2023), bulk geochemistry for soil erosion and diatom productivity (Geirsdóttir et al., 2009, 2013, 2019, 2020, 2022; Larsen et al., 2012; Blair et al., 2015; Harning et al., 2018a; Tinganelli et al., 2018; Bates et al., 2021), lipid biomarkers for fire activity (Ardenghi et al., 2024), and chironomids and lipid biomarkers for quantitative temperature (Caseldine et al., 2003; Axford et al., 2007, 2009; Langdon et al., 2010; Holmes et al., 2013; Harning et al., 2020; Richter et al., 2020). The Holocene Thermal Maximum (7900 to 5500 cal a BP, Caseldine et al., 2006; Geirsdóttir et al., 2013) has been a particular focus as it provides a potential analogue for future environmental change – current estimates suggest that summer temperatures were ~3 ºC warmer than present (Flowers et al., 2008; Harning et al., 2020). As such, these proxy records have then been used to test and validate glacier models (Flowers et al., 2008; Anderson et al., 2018) and project future environmental scenarios (Anderson et al., 2019).

Research on Iceland's Holocene paleoclimate has also centered around the impact of human settlement during the last millennium. The classic paradigm is that following the settlement of Iceland (i.e., *Landnám,* ~870 CE, Vésteinsson and McGovern, 2012), soil erosion was intiated due to deforestation and overgrazing by newly introduced livestock (e.g., Thórarinsson, 1944, 1961; Dugmore and Buckland, 1991; Dugmore and Erskine, 1994; Hallsdóttir, 1995) with climate and volcanic forcings playing a secondary role (Thórarinsson, 1961; Gerrard, 1991). While human impact certainly affected the Icelandic landscape, empirical evidence demonstrates that the natural decline of woody vegetation (Streeter et al., 2015) and increased and sustained soil erosion began at least several centuries prior to known human presence (Geirsdóttir et al., 2009, 2020). These natural changes have been ascribed to Late Holocene cooling, due to diminishing Northern Hemisphere summer insolation and the southward migration of the Polar Front and sea ice towards Iceland (e.g., Axford et al., 2007; Geirsdóttir et al., 2013; Cabedo-Sanz et al., 2016; Harning et al., 2021), as well as volcanic eruptions whose tephra deposits initiate erosion through the abrasion and destruction of vegetation that stabilizes the underlying soil (Larsen et al., 2012; Geirsdóttir et al., 2013; Blair et al., 2015; Eddudóttir et al., 2017). Icelandic lake sediment studies provide optimal archives to explore the relationship and resilience of the landscape to climate and human impacts due to the lake's continuous sedimentation and high sedimentation rates. These conditions afford sub-centennial records of environment and climate variability and robust age control derived from geologically instantaneous tephra markers (e.g., Thórarinsson, 1944; Larsen and Eiríksson, 2008), among

Deleted: t

Deleted: phasing

Deleted: these various mechanisms

Deleted: that

other geochronological techniques (i.e., radioactive isotopes and paleomagnetic secular variations, PSV, Ólafsdóttir et al., 2013).

Icelandic volcanism has featured both effusive and explosive mafic eruptions during the Holocene, where the latter have often been influenced by frequent subglacial and subaqueous/submarine interactions resulting in considerable tephra production. Although less common, rhyolitic eruptions from central volcanoes are frequent in Iceland and typically more explosive than their mafic counterparts (e.g., Thordarson and Larsen, 2007; Thordarson and Höskuldsson, 2008; Larsen and Eiríksson, 2008). Due to their intensity, many of these rhyolitic eruptions have produced widespread, light-colored tephra layers that form the backbone of tephrochronological frameworks on both sides of the North Atlantic (e.g., Abbott and Davies, 2012; Lawson et al., 2012). Most Icelandic tephra layers have been dated in soil and sedimentary sections via radiocarbon (^{14}C) and soil/sediment accumulation rates (Mangerud et al., 1984, 1986; van den Bogaard et al., 1994, 2002; Dugmore et al., 1995; Pilcher et al., 1995, 1996; Birks et al., 1996; Wastegård et al., 2001; Langdon and Barber, 2001; Bergman et al., 2004; Óladóttir et al., 2005, 2007, 2011; Gudmundsdóttir et al., 2011, 2016, 2018; Timms et al., 2017, 2018; Harning et al., 2018b, 2019) in addition to annual layer counting in Greenland ice cores (Grönvold et al., 1995; Rasmussen et al., 2006; Davies et al., 2024). However, despite the vast existing literature and the high frequency of tephra-producing eruptions from Iceland during the Holocene (n ≈ 2400; Thordarson and Höskuldsson, 2008), the Icelandic record is incomplete due to a combination of preservation and the relatively few records with complete tephra layer inventories (e.g., Larsen et al., 2002; Thordarson and Larsen, 2007). Given Iceland's proximity to major regions of paleoenvironmental research, and the community's growing reliance on its tephra layers for age control and correlation between sites, continuing to work towards a well-dated and compositionally well-defined master tephra stratigraphy is paramount.

Here, we revisit the sediment of Torfdalsvatn, a lake in North Iceland (Fig. 1), to address several outstanding research gaps. Due to it being the only known non-marine sedimentary record in Iceland that extends to ~12000 cal a BP, Torfdalsvatn's lacustrine record has attracted considerable attention (e.g., Björck et al., 1992; Rundgren, 1995, 1998; Rundgren and Ingólfsson, 1999; Florian, 2016; Alsos et al., 2021; Harning et al., 2024). Important contributions include the major elemental composition of regional marker tephra layers (Björck et al., 1992; Alsos et al., 2021), which for the Early Holocene section have been recently revised (Harning et al., 2024). In addition, several paleoenvironmental records have been developed using pollen, macrofossils, chironomids, and plant *sed*aDNA to explore questions related to the postglacial colonization of plants and Holocene temperature variability (Björck et al., 1992; Rundgren, 1995, 1998; Axford et al., 2007; Alsos et al., 2021). However, currently, there has been no systematic study of all tephra layers preserved in Torfdalsvatn's sediment record and the response of the lake's aquatic environment to Holocene climate change has not been thoroughly explored. Therefore, in this study, we first use two lake sediment cores from Torfdalsvatn to construct a high-resolution age model derived from historical marker tephra layers, paleomagnetic secular variation, and radiocarbon. We then apply this robust age constraint to support a detailed tephrochronology (>2200 grains analyzed in 33 tephra horizons) and sub-centennial geochemical (MS, TOC, C/N, δ^{13}C, and BSi) and algal pigment proxy records. Collectively, and along with previously published proxy records from

Deleted: In this study

Deleted: ≤

Deleted: its

Deleted: Here

Deleted: complete

Torfdalsvatn, these new terrestrial and aquatic records provide key insight into the paleoenvironmental history of North Iceland during the Holocene and serve as a key template for this region of Iceland.

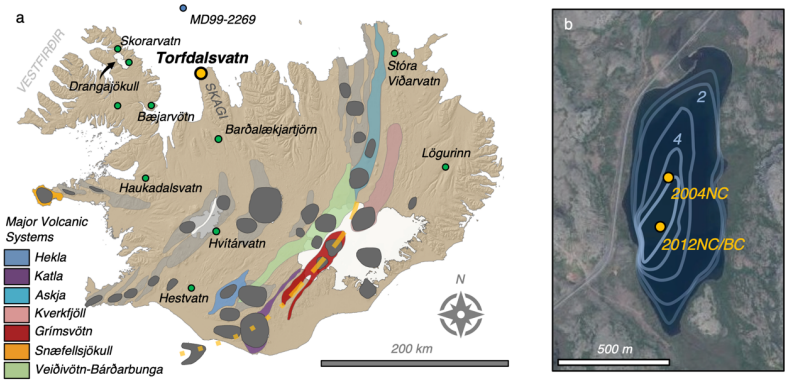

Figure 1: Overview map of Iceland. a) Locations of major volcanic systems (dark gray denotes central volcano and color corresponds to volcanic system IDs in the legend), and terrestrial (green) and marine sites (blue) mentioned in the text, with Torfdalsvatn highlighted in yellow. b) Close-up of Torfdalsvatn, its bathymetry (1-m isolines), and location of lake sediment core sites for 2012NC (this study), 2012 BC (Harning et al., 2024), and 2004NC (Axford et al., 2007). Base aerial imagery courtesy of Loftmyndir ehf.

2 Methods

2.1 Study site and sediment core collection

Torfdalsvatn (66.06°N, 20.38°W) is a relatively small (0.4 km^2), shallow (5.8 m depth) lake located at 52 m asl on the northwest coast of the Skagi peninsula with a catchment area of 2.76 km^2 (Fig. 1). The surrounding bedrock is composed of Pliocene-Pleistocene age (3.3 to 0.8 Ma) basaltic lava successions separated by thin sedimentary units (Harðarson et al., 2008). Soils within the low-relief lake catchment are thin and sparse, but where present, are composed of brown to histic andosols as well as some peat (Arnalds and Gretarsson, 2001). Our summer field visits indicate that the modern vegetation is broadly characterized as moss heathland.

In February 2012, we recovered lake sediment cores from the lake's depocenter using a Nesje piston coring system atop a lake-ice platform. We captured ~8.4 m of continuous sediment in two successive drives (TORF12-2A-1N and TORF12-2A-2N; referred to as 2012NC) reaching dense, deglacial sediment at the base (Fig. 1b, note: another core 2012BC was taken from the same location, Harning et al., 2024). The cores were split and measured for density and magnetic susceptibility at 2-cm resolution on a GEOTEK (MSCL-S) core scanner at the University of Iceland. Here, we also present new tephra compositional data from a 5.4 m-long sediment record collected from a shallower water depth in February 2004 (04-TORF-01, i.e., 2004NC, Fig. 1b) previously studied for chironomid assemblages (Axford et al., 2007).

Deleted: The

2.2 Tephra sampling and compositional analysis

Tephra layers from 2012NC and 2004NC were located by visual inspection (or high MS values for those that are not visible, i.e., cryptotephra) (Fig. 2) and sampled along the vertical axis. For the ~26 cm thick G10ka Series unit in 2012NC, samples were taken every 1 cm. Each sample was sieved to isolate glass fragments between 125 and 500 µm and embedded in epoxy plugs. Tephra glass from 2012NC along with some layers from 2004NC were analyzed at the University of Iceland on a JEOL JXA-8230 electron microprobe using an acceleration voltage of 15 kV, beam current of 10 nA and beam diameter of 10 µm (see Supporting Data). The international A99 standard was used to monitor for instrumental drift and maintain consistency between measurements (see Supporting Data).

Using the compositional dataset, tephra layer origins were then assessed following the systematic procedures outlined in Jennings et al. (2014) and Harning et al. (2018b). Briefly, based on SiO_2 wt% vs total alkali (Na_2O+K_2O) wt%, we determine whether the tephra volcanic source is mafic (tholeiitic or alkalic), intermediate and/or rhyolitic. From here, we objectively discriminate the source volcanic system through a detailed series of bi-elemental plots produced from available compositional data on Icelandic tephra (see Supporting Data and Figs. S1-3). Merging the volcanic system source with relevant stratigraphic and chronologic information permits the identification of the source eruption if the eruption is previously known. If a tephra horizon conforms to the composition of tephra of known age, then it forms a fixed point in the age model (i.e., marker tephra layer). If this is not possible, then an age is extracted from the age model (see Section 2.3.3) and named according to its volcanic source and modeled time of deposition. As an example, the Katla tephra layer identified at 142.5 cm depth (1270 cal a BP) is termed "Katla 1270" (Table 2). However, tephra layers from the historical period are classically labeled as age CE,

Deleted: i

Deleted: Table 1 and

Deleted: 5

which we specify where needed.

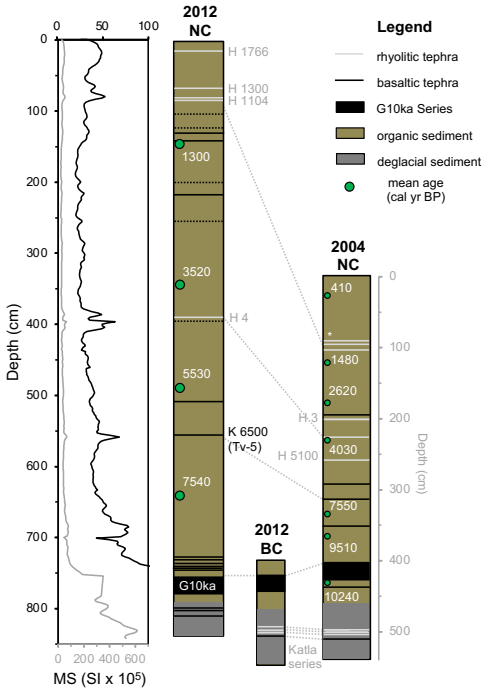

Figure 2: Physical and lithological characteristics of Torfdalsvatn lake sediment. Magnetic susceptibility (MS, black and gray are two different scales) record and simplified lithostratigraphy shown for core 2012NC (this study), and lithostratigraphy for cores 2012BC (Harning et al., 2024) and 2004NC (Axford et al., 2007). Note that the 2004NC log is plotted on its own depth axis (gray). See Fig. 8 for stratigraphic detail of the Hekla 1104 CE tephra layers in core 2004NC. Key marker tephra layers are labeled in each core, and tephra layer correlations between records are highlighted with dashed gray lines. Depth and mean calibrated ^{14}C ages of macrofossils samples shown for 2012NC and 2004NC with green circles. See Table 1 for complete radiocarbon information.

Table 1: Lake sediment radiocarbon information used in this study. All calibrated ages use the most recent radiocarbon calibration curve (IntCal20, Reimer et al., 2020).

Lab ID	Core name	Depth (cm)	Material	Conventional ^{14}C age ± σ	Calibrated age BP ± σ	Reference
CURL-15806	2012NC	148	Aquatic macrofossil	1390 ± 15	1300 ± 10	This study

Deleted:

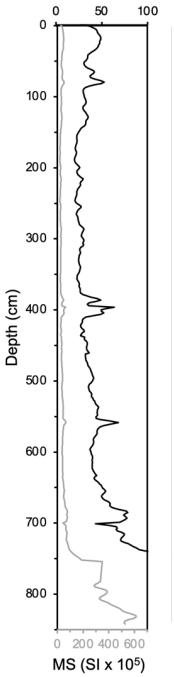

CURL-15814	2012NC	346	Aquatic macrofossil	3305 ± 15	3520 ± 40	This study
CURL-15812	2012NC	489.5	Aquatic macrofossil	4785 ± 20	5530 ± 50	This study
CURL-15794	2012NC	642	Aquatic macrofossil	6660 ± 20	7540 ± 30	This study
AA60639	2004NC	27.5	Plant macrofossil	370 ± 40	410 ± 80	Axford et al. (2007)
NSRL-14520	2004NC	120	Plant macrofossil	1635 ± 20	1480 ± 60	Axford et al. (2007)
NSRL-14765	2004NC	180	Humic acid	2515 ± 20	2620 ± 100	Axford et al. (2007)
NSRL-14517	2004NC	227.5	Humic acid	3685 ± 15	4030 ± 50	Axford et al. (2007)
NSRL-14519	2004NC	337.5	*Betula* leaf	6690 ± 20	7550 ± 30	Axford et al. (2007)
NSRL-14766	2004NC	369	Humic acid	8505 ± 15	9510 ± 20	Axford et al. (2007)
NSRL-14518	2004NC	432	Humic acid	9100 ± 25	10240 ± 10	Axford et al. (2007)

2.3 Chronology

2.3.1 Paleomagnetic secular variation

Continuous u-tube channels of sediment were taken from the center of core 2012NC and measured for paleomagnetic secular variation (PSV) following the methods of Ólafsdóttir et al. (2013). Torfdalsvatn's distinct characteristic remanent magnetization (ChRM) declination and inclination features were tuned to the master GREENICE PSV stack through 14 tie points (Fig. S4). The GREENICE chronology is based on 47 ^{14}C dates derived from two PSV-synchronized marine sediment cores (MD99-2269 and MD99-2322, Stoner et al., 2007, 2013), in addition to eight marker tephra layers of known age (Kristjánsdóttir et al., 2007).

2.3.2 Radiocarbon

2012NC was inspected for aquatic plant macrofossils to provide additional chronological control. Aquatic plants are generally favorable for ^{14}C dating in Iceland as there is no hardwater effect in lakes and terrestrial macrofossils have longer transport times that may result in ages that are stratigraphically too old. The four aquatic macrofossil fragments picked from 2012NC (Fig. 2) were gently rinsed with deionized water to remove sediment and freeze-dried. Samples were given an acid-base-acid pretreatment (Bradley and Stafford, 1994) and graphitized at the University of Colorado Boulder, then measured by AMS at

Deleted: 3a-b

Deleted: 4

Deleted: Terrestrial macrofossils were avoided as it has been shown that their ^{14}C ages are typically too old for their stratigraphic position in Icelandic lake sediments (Sveinbjörnsdóttir et al., 1998; Geirsdóttir et al., 2009).

the University of California Irvine. Conventional ^{14}C ages were calibrated using OxCal 6.0 (Bronk Ramsey, 2009) and the IntCal20 calibration curve (Reimer et al., 2020), and are reported in cal a BP, where BP is years before present (1950 CE, Table 1).

2.3.3 Age model

The 2012NC age model relies on a combination of key marker tephra layers whose ages are known from the historical period (n=2, Hekla 1766 and Hekla 1300, e.g., Thórarinsson, 1967), PSV tiepoints (n=14), and ^{14}C-dated macrofossils (n=4). An age model was generated using the open-source R package rbacon (Blaauw and Christen, 2011; R Core Team, 2021), the IntCal20 calibration curve for the ^{14}C samples (Reimer et al., 2020), and an uncertainty of ± 50 cal a BP for each PSV tie point (e.g., Ólafsdóttir et al., 2013) (Fig. 3a). Given the thin nature of tephra layers typically less than 1 cm, we did not remove tephra layer thicknesses from the model. Non-marker tephra layer ages are derived from basal depth of the layer, the median value of model iterations (red line), and the 95% uncertainty envelope (grey lines) (Fig. 3a).

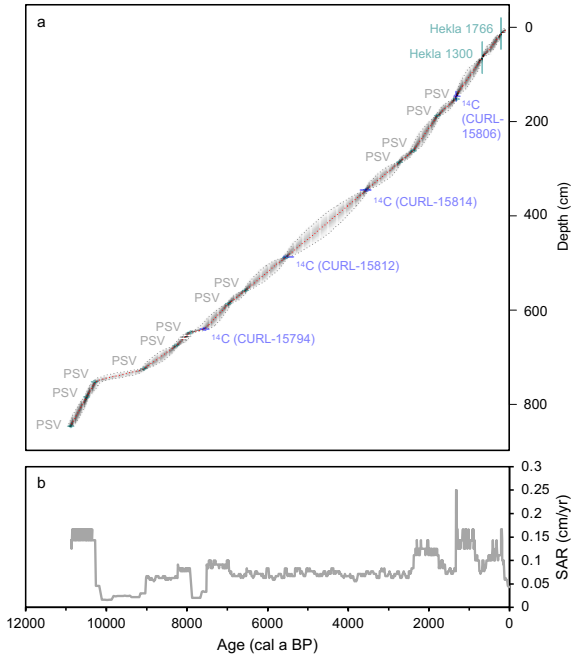

Deleted: 5
Deleted: Chronology and a
Deleted: from
Deleted: c
Deleted: an
Deleted: 3c

Figure 3: Age model results. a) rbacon age model constructed from the PSV tie points (gray, *n* = 14), historical marker tephra layers (green, *n* = 2), and radiocarbon ages of plant macrofossils (blue, *n* = 4) (Blaauw and Christen, 2011; R Core Team, 2021), where solid red line reflects the median of model iterations, and the outer gray lines reflect the 95% confidence envelope. See Fig S4 for PSV results. b) Sedimentation accumulation rates (SAR, cm/yr) derived from the rbacon age model.

2.4 Bulk geochemistry

Samples were taken for bulk geochemistry at 2-cm resolution (1-cm thick), avoiding tephra layers, then ground and homogenized with an agate mortar and pestle. Total carbon (TC), total nitrogen (TN), and $\delta^{13}C$ (relative to VPDB) were measured using a CE NC 2500 elemental analyzer interfaced to a Finnigan Delta V isotope ratio mass spectrometer at the Carnegie Geophysical Laboratory. Isotopic ratios were corrected for drift using an acetanilide standard, and duplicate analyses show a precision of less than 0.2 ‰ for each isotope ratio. For a subset of these samples (*n*=281), we also measured biogenic silica (BSi) by Diffuse Reflectance Fourier Transform Infrared Spectrometry (FTIRS) on a Bruker Vertex 70 with a Praying Mantis diffuse reflectivity accessory (Harrick) at the University of Colorado Boulder, integrating between 1000 and 1250 cm^{-1}. Since published calibrations to wt% biogenic silica are linear and do not influence the nature of the proxy curve (e.g., Vogel et al., 2008), we report values in FTIRS absorbance units. Previous studies in Iceland report low instrumental uncertainty for this method (0.087 to 4.334 absorbance units, Harning et al., 2018a).

2.5 Algal pigments

Samples for algal pigments were taken at 2-cm resolution above 226 cm depth (~2000 cal a BP) and at 4-cm resolution below, where each corresponds to an interval previously sampled for bulk geochemistry as described above. Algal pigments were measured at the University of Colorado Boulder following the methodology described in Leavitt and Hodgson (2001) to minimize pigment degradation. The archive half of sediment core was used for pigment analysis because it was sealed, stored cold, and not visibly oxidized at the time of sampling and all subsamples were kept frozen under nitrogen until the time of measurement. Briefly, following core splitting, algal pigments were immediately solvent extracted from 246 freeze dried sediment samples using 6 mL of acetone:methanol (80:20, v/v) overnight in amber vials under N_2 at -10 °C. Samples were touch mixed and sonicated to disperse sediment and increase extraction efficiency, then filtered through a 0.2 µm PTFE syringe filter which was then rinsed with 2 ml of acetone to recover sample residue from the filter. The extract was dried down and rehydrated with a known volume of acetone containing a known concentration of α-tocopherol standard. Samples were placed in the refrigerated autosampler of an Agilent 1200 series HPLC and derivatized to improve chromatographic behavior immediately prior to injection with an equal volume of 28 mM tetrabutyl ammonium acetate in water. A binary mobile phase system was used with solvent A composed of methanol:28 mM tetrabutyl ammonium acetate (70:30, v/v) in water and solvent B composed of pure methanol at a flow rate of 1 mL min^{-1}. An Agilent Eclipse XDB-C18 4.6 x 150 mm column was used to separate pigments whose absorbance of visible light was detected by an Agilent Diode Array Detector (DAD) scanning between 400 and 750 nm. Pigments were identified by comparing characteristic absorbance spectra with that stored in a library

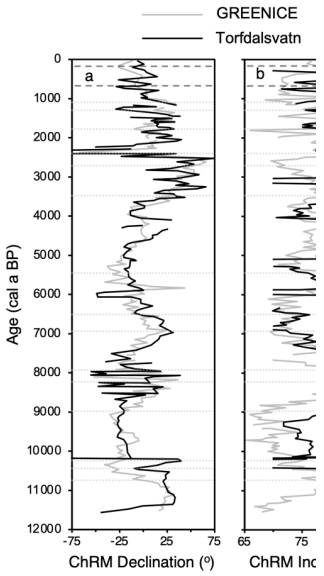

Deleted:

Deleted: **PSV data from core 2012NC (black) compared to the master GREENICE record (gray) in terms of a) declination and b) inclination. Marker tephra layers used in the PSV synchronization are shown with dark gray dashed lines and PSV tie points used in the age model are shown with light gray solid lines. c…**

Deleted: **d**

Deleted: **6**

Deleted: on

Deleted: 407 samples

Deleted: W

Deleted: - Fourier Transform Infrared Spectroscopy

Deleted: e.g.,

Deleted: **7**

Deleted: 80:20 mixture of

Deleted: [2]

Deleted: a 70:30 mixture of

created from a suite of standards obtained from DHI Denmark and reported as concentration normalized to organic carbon (µg pigment/mg OC).

2.6 Statistics

To compare the (dis)similarity of different proxy records and reduce their overall dimensionality, we performed Principal Coordinate Analysis (PCoA) using a Bray-Curtis dissimilarity matrix on both the bulk geochemistry and algal pigment proxy datasets. Bulk geochemistry datasets include SAR, %TOC, C/N, $\delta^{13}C$, and BSi, but not MS due to the interference of tephra layers. Algal pigment datasets include total pigments, total chlorins, diatom pigments, lutein/diatoxanthin, and canthaxanthin. For each analysis, sample sets were reduced to the lowest common resolution. All analyses were performed in the open-source platform R (R Core Team, 2021) using the phyloseq package (McMurdie and Holmes, 2013).

3 Results

3.1 Tephra stratigraphy and age model

Torfdalsvatn's tephra stratigraphy is shown in Figure 2 and Table 2, where age and origin are indicated along with correlations between the 2012NC/BC and 2004NC cores. Detailed tephra layer descriptions (n = 33), compositional datasets (>2200 grains analyzed), and elemental plots used to identify the tephra layers are provided in the Supporting Data and Information. We stress, unless otherwise noted, that our chemical data is obtained from pristine basaltic to silicic tephra grains that feature delicate protrusions (e.g., Harning et al., 2024). In samples regarded as representing pristine tephra fall, the grains in the mafic realm (basalt to andesite) range from (i) non- to poorly (<20 %) vesicular, black blocky glass grains defined by brittle fracture surfaces to (ii) poorly- to highly-vesicular (20 to 60 %) black to brown glass grains with vesicle-pitted surfaces to (iii) highly vesicular (>60 %) translucent (sideromelane), brown to pale brown glass grains with very convolute outlines to (iv) achneliths defined by coherent shiny black glazed/fused outer surfaces (e.g., Walker and Croasdale, 1972; Thordarson et al., 1996). The felsic (high-silica andesite, dacite to rhyolite) realm are highly vesicular (>60 %) grains and are either pumice fragments with irregular outlines or fragments dominated by tube-vesicles or vesicle-wall/bubble-junction glass shards (e.g., Fisher and Schmincke, 1984).

The age model for core 2012NC uses 2 historic marker tephra layers of well-established age (Hekla 1766 and Hekla 1300, Thórarinsson, 1967), 14 PSV tiepoints, and 4 ^{14}C-dated macrofossils (Fig. 3a). With the lowest PSV tie point assigned to an age of 10868 cal a BP, the high density of chronological control points (n = 20) results in an average of about 1 every 500 years. Combined with the Bayesian modeling approach, the age model therefore provides relatively precise estimates on the ages of new tephra layers as well as the timing of past paleoenvironmental change derived from proxy records (e.g., Blaauw et al., 2018). Based on this age model, sedimentation accumulation rates (SAR) have minimal variation throughout the entirety of the Holocene record (Fig. 3b), particularly compared to SARs of other non-glacial lakes in Iceland (e.g., Geirsdóttir et al.,

Deleted: 8

Deleted: 3c

Deleted: our

Deleted: and high-quality

Deleted: 3d

2013). Due to the near linear sedimentation rate, we do not present the following proxy data as fluxes as this results in negligible changes to the structure of proxy records.

Table 2: Summary of Torfdalsvatn tephra stratigraphy and chronology. See Supporting Data for major element compositions and chemical identification of the tephra layers.

Tephra ID[1]	Dominant composition	Cumulative depth (cm)[2]	Thickness (cm)	Age (cal a BP)	Number of events[4]
H 1766*	Rhyolite to icelandite	15	0.1	184	3
H 1300*	Rhyolite to icelandite	66	0.1	650	3
H 1104*	Rhyolite	84	0.7	846	3
C 990	Mix	104	-	990 ± 80	4
C 1180	Mix	125	-	1180 ± 70	2
K 1220	Alkali basalt	131	1	1220 ± 50	3
K 1270	Alkali basalt	142.5	2	1270 ± 40	2
C 1850	Mix	202	-	1850 ± 50	3
K/G 1990	Mix	219	0.4	1990 ± 140	3
C 2320	Mix	257	-	2320 ± 70	4
H C*	Icelandite	~340	0.5	2800 ± 80	2
H 3*	Icelandite, rhyolite	~349	2	3060 ± 30	2
H 4*	Rhyolite	391	1.3	4260 ± 10	2
H 4270	Alkali basalt	397	-	4270 ± 180	2
H 5100	Rhyolite and alkali basalt	~450	0.8	~5100	1
A 5700	Primitive basalt	~505	0.1	~5700	1
Kv/K 5850	Tholeiite basalt	512	0.1	5850 ± 200	2
K 6500 (Tv-5)	Alkali basalt	557	1.1	6490 ± 130	1
G/K 8500	Tholeiite/alkali basalt	675	0.1-0.2	~8500	2
G? 9260	Tholeiite basalt	730	0.3	9260 ± 300	1
G 9410 (G10ka Series #13)*	Tholeiite basalt	734	0.6	9410 ± 340	2
G 9630 (G10ka Series #12)*	Tholeiite basalt	739.5	1.1	9630 ± 350	1
G 9740 (G10ka Series #11)*	Tholeiite basalt	742.5	0.5	9740 ± 320	2
G 9850 (G10ka Series #10)*	Tholeiite basalt	746	0.9	9850 ± 300	2
G 9960 (G10ka Series #9)*	Tholeiite basalt	749	1	9960 ± 240	1
G-10120-10400 G10ka Series (1-8) (Tv-4)*	Tholeiite basalt	756-781	25	10120-10400	7
H 10550	Alkali basalt	802	0.3	10550 ± 150	2
I-THOL-I? (Tv-3)*	Tholeiite basalt	804	0.3	10560 ± 150	2
Kv 10630	Tholeiite basalt	812.5	0.3	10630 ± 150	3
K 11170	Rhyolite, intermediate, alkali basalt	827	0.4	11200 ± 330[3]	3
K 11295	Rhyolite, intermediate, alkali basalt	836	0.9	11360 ± 340[3]	1
K 11315 (Tv-2)	Rhyolite, intermediate, alkali basalt	837	1.1	11375 ± 330[3]	1
H 11390 (Tv-1)	Alkali basalt	845	0.6	11390 ± 180[3]	1

[1] Abbreviation in the tephra ID column are as follows: A, Askja: C, cryptotephra; G, Grímsvötn; H, Hekla; K, Katla; Kv, Kverkfjöll; V-B, Veiðivötn-Bárðarbunga.
[2] Refers to depth in 2012NC sediment core.
[3]Ages reported in Harning et al. (2024).
[4] Indicates number of tephra fall events represented within individual tephra horizons. Total is 78.
*Established marker tephra layers from Iceland.
Bold ID indicates that residual sulfur content was measured in the groundmass glass of the tephra.
Underlined ID indicates potential regional markers.

3.2 Bulk geochemistry

Due to the high sampling density of bulk geochemistry (n = 407) and BSi (n = 284), the temporal resolution of Torfdalsvatn's record equates to an average of 1 sample every 27 and 39 years, respectively. Torfdalsvatn's magnetic susceptibility (MS) record shows the highest values at the base of the sediment core, which subsequently decrease to relatively low and stable values around 7000 cal a BP before rising again at 1350 cal a BP (Fig. 4a). %TOC ranges from 0.85 to 10.44 % with lowest values at the beginning of the record and highest values in the most recent portion, where a significant mean shift occurs at 8000 cal a BP (Fig. 4b). C/N values range from 5.33 to 11.13 with relatively high values from the beginning of the record to 7400 cal a BP, followed by a minimum between 7300 and 1080 cal a BP, before rising to reach a second maxima during the last several centuries (Fig. 4c). $\delta^{13}C$ values range from -23.05 to -15.87 ‰ and show large centennial-scale variability with the most ^{13}C-depleted values occurring near the base and top of the record and inversely correlated with C/N (Fig. 4d). Along with C/N values, $\delta^{13}C$ values are consistent with organic matter originating from a combination of aquatic and terrestrial sources, where their coincident changes (C/N increase and ^{13}C-depletion) at 1800 cal a BP are consistent with a shift to a larger proportion of terrestrial organic matter to the lake (e.g., Geirsdóttir et al., 2020) (Fig. 4c-d). Finally, BSi ranges from 77 to 150 absorbance units, with the lowest values at the base and top of the record, and relatively higher but variable values in between (Fig. 4e).

PCoA results for the bulk geochemistry proxy datasets show that axis 1 explains 52.4 % of the data's similarity (Fig. S5). PCoA axis 1 shows the highest values at the base of the record followed be a gradual decrease to a low at 7650 cal a BP (Fig. 4f). During the Middle Holocene, the PCoA values show some centennial scale variability, although millennial scale variability is relatively stable before a step shift at 1080 cal a BP (Fig. 4f). The major changes observed, such as the Early Holocene decrease, Middle Holocene centennial-scale variability and step shift at 1080 cal a BP, coincide with either erosional signals and/or tephra deposits (gray bars, Fig. 4). We therefore interpret PCoA axis 1 of bulk geochemistry to reflect relative changes in erosional activity.

Deleted: average

Deleted: s

Deleted: e

Deleted: broadly anticorrelated

Moved (insertion) [1]

Deleted: and algal pigment

Deleted: and 71 % of the variance, respectively

Deleted: A

Deleted: for bulk geochemistry proxies

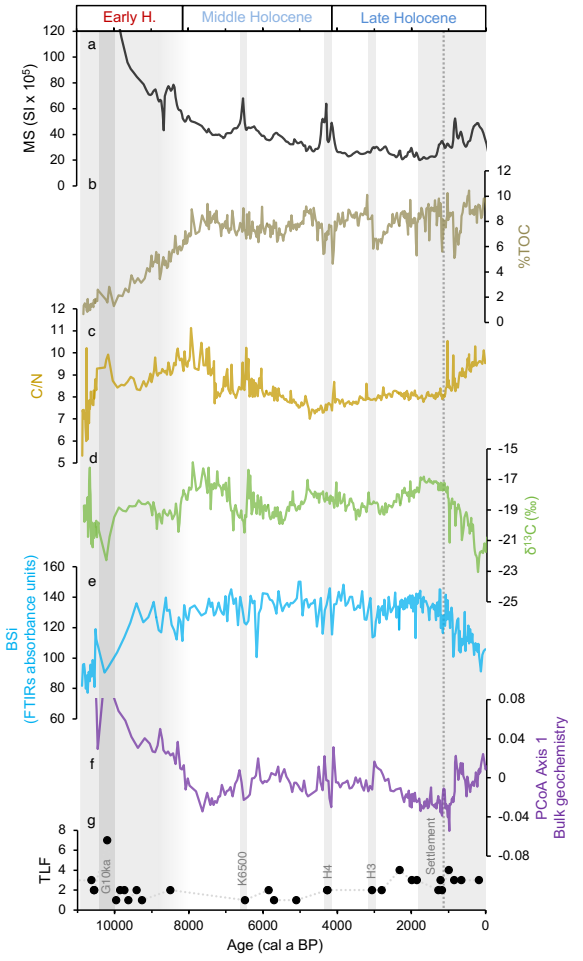

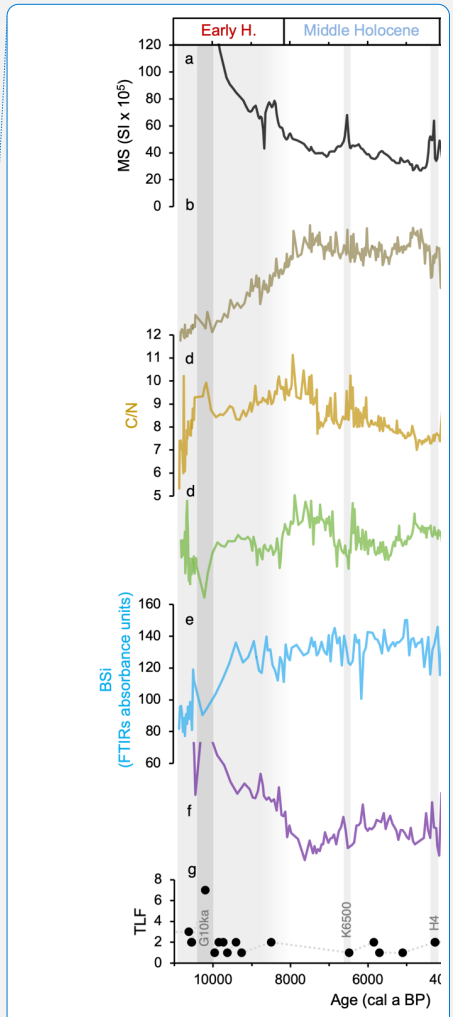

Figure 4: Bulk physical and geochemical proxy records (a-e), PCoA Axis 1 of bulk geochemistry proxies (f), and tephra layer frequency (TLF, g) from core 2012NC. Note that MS in panel a is truncated at 120 SI x 10^5 and values at the base of the record reach up to 523 SI x 10^5. Grey bars reflect landscape disturbances associated with large tephra layer deposits and erosion and dashed gray line denotes the timing of presumed human settlement (1080 cal a BP).

Deleted:

Deleted: f

Deleted: G

Deleted: H

3.3 Algal pigments

The temporal resolution of Torfdalsvatn's algal pigment sampling (n = 246) equates to an average of 1 sample every 44 years. Algal pigment results are presented as the concentration of total chlorins (chlorophyll + degradation products pheophytin and pheophorbide), concentration of diatom pigments (fucoxanthin + diatoxanthin + diadinoxanthin), lutein to diatoxanthin ratio (L/D, ratio of green algae and higher plants to diatoms and chrysophytes, Leavitt and Hodgson, 2001), and the concentration of the cyanobacterial pigment canthaxanthin (Fig. 5). In all samples measured, chlorins are the most abundant pigments (Fig. 5a), making up between ~65 and 95 % of total pigments detected. In the earliest part of the record, chlorin concentrations are at their highest and rapidly decrease through 9450 cal a BP with a subsequent period of relatively elevated concentrations between 6030 and 3020 cal a BP (Fig. 5a). The proportion of diatom pigments is variable, ranging from ~1 to 27% of total pigment with the lowest relative abundance of diatom pigments occurring at the beginning of the record (Fig. 5b). After peaking at 8720 cal a BP, diatom pigment abundance begins to decrease, and along with inverse correlations with L/D, suggests that green algae became more abundant (Fig. 5b-c). Lutein-producing (green) species remain dominant, and the relative proportion of diatom pigments is low until 5560 cal a BP (Fig. 5b-c). Between 5560 and 1800 cal a BP, diatom pigments steadily increase, and L/D stays low (Fig. 5b-c), suggesting elevated diatom relative abundance through this interval before a change in sign in both proxies (low diatom pigments and increased L/D) during the last 1800 years. The only detectable pigment biomarker of cyanobacteria in Torfdalsvatn is canthaxanthin, present throughout the sediment core at low relative abundance between ~0.5 and 2.5% of total pigment (Fig. 5d). *Nostoc* sp. were commonly observed on shoreline rocks while sampling the epilithon in July 2014 and may therefore be a likely source of canthaxanthin. Except for the highest concentrations at the base of the record, cyanobacterial pigments are generally low until 8600 cal a BP, then steadily increase until 8040 cal a BP (Fig. 5d). Canthaxanthin concentrations remain high until ~5450 cal a BP, albeit with some variability, decreasing thereafter until reaching minimum values during the last 500 years (Fig. 5d). Post-depositional diagenesis does not appear to control any of the observed trends as pigment concentrations do not systematically decrease downcore and the highest concentrations are found in the oldest sediments.

PCoA results for the algal pigment proxy datasets show that axis 1 explains 71 % of the data's similarity (Fig. S6). PCoA axis 1 closely resembles total diatom and chlorin pigments and shows relatively large centennial scale variability compared to the relatively stable millennial scale variability. Major deviations in the trends include a low from ~7250 cal a BP to 4950 cal a BP and a steady decline from 1800 cal a BP towards present (Fig. 5f). Given the strong similarity to algal pigment trends, we interpret PCoA axis 1 to reflect relative changes in total algal productivity.

Deleted: average

Deleted: ing

Deleted: until

Deleted: 20

Deleted: anti

Deleted: relatively

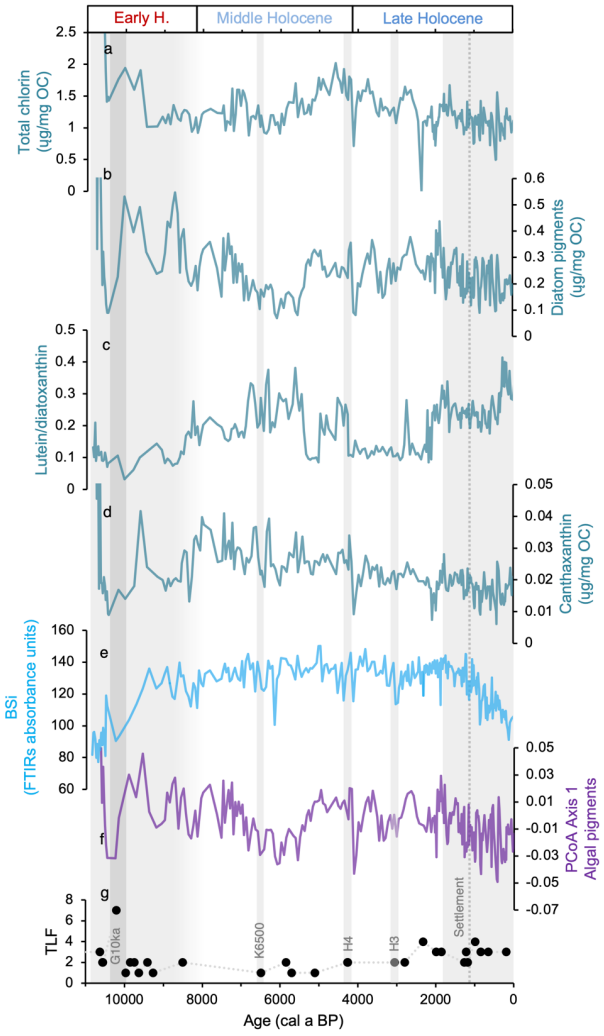
Early H.
Middle Holocene
Late Holocene
a
b
c
d
e
f
g
Total chlorin (µg/mg OC)
Diatom pigments (µg/mg OC)
Lutein/diatoxanthin
Canthaxanthin (µg/mg OC)
BSi (FTIRs absorbance units)
PCoA Axis 1 Algal pigments
TLF
G10ka
K6500
H4
H3
Settlement
Age (cal a BP)

Figure 5: Algal pigment proxy records (a-d), bulk geochemical BSi (e), PCoA Axis 1 of algal pigment proxies (f), and tephra layer frequency (TLF, g) from core 2012NC. Grey bars reflect landscape disturbances associated with large tephra layer deposits and erosion and dashed gray line denotes the timing of presumed human settlement (1080 cal a BP).

4 Discussion

4.1 Holocene tephra records

We identified 28 visible tephra and 5 cryptotephra horizons in the lake sediment of Torfdalsvatn. In total, these tephra horizons represent at least 78 separate fall events (Table 2) as the majority (n=24; 73%) feature tephra fall from more than one volcanic system. On 9 occasions (27%), the horizons contain tephra with composition indicating a single system as the source. Most common are tephra horizons with 2 source systems (n=13; 39%), then those with 3 source systems (n=8; 24%), followed by 4 (n=2; 6%) and then 7 (n=1; 3%). In 19 out of 24 (79%) tephra horizons, the tephra populations indicate additional source systems present as minor components, and in some instances only by a single grain. In 6 instances (18%), the different source system populations are present in more equal proportions and 4 of those cases (12%) are represented by the cryptotephra horizons. The source systems indicated are Grímsvötn (n=31; 40%), Hekla (n=17; 22%), Katla (n=14; 19%), Veiðivötn-Bárðarbunga (n=7; 9%), Askja (n=3; 4%), Kverkfjöll (n=3; 4%), and unknown (n=2; 3%) (SDT2). All these systems are distal to Torfdalsvatn, where Katla is farthest away (~270 km) and Askja is closest (~200 km). Consequently, only the more powerful explosive eruptions at these systems had the potential to produce tephra fall at Torfdalsvatn. Please see Supporting Information for more details on the implications of Torfdalsvatn's tephra stratigraphy.

Most lake sediment records in Iceland that report tephra compositional analyses only do so for key marker tephra to provide age control for accompanying proxy records. Currently, there are 5 regional lake record stratigraphies that provide complete tephra inventories for the sedimentary sequences (Fig. 6). Compared to these other detailed tephra stratigraphies, the 78 volcanic events identified in Torfdalsvatn are relatively extensive and only superseded by the lake Lögurinn record, which contains 149 volcanic events based on compositional analyses (Fig. 6, Gudmundsdóttir et al., 2016). Surprisingly, the tephra record from Hestvatn, which is located close to many of the active volcanic centers in south Iceland only archives 38 distinct volcanic events (Fig. 6, Geirsdóttir et al., 2022). The records from west (Haukadalsvatn) and northwest Iceland (Vestfirðir) contain 37 and 27 tephra layers, respectively (Harning et al., 2018, 2019). While various factors can influence the preservation of tephra layers in individual lake sediment records (e.g., Boygle, 1999), the simplest explanation for the regional variability in tephra layer occurrence is the direction of prevailing atmospheric winds around Iceland. In the stratosphere (7-15 km altitude), where explosive ash plumes are predominately injected to, the prevailing winds are westerly (Lacasse, 2001). However, if ash plumes are in the troposphere (<7 km altitude), upper stratosphere (>15 km altitude), or occur during the spring/summer when the prevailing stratospheric westerlies shift to weak easterlies (Lacasse, 2001), tephra can be carried westward.

Deleted: ¶
3.4 Statistics

Moved up [1]: PCoA results for the bulk geochemistry and algal pigment proxy datasets show that axis 1 explains 52.4 % and 71 % of the variance, respectively. PCoA Axis 1 for bulk geochemistry proxies shows the highest values at the base of the record followed be a gradual decrease to a low at 7650 cal a BP (Fig. 4f). During the Middle Holocene, the PCoA values show some centennial scale variability, although millennial scale variability is relatively stable before a step shift at 1080 cal a BP (Fig. 4f). The major changes observed, such as the Early Holocene decrease, Middle Holocene centennial-scale variability and step shift at 1080 cal a BP, coincide with either erosional signals and/or tephra deposits (gray bars, Fig. 4). PCoA Axis 1 for algal pigments closely resembles total diatom and chlorin pigments and shows relatively large centennial scale variability compared to the relatively stable millennial scale variability. Major deviations in the trends include a low from ~7250 cal a BP to 4950 cal a BP and a steady decline from 1800 cal a BP towards present (Fig. 5f). We interpret PCoA Axis 1 of bulk geochemistry and algal pigments to reflect relative changes in erosional activity and total algal productivity, respectively.¶

Deleted: PCoA results for the bulk geochemistry and algal pigment proxy datasets show that axis 1 explains 52.4 % and 71 % of the variance, respectively. PCoA Axis 1 for bulk geochemistry proxies shows the highest values at the base of the record followed be a gradual decrease to a low at 7650 cal a BP (Fig. 4f). During the Middle Holocene, the PCoA values show some centennial scale variability, although millennial scale variability is relatively stable before a step shift at 1080 cal a BP (Fig. 4f). The major changes observed, such as the Early Holocene decrease, Middle Holocene centennial-scale variability and step shift at 1080 cal a BP, coincide with either erosional signals and/or tephra deposits (gray bars, Fig. 4). PCoA Axis 1 for algal pigments closely resembles total diatom and chlorin pigments and shows relatively large centennial scale variability compared to the relatively stable millennial scale variability. Major deviations in the trends include a low from ~7250 cal a BP to 4950 cal a BP and a steady decline from 1800 cal a BP towards present (Fig. 5f). We interpret PCoA Axis 1 of bulk geochemistry and algal pigments to reflect relative changes in erosional activity and total algal productivity, respectively.¶

Deleted: During the Holocene, Icelandic volcanism has featured both effusive and explosive mafic eruptions, where the latter have often been influenced by frequent subglacial and subaqueous/submarine interactions. Although less common, rhyolitic eruptions from central volcanoes are frequent in Iceland and typically more explosive than their mafic counterparts (e.g., Thordarson and Larsen, 2007; Thordarson and Höskuldsson, 2008; Larsen and Eiríksson, 2008). Due to their added intensity, many of these rhyolitic eruptions have produced widespread, light-colored tephra layers that form the backbone of tephrochronological frameworks on both sides of the North Atlantic (e.g., Abbott and Davies, 2012; Lawson et al., 2012). Most of these tephra laye ... [1]

Deleted: 6

Deleted: s

Deleted: a stratigraphies and chronologies for all tephra identified in

Deleted: complete

Deleted: high

In addition to the established Holocene tephra marker layers in the Icelandic record (highlighted with an * in Table 2), our high-resolution age model allows 14 additional tephra layers in Torfdalsvatn to serve as regional marker horizons in north Iceland. These include 1) the thick and closely-spaced Late Holocene basaltic Katla 1220 and Katla 1270 tephra layers, 2) the Middle Holocene sequence of Hekla 5100, Kverkfjöll/Katla 5850, Askja 6100 and Katla 6500 (Tv-5) series, 3) the Early Holocene Grímsvötn/Katla tephra pair G/K 8500 and Grímsvötn 9260, and 4) the pre-G10ka Series basaltic Hekla tephra layers, Hekla 10,550 and Hekla 11,390 (Tv-1), as well as the bimodal Katla tephra layers (Katla 11,170, Katla 11,295 and Katla 11,315, see Harning et al., 2024).

Finally, in this study, the residual sulfur content was measured in a selected suite of tephra samples (bold font, Table 2) to assess whether the events that produced those tephra layers involved interaction with external water upon eruption. Evidence of such interaction is an indicator of wet vent environment and thus may serve as a proxy for eruptions from within glaciers or through standing body of water (lake or the sea). We refer the reader to the Supporting Information for more details.

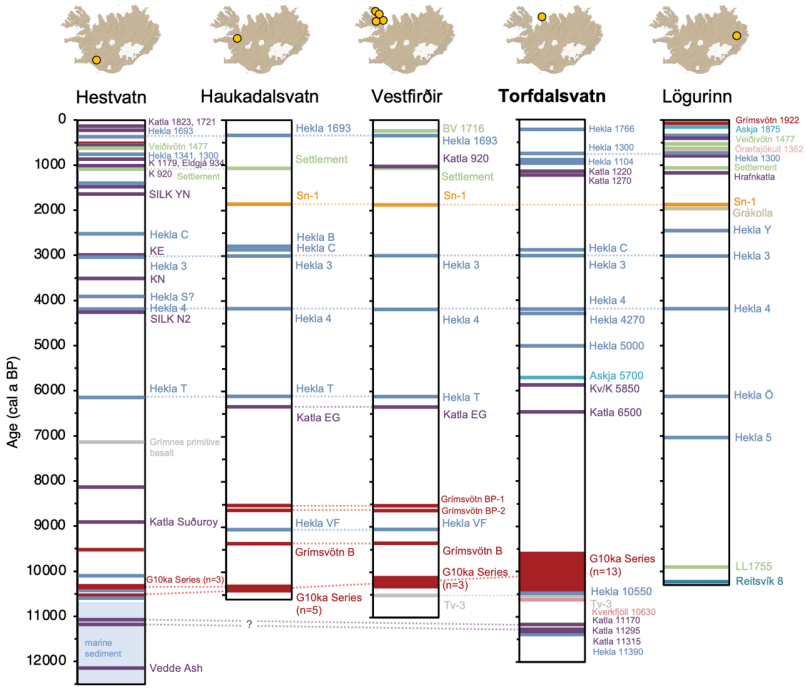

Figure 6: Regional Icelandic tephra stratigraphies based on high-resolution lake sediment records from Hestvatn (Geirsdóttir et al., 2022), Haukadalsvatn (Harning et al., 2019), Vestfirðir (Harning et al., 2018), Torfdalsvatn (this study, Björck et al., 1992; Alsos et al., 2021; Harning et al., 2024), and Lögurinn (Gudmundsdóttir et al., 2016). For lake Lögurinn (east Iceland), we note that 149 total tephra layers have been identified and compositionally analyzed (Gudmundsdóttir et al., 2016), although we only show the key marker tephra layers for simplicity. All tephra layers are colored according to volcanic systems shown in Fig. 1a, and correlations between records indicated by dashed gray lines. Note: ages for tephra layers younger than the Settlement layer at ~1080 cal a BP (i.e., historical tephra) are presented in CE and not BP.

4.2 Holocene climate and landscape evolution

Continuous records of past landscape stability and soil erosion can be reconstructed by comparing proxies for minerogenic flux (magnetic susceptibility, MS) and terrestrial versus aquatic organic matter source (C/N and $\delta^{13}C$) (e.g., Geirsdóttir et al., 2009, 2013, 2019, 2020). The controlling factors on the quantity of magnetic material that enters the lake are the amount of fine-grained minerogenic material available (from receding glaciers or tephra deposition), how well stabilized this material is by vegetation, and the strength of a transport mechanism (erosion by wind or water). In Iceland, organic matter source can be distinguished as either terrestrial or aquatic via C/N and $\delta^{13}C$ composition (Wang and Wooller, 2006; Skrzypek et al., 2008; Langdon et al., 2010; Florian, 2016), where terrestrial plants typically have high C/N (10 to 205) and low $\delta^{13}C$ values (-31 to -22 ‰) and aquatic plants have low C/N (7 to 26) and high $\delta^{13}C$ values (-30 to -11 ‰), with some overlap between end-members. Bulk sediment values therefore reflect the relative biomass in each environment, as well as efficiency of the transport of stored terrestrial material by soil erosion, which in Iceland, is easily accomplished by both wind and water due to the lack of cohesion of andosol soil (Arnalds, 2015). An increase in magnetic material (here inferred from magnetic susceptibility) without associated increase in C/N represents either an increase in available source material (such as tephra) or a relatively small carbon-producing biomass that reduces dilution of minerogenic material.

Biogenic silica (BSi), which reflects the relative amount of siliceous material produced by lake algae (mostly diatoms), is a commonly used measure for reconstructing total aquatic productivity (Conley and Schelske, 2001), and in Iceland, spring temperatures as well (Geirsdóttir et al., 2009). On the other hand, algal pigments provide a more comprehensive view of past aquatic productivity as they reflect all taxonomic groups, rather than just those that produce silicified structures (Leavitt and Hodgson, 2001), and primarily respond to broad changes in climate and nutrients (Smith, 1979; Smol and Cumming, 2000). Algal pigment concentrations and ratios, such as those presented here, can be used to characterize both total aquatic productivity and the relative contribution of major algal groups as most pigments used are relatively stable, reducing the bias of variable pigment preservation through time (Bianchi et al., 1993; Leavitt and Hodgson, 2001).

4.2.1 Deglaciation to Early Holocene (~12000 to 8200 cal a BP)

Based on the basal age of the Torfdalsvatn lake sediment core, deglaciation of this region of north Iceland is estimated to be around 12000 cal a BP (Harning et al., 2023). Subsequently, the receding Icelandic Ice Sheet left abundant, easily erodible minerogenic material upon the local landscape. Plant *sed*aDNA records from Torfdalsvatn indicate that the first pioneer forb,

Deleted: Shortly after deglaciation

Deleted: ,

graminoid and bryophyte taxa were present in the catchment no earlier than 12,000 cal a BP (Fig. 7c, Alsos et al., 2021; Harning et al., 2024). The lack of a substantial terrestrial ecosystem needed to stabilize the landscape at this time is consistent with the highest MS values in Torfdalsvatn's Holocene record (Fig. 4a). MS then decreases as the quantity of easily erodible material was depleted and vegetation cover developed (Alsos et al., 2021). Woody taxa, such as *Salix* and *Betula*, then appear in the lake catchment by 10,300 and 9500 cal a BP, respectively (Alsos et al., 2021; Harning et al., 2023), straddling the deposition of the G10ka Series tephra and during the dominant period of terrestrial plant colonization (Alsos et al., 2021). MS values continue to steadily decrease through the G10ka Series tephra, although C/N increases, indicating a period of increased plant and soil erosion around Torfdalsvatn that has been previously associated with the massive amount of tephra fallout from the Grímsvötn eruptions (Rundgren, 1998; Hallsdóttir and Caseldine, 2005; Eddudóttir et al., 2015; Florian, 2016).

Throughout the Holocene record, chlorins are the most abundant algal pigment in Torfdalsvatn, consistent with their ubiquity in photosynthetic organisms and function as light-harvesting pigments (Simkin et al., 2022). In the Early Holocene, chlorin concentrations peak at 10760 cal a BP (Fig. 5a). At this time, significant terrestrial biomass had yet to develop on the landscape (Alsos et al., 2021), meaning most organic matter was aquatic and algal pigment-rich, which is supported by low C/N and high $\delta^{13}C$ values in bulk sediment (Fig. 4c-d). This is also consistent with a high proportion of unidentified *sed*aDNA reads, which is presumed to derive from algae due to limited reference material currently available (Alsos et al., 2021). The subsequent decrease in chlorin concentrations (Fig. 5a) therefore likely reflects terrestrial biomass development (Alsos et al., 2021) and influx of algal pigment-poor material. This interpretation is supported by increasing C/N ratios, which indicate increased proportion of terrestrial carbon through this interval (Fig. 4c). The proportion of diagnostic pigments from algal groups (e.g., diatoms, L/D, and canthaxanthin) are variable during the Early Holocene. Diatom pigments become more abundant after the deposition of the G10ka Series tephra and an increase in BSi during this interval suggests an increase in diatom productivity (Fig. 5b and e). These changes occur during a period of broad summer warming in Iceland, most clearly manifested in the rapid retreat and likely disappearance of residual Icelandic ice caps (Larsen et al., 2012; Harning et al., 2016b; Anderson et al., 2019). After peaking at 8720 cal a BP, diatom pigment concentrations decrease, inversely correlated with the ratio of lutein to diatoxanthin (Fig. 5b-c). This, along with a decrease in C/N (Fig. 4c), suggests that green algae and/or aquatic higher plants became more abundant at the expense of diatoms.

During the Early Holocene, marine sediment proxy records from the North Iceland Shelf indicate that surface currents were generally dominated by warm Atlantic Water and restricted sea ice (e.g., Kristjánsdóttir et al., 2017; Xiao et al., 2017; Harning et al., 2021) (Fig. 7). However, lake sediment and mire records from north Iceland document an interruption in woody taxa succession inferred from pollen and increased soil erosion from ~8800 to 7900 cal a BP (e.g., Hallsdóttir, 1995; Hallsdóttir and Caseldine, 2005; Eddudóttir et al., 2015, 2018; Geirsdóttir et al., 2020). This time window includes the well-known 8.2 ka event (e.g., Barber et al., 1999; Alley and Ágústsdóttir, 2005; Rohling and Pälike, 2005) as well as additional freshwater pulses that originated from the decaying Laurentide Ice Sheet (e.g., Jennings et al., 2015) that are known to have driven oceanographic cooling around Iceland via a slowdown of the North Atlantic ocean circulation (e.g., Quillmann et al., 2012; Moossen et al., 2015). PCoA results for Torfdalsvatn soil erosion demonstrate that while the catchment was in transitional state towards

Deleted: , including Drangajökull (Harning et al., 2016b), located ~75 km to the west of Torfdalsvatn (Fig. 1a)

Deleted: anti

Deleted: increasingly

Deleted: additional

stabilization (Fig. 7a), algal productivity generally decreases in response to cooling in the ~8800 to 7900 cal a BP window (Fig. 7b). In terms of vegetation, plant *sed*aDNA species richness shows no change in woody, forbs, and bryophyte plant functional groups at this time, whereas others, such as graminoids and aquatic plants may have decreased. However, the low resolution of the *sed*aDNA record (>250 years, Fig. 7c) makes it challenging to confidently attribute changes to the ~8800 to 7900 cal a BP climate window specifically.

Deleted: little

Deleted: disturbances to

Deleted: some

Deleted: we note that

Deleted: this lack of response in some plant groups may partially be due to …

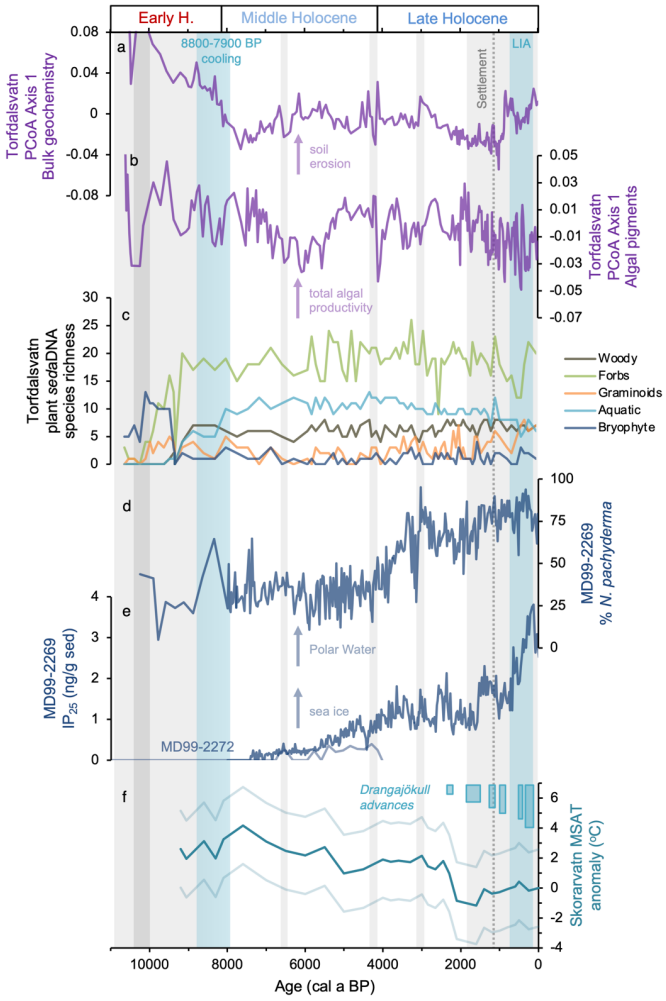

600

Figure 7: Comparison of Torfdalsvatn's PCoA results with regional marine and terrestrial environmental records. a) Torfdalsvatn PCoA Axis 1 of bulk geochemistry (this study), b) Torfdalsvatn PCoA Axis 1 of algal pigments (this study), c) Torfdalsvatn species richness of various plant functional groups based on *sed*aDNA (Alsos et al., 2021), d) relative abundance of Arctic planktic foraminifera *N. pachyderma* from marine core MD99-2269 (Harning et al., 2021), e) concentration of sea ice algae biomarker IP_{25}

from marine core MD99-2269 (dark blue, Cabedo-Sanz et al., 2016) and MD99-2272 (light blue, Xiao et al., 2017), and f) Drangajökull ice cap advances (blue, Harning et al., 2016a, 2018a) and mean summer air temperature anomaly (ºC) from Skorarvatn, NW Iceland (teal) with uncertainty estimates (light teal) (Harning et al., 2020). Grey bars reflect landscape disturbances associated with large tephra layer deposits and erosion and dashed gray line denotes the timing of presumed human settlement (1080 cal a BP).

4.2.2 Middle Holocene (8200 to 4200 cal a BP)

Overall, MS continues to decrease through the Middle Holocene, except for periodic spikes at 6500 and 4260 cal a BP reflecting the presence and impact of major tephra fall from Katla and Hekla eruptions, respectively (Fig. 4a). For the Katla 6500 tephra, increased C/N and $\delta^{13}C$ values indicate increased soil erosion immediately following its deposition, which lasted for several centuries (Fig. 4c-d). Similarly, Hekla 4 is known to have disturbed the terrestrial landscape in Icelandic lake catchments (Geirsdóttir et al., 2019), and in Torfdalsvatn, the period of increased erosion inferred from increased C/N and $\delta^{13}C$ values indicates that it only lasted for about a century (Fig. 4c-d). Eddudottir et al. (2017) suggest that lowland areas with presumably more substantial *Betula* woodland cover, such as Torfdalsvatn, are more resilient to tephra fall compared to higher elevation areas that were already at the climatic/ecological limit. The persistence of woody taxa around Torfdalsvatn through these large tephra fall events (Alsos et al., 2021) is consistent with this inference and suggests that the impact of periods of increased erosion were relatively shorter or less severe around Torfdalsvatn than they would otherwise be at higher elevation sites. However, we note that sampling resolution for *sed*aDNA in this portion of the record is over 100 years (Alsos et al., 2021), which may miss short-term impacts of tephra to the catchment ecosystem. In terms of aquatic proxies, we note that all algal pigments as well as BSi indicate short-lived increases in algal productivity during both the Katla 6500 and Hekla 4 eruptions. This process is consistent with lake studies in other volcanic regions that document increased diatom and algal productivity following volcanic eruptions due to the increased supply of silica and nutrients (e.g., Telford et al., 2004; Egan et al., 2019).

Chlorin concentrations remain generally low during the first two millennia of the Middle Holocene before increasing to peak values at 4580 cal a BP (Fig. 5a). These higher chlorin values are associated with increasing diatom pigments (Fig. 5b), decreasing L/D ratios (Fig. 5c), and the lowest C/N of the record (Fig. 4c), indicating a shift of organic matter towards a more aquatic plant source around this time. Interestingly, BSi does not track diatom pigment abundance for much of the record, which may be due to several complicating factors related to using both organic and inorganic indicators to reconstruct past algal biomass. Both proxies (i.e., diatom pigments and BSi) can be influenced by differences in amount of each compound per unit of algal biomass, varying species assemblage, and environmental conditions (Alberte et al., 1981; Lavaud et al., 2002; Rousseau et al., 2002; Stramski et al., 2002; Finkel et al., 2010), all of which are challenging to individually constrain in paleoenvironmental reconstructions. In any case, during the Middle Holocene, terrestrial pollen (Rundgren, 1998; Hallsdóttir and Caseldine, 2005; Eddudóttir et al., 2015) and plant *sed*aDNA records (Alsos et al., 2021) indicate that catchment vegetation communities were well-developed, which likely stabilized the catchment and reduced the influx of terrestrial organic matter to the lake. In addition, aquatic plants make up the dominant proportion of *sed*aDNA reads at this time (Alsos et al., 2021),

Deleted: At least f

Deleted: has

Deleted: similarly

Deleted: other

Deleted: , however,

Deleted:

Deleted:

Deleted: . One possibility is that there are

Deleted: these

which likely results from the small, shallow nature of the lake basin that permits light penetration for submerged taxa (Fig 1b), consistent with the increased general productivity of the aquatic environment.

Finally, cyanobacterial populations have been shown to quickly increase in response to higher temperature and nutrient levels and may therefore be an important indicator species for past lake conditions (De Senerpont Domis et al., 2007; Paerl and Paul, 2012). The only detectable pigment of cyanobacteria in Torfdalsvatn is canthaxanthin, present throughout the core at low concentrations. Canthaxanthin concentrations remain elevated until ~5450 cal a BP, albeit with some variability, decreasing thereafter until reaching minimum values during the last 500 years (Fig. 5d). The pattern of change in canthaxanthin concentrations mirrors other relative and quantitative temperature records derived from Icelandic lake sediment BSi composites and lipid biomarkers records, respectively, which peak during the Holocene Thermal Maximum (7900 to 5500 cal a BP) and decrease in a stepwise manner through the Middle Holocene to the Little Ice Age (700 to 50 cal a BP, 1250 to 1900 CE) (Larsen et al., 2012; Geirsdóttir et al., 2013, 2019, 2020; Harning et al., 2020). This suggests that the abundance of cyanobacteria may be controlled more closely by lake water temperature and length of summer than the other algal groups in Torfdalsvatn, such as diatoms.

PCoA results from bulk geochemistry and plant *sed*aDNA species richness demonstrate that the Middle Holocene terrestrial landscape around Torfdalsvatn was generally stable, whereas algal productivity diminished between 7500 and 5000 cal a BP (Fig 7a-c). This terrestrial stability is consistent with the corresponding marine environment along the North Iceland Shelf, where the ocean surface was dominated by warm Atlantic Water at this time (e.g., Kristjánsdóttir et al., 2017; Harning et al., 2021), reflected well by low abundances of Arctic planktic foraminifera (e.g., *N. pachyderma*, Harning et al., 2021) and sea ice algae proxies (e.g., IP_{25}, Cabedo-Sanz et al., 2016; Xiao et al., 2017) (Fig. 7d-e). The decrease in algal productivity between 7500 and 5000 cal a BP in the PCoA results largely stems from decreases in diatom pigments as well as minor decreases in chlorins at the expense of lutein-producing green algae and/or higher plants (Fig. 5). As there is no indication of local climate change during the 7500 to 5000 cal a BP interval in either the Icelandic marine or terrestrial realms, it is possible that the changes resulted from internal lake dynamics, such as nutrient availability. However, without further proxy information, the processes behind the changes in algal productivity are currently challenging to diagnose.

Deleted: logical

Deleted: were induced by

Deleted: processes

4.2.3 Late Holocene (4200 cal a BP to present)

After about two millennia of relative stability in Torfdalsvatn following the Hekla 4 tephra layer, individual algal pigment concentrations, BSi, and algal pigment PCoA results begin to decrease at 1800 cal a BP (150 CE, Fig. 5). These consistent changes indicate broad decreases in total algal productivity likely driven by ambient changes in climate and/or shorter ice-free seasons that inhibit light availability. However, we do not find an increase in C/N or soil erosion accompanying algal productivity changes around Torfdalsvatn, similar to other high-resolution lake sediment proxy records in Iceland (e.g., Geirsdóttir et al., 2013, 2019, 2020). This is consistent with the low elevation and low relief nature of Torfdalsvatn's catchment and relative stability of the various terrestrial plant functional groups in the lake catchment derived from *sed*aDNA (Fig. 7C, Alsos et al., 2021). However, regime shifts in offshore marine climate records demonstrate that around this time (i.e., ~1800

Deleted: In contrast to other high resolution lake sediment C/N proxy records in Iceland (Geirsdóttir et al., 2019, 2020)

Deleted: .

cal a BP, 150 CE) the Polar Front advanced southward around Iceland, bathing the North Iceland Shelf with cool, sea-ice bearing Polar Water (Harning et al., 2021). This shift in ocean surface water source is reflected well by the increase in Arctic planktic foraminifera *N. pachyderma* (Harning et al., 2021) and sea ice algae proxy IP_{25} (Cabedo-Sanz et al., 2016) from sediment cores on the North Iceland Shelf just north of Torfdalsvatn (MD99-2269, Figs. 1A and 7d-e), and led to substantial summer cooling in the area around Skorarvatn, NW Iceland, resulting in the marginal expansion of the nearby Drangajökull ice cap, just west of Torfdalsvatn (Figs. 1a and 7f, Harning et al., 2016a, 2018a, 2020).

At 880 cal a BP (1070 CE), bulk geochemistry PCoA results indicate a substantial increase in landscape instability and soil erosion around Torfdalsvatn (Fig. 7a). Norse settlers are estimated to have arrived in Iceland earlier, i.e., around 1080 cal a BP (870 CE), and *assumed* to have quickly impacted the landscape through woodland clearing and agricultural and pastoral farming that prohibited natural plant regeneration (e.g., Thórarinsson, 1944; Arnalds, 1987; Hallsdóttir, 1987; Smith, 1995; Lawson et al., 2007). However, these datasets are largely based on soil and sedimentary records with coarser resolution and/or age control than Torfdalsvatn. For Torfdalsvatn, the earliest known presence of humans around the lake is later than both the geochemical record and assumed settlement in 665 cal a BP (1285 CE), when the local farms sharing the lake are mentioned in a letter as being owned by the Þingeyrarklaustur monastery (DI, 1857-1986). The plant *sed*aDNA record from Torfdalsvatn indicates that while some woody taxa, such as *Salix* and *Betula*, are present through the presumed timing of human colonization around 1080 cal a BP (870 CE), *J. communis* (juniper) disappears and species diversity of forbs decrease slightly earlier than our bulk geochemistry record and documentary evidence of human presence (1055 cal a BP, 895 CE, Fig. 7C, Alsos et al., 2021). We note, however, that while environmental impacts from settlers have been independently confirmed in lake sediments on the Faroe and Lofoten Islands using fecal biomarkers and/or sheep *sed*aDNA (D'Anjou et al., 2012; Curtin et al., 2021), these tools have so far proved challenging for use in Icelandic sediments and are needed for confirmation (Ardenghi et al., 2024). Hence, it is difficult to correlate whether the changes in soil erosion around Torfdalsvatn are related to human pressure or otherwise. In any case, it is unlikely that the small populations that initially settled Iceland (~30,000 people, *Landnámabók*, i.e. The book of Settlement) would have had a substantial and immediate impact on the landscape. If we can independently confirm human presence in Torfdalsvatn sedimentary record through future application of molecular approaches, such as fecal biomarkers and mammalian *sed*aDNA, our record from Torfdalsvatn will provide a well-constrained benchmark for changes in the ecosystem linked to human practices in north Iceland.

Following the initiation of increased long-term soil erosion that began around 880 cal a BP, we observe distinct disturbances to the Hekla 1104 CE (846 cal a BP) tephra layer stratigraphy. In core 2004NC, Hekla 1104 CE tephra is present over a 15.4 cm interval (88.1 to 103.5 cm depth) as three distinct and separate layers/wedges connected by mm-thick, irregular light-colored stringers with intermittent shear planes (Fig. 8). The 30 cm above the uppermost wedge is characterized by fining upward pumice grains suggesting an origin within a gravity current (Fig. 8). In core 2012NC, it is present as two distinct layers at depths of 80.5 cm (0.1 cm) and 84.5 cm (0.7 cm) (see Supporting Information), where the upper layer has a modeled age of 800 cal a BP (1150 CE). Hekla 1104 CE is also found in a previously published record from Torfdalsvatn (Alsos et al., 2021), where the stratigraphy is also discontinuous with stringers below and above the main tephra layer horizon (Bender, 2020). The

Deleted: and

Deleted: s

Deleted: this interval

Deleted: , which may partially be due to variable age control between the two sedimentary records

Deleted: , and

Deleted: s

Deleted: 10

Deleted: 1150 CE

cause of this disturbance is unlikely to relate to sediment coring as it is found in the middle of the core segments between undisturbed organic lake sediment and identified in three independent records. Instead, this indicates that an external factor likely impacted the sedimentary sequence after the Hekla 1104 CE tephra layer was deposited, such as a slope failure. As the catchment and bathymetry of Torfdalsvatn are both low relief (Fig. 1b, Florian, 2016), a slope failure would require a trigger event. Local documentary records indicate that a large earthquake occurred in 1260 CE (Storm, 1977a, 1977b, 1977c), which we propose as a likely candidate based on the slightly younger age compared to the tephra deposit. Similar soft sediment deformation structures in tephra layers have been identified in New Zealand lakes and linked to seismic activity (termed tephra-seismites, Kluger et al., 2023), supporting our reasoning for Torfdalsvatn's stratigraphy. While the disturbance is relatively short-lived, the Torfdalsvatn records indicate the susceptibility of even low-relief environments to seismic activity that may confound the continuity and interpretation of lake sediment proxies in Iceland.

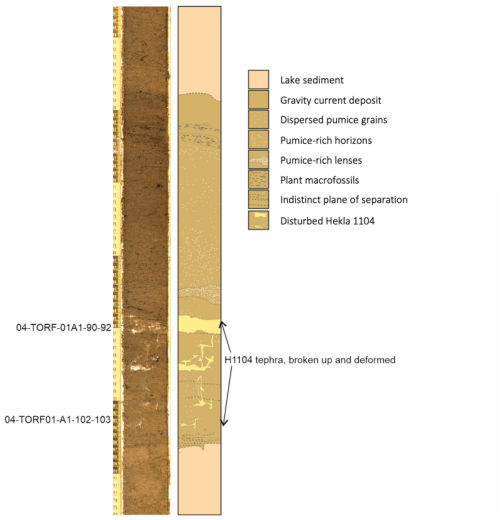

Figure 8: Lithostratigraphy of the deformed Hekla 1104 CE tephra layer (i.e., tephra-seismite) in core 2004NC. On the left is a photo image and on the right is a simplified schematic based on the major identified sediment types.

Finally, the general cooling reflected in decreased algal productivity that commenced at 1800 cal a BP (150 CE) culminated with the lowest Late Holocene values at 450 cal a BP (1500 CE, Fig. 7b). This coincides with the Little Ice Age (LIA, ~700 to 100 cal a BP, 1250 to 1850 CE, blue bar, Fig. 7, Geirsdóttir et al., 2013), a period marked by the coolest Holocene conditions in Iceland. Regionally, the Little Ice Age is well reflected in environmental conditions such as the maximum Holocene extent of Polar Water and sea ice on the North Iceland Shelf (Fig. 7d-e, Cabedo-Sanz et al., 2016; Harning et al.,

Deleted: around

2021) and largest Holocene dimensions of Icelandic ice caps (Fig. 7f, Larsen et al., 2011; Harning et al., 2016b; Hannesdóttir et al., 2015, 2020). In terms of Torfdalsvatn plant communities, species richness patterns show troughs in forbs and aquatic taxa and peaks in graminoids and bryophytes during this interval (Fig. 7c). Alsos et al. (2021) also note an increase of high arctic taxa such as *O. digyna*, *K. islandica*, *Epilobium anagallidifolium*, *S. acaulis*, and *D. octopetala* at Torfdalsvatn during the Little Ice Age. Despite these broad changes in Torfdalsvatn's terrestrial and aquatic environments during the coldest part of the Holocene – that would be expected to result in enhanced landscape instability as observed in other Icelandic lake records (e.g., Geirsdóttir et al., 2009, 2020) – we observe a decrease in soil erosion between 650 and 100 cal a BP (1300 to 1850 CE, Fig. 7a). The northern latitudinal position of the lake abutting the harsh Polar marine climate on the North Iceland Shelf and minima in Northern Hemisphere summer insolation (Berger and Loutre, 1991) would have resulted in shorter summers and possibly reduced mobilization of soil in a more perennially frozen landscape, and therefore explain a decrease in soil erosion. Following the termination of the Little Ice Age (100 cal a BP, 1850 CE), the Torfdalsvatn record indicates a slight decrease in soil erosion and algal productivity to present (Fig. 7a-b). While it is challenging to directly tie this period to Iceland's instrumental temperature record because 1) we lack secure chronological control from the last century (e.g., ^{137}Cs) and 2) this period is only represented by several data points, these proxy trends suggest that the broad warming trend that followed the end of the Little Ice Age (Hanna et al., 2004) may have resulted in reduced soil erosion and algal productivity. However, with the contaminant rise in Iceland's population (Hagstofa Íslands, 2024), increased human pressure may have also impacted the landscape. Future higher-resolution studies focusing on the last several centuries in Icelandic lakes will be instrumental in deciphering the most recent changes in the environment and how that relates to human and climate drivers.

5 Conclusions

We present a multi-proxy analysis of lake sediments from Torfdalsvatn, the longest known lacustrine record in Iceland of ~12000 years. These analyses include a high-resolution age model (n = 22 control points), an expanded and comprehensive Holocene tephra stratigraphy and chronology (>2200 grains analyzed in 33 tephra horizons), and sub-centennial bulk geochemical and algal pigment proxy records. Collectively, we use these datasets to address the following topics:

- *Tephrochronology:* We identified 33 distinct tephra layers, which represent 78 separate volcanic events from 6 volcanic systems. Compared to tephra stratigraphies from other lake sediment records in Iceland, these are relatively high numbers. Key marker tephra layers include I-THOL-I, the G10ka Series (13 events), Katla 6500, Hekla 4, Hekla 3, Hekla C, Hekla 1104, Hekla 1300, and Hekla 1766. In addition, we present evidence for a previously unidentified basalt tephra (Askja 6100) with a distinct primitive composition and a bimodal (rhyolite-basalt) tephra layer (Hekla 5100).
- *Catchment instability and soil erosion:* Bulk physical and geochemical proxy records capture past intervals of soil erosion around Torfdalsvatn due to combinations of Middle Holocene volcanic eruptions, Late Holocene climate cooling and after presumed human settlement at 880 cal a BP (1070 CE). Compared to other lake sediment records in Iceland, we do not observe clear long-term increases in soil erosion beginning prior to human settlement but starting

Deleted: Holocene terrestrial

Deleted: -

Deleted: climate cooling,

~200 years later. The stratigraphy (i.e., tephra-seismite) of sediment during the last millennium also suggests the occurrence of a seismic-induced slope failure in or around the lake.

- *Algal productivity:* Torfdalsvatn's algal group ontogeny progressed from mainly diatoms shortly after the G10ka Series tephra, to predominantly green algae, aquatic macrophytes and cyanobacteria. This is assumed to have been driven by increased temperatures and length of summer during the HTM where the timing of peak cyanobacterial abundance likely represents the warmest Holocene temperatures in Torfdalsvatn. After the HTM, algal productivity remains generally stable until 1800 cal a BP, when changes in regional climate led to decreased algal productivity that reached the lowest values during the Little Ice Age (700 to 100 cal a BP, 1250 to 1850 CE).
- The changes in algal productivity and soil erosion observed beginning around 1800 (150 CE) and 880 cal a BP (1070 CE), respectively, highlight the impact of both natural and possibly anthropogenic factors on Late Holocene aquatic and terrestrial environmental changes in north Iceland. Importantly, they emphasize that while local climate was cooling prior to known human settlement, some low-elevation coastal regions such as Torfdalsvatn, may have been more resistant to natural pre-settlement changes in vegetation cover and soil erosion than observed in other regions of Iceland.

Data Availability

Data associated with this manuscript is available in the Supporting Information and at the NOAA NCEI Paleoclimatology database (https://www.ncei.noaa.gov/access/paleo-search/study/39580).

Author Contributions

ÁG and GHM conceptualized and funded the research; ÁG, GHM, CRF and YA acquired lake sediment cores; SÓ performed PSV analyses; DJH and TT performed EMP analyses and generated the age model; CRF analyzed bulk geochemistry and algal pigments; DJH, CRF, ÁG and TT wrote the paper with contribution from all co-authors.

Competing Interests

The authors declare that they have no conflict of interest.

Acknowledgements

We kindly thank Guðrún Eva Jóhannsdóttir for her contribution to electron microprobe measurements and Þorsteinn Jónsson, Sveinbjörn Steinþórsson, Jason Briner, Yiming Wang, and Matt Wooller for assistance in the field. CRF acknowledges support from the Doctoral Grant of the University of Iceland. This project has been principally supported by the Icelandic Center for Research (RANNÍS) through Grant-of-Excellences #022160002-04, #70272011-13 and #141573051-3, the University of Iceland Research Fund, and the National Science Foundation ARCSS #1836981, awarded to ÁG and GHM.

References

Abbott, P. M., and Davies, S. M.: Volcanism and the Greenland ice-cores: the tephra record, Earth-Science Reviews, 115, 173-191, https://doi.org/10.1016/j.earscirev.2012.09.001, 2012.

Alberte, R. S., Friedman, A. L., Gustafson, D. L., Rudnick, M. S., and Lyman, H.: Light-harvesting systems of brown algae and diatoms. Isolation and characterization of chlorophyll a c and chlorophyll a fucoxanthin pigment-protein complexes, Biochimica et Biophysica Acta (BBA) - Bioenergetics, 635, 304–316, https://doi.org/10.1016/0005-2728(81)90029-3, 1981.

Alley, R., and Ágústsdóttir, A.: The 8k event: Cause and consequences of a major Holocene abrupt climate change, Quaternary Science Reviews, 24, 1123-1149, https://doi.org/10.1016/j.quascirev.2004.12.004, 2005.

Alsos, I. G., Lammers, Y., Kjellman, S. E., Merkel, M. K. F., Bender, E. M., Rouillard, A., Erlendsson, E., Guðmundsdóttir, E. R., Benediktsson, I. Ö., Farnsworth, W. F., Brynjólfsson, S., Gísladóttir, G., Eddudóttir, S. D., and Schomacker A.: Ancient sedimentary DNA shows rapid post-glacial colonisation of Iceland followed by relatively stable vegetation until the Norse settlement (Landnám) AD 870, Quaternary Science Reviews, 259, 106903, https://doi.org/10.1016/j.quascirev.2021.106903, 2021.

Anderson, L. S., Flowers, G. E., Jarosch, A. H., Aðalgeirsdóttir, G. Th., Geirsdóttir, Á., Miller, G. H., Harning, D. J., Thorsteinsson, T., Magnússon, E., and Pálsson, F.: Holocene glacier and climate variations in Vestfirðir, Iceland, from the modeling of Drangajökull ice cap, Quaternary Science Reviews, 190, 39-56, https://doi.org/10.1016/j.quascirev.2018.04.024, 2018.

Anderson, L. S., Geirsdóttir, Á., Flowers, G. E., Wickert, A. D., Aðalgeirsdóttir, G. Th., and Thorsteinsson, T.: Controls on the lifespans of Icelandic ice caps, Earth and Planetary Science Letters, 527, 115780, https://doi.org/10.1016/j.epsl.2019.115780, 2019.

Ardenghi, N., Harning, D. J., Raberg, J. H., Holman, B. R., Thordarson, T., Geirsdóttir, Á., Miller, G. H., Sepúlveda, J.: A Holocene history of climate, fire, landscape evolution, and human activity in Northeast Iceland, Climate of the Past, in press, https://doi.org/10.5194/cp-2023-74, 2024.

Arnalds, A.: Ecosystem disturbance in Iceland, Arctic and Alpine Research, 19, 508-513, https://doi.org/10.2307/1551417, 1987.

Arnalds, O.: The Soils of Iceland. Springer, 2015.

Arnalds, O., and Gretarsson, E.: Soil map of Iceland. Agricultural Research Institute, Reykjavík, 2021.

Arnolds, Ó., Marteinsdóttir, B., Brink, S.H., and Órsson, J.: A framework model for current land condition in Iceland, PloS ONE, 18, e0287764, https://doi.org/10.1371/journal.pone.0287764, 2023.

Axford, Y., Geirsdóttir, Á., Miller, G. H., and Langdon, P.: Climate of the Little Ice Age and the past 2000 years in northeast Iceland inferred from chironomids and other lake sediment proxies, Journal of Paleolimnology, 41, 7-24, https://doi.org/10.1007/s10933-008-9251-1, 2009.

Axford, Y., Miller, G. H., Geirsdóttir, Á., and Langdon, P.: Holocene temperature history of northern Iceland inferred from subfossil midges, Quaternary Science Reviews, 26, 3344-3358, https://doi.org/10.1016/j.quascirev.2007.09.003, 2007.

Bates, R., Erlendsson, E., Eddudóttir, S. D., Möckel, S. C., Tinganelli, L., and Gísladóttir, G.: *Landnám*, land use and landscape change in Kagaðarhóll in Northwest Iceland, Environmental Archaeology, 27, 211-227, https://doi.org/10.1080/14614103.2021.1949680, 2021.

Barber, D. C., Dyke, A., Hillaire-Marcel, C., Jennings, A. E., Andrews, J. T., Kerwin, M. W., Bilodeau, G., McNeely, R., Southon, J., Morehead, M. D., and Gagnon, J. M.: Forcing of the cold event of 8,200 years ago by catastrophic drainage of Laurentide lakes, Nature, 400, 344-348, https://doi.org/10.1038/22504, 1999.

Bender, E. M.: Late Quaternary tephra stratigraphy and paleoenvironmental reconstruction based on lake sediments from North and Northeast Iceland, MS thesis, UiT The Arctic University of Norway, 2020.

Berger, A., and Loutre, M. F.: Insolation values for the climate of the last 10 million years, Quaternary Science Reviews, 10, 297-317, https://doi.org/10.1016/0277-3791(91)90033-Q, 1991.

Bergman, J., Wastegård, S., Hammarlund, D., Wohlfarth, B., and Roberts, S. J.: Holocene tephra horizons at Klocka Bog, west-central Sweden: aspects of reproducibility in subarctic peat deposits, Journal of Quaternary Science, 19, 241-249, https://doi.org/10.1002/jqs.833, 2004.

Bianchi, T. S., Dibb, J. E., and Findlay, S.: Early diagenesis of plant pigments in Hudson River sediments, Estuarine, Coastal and Shelf Science, 36, 517–527, https://doi.org/10.1006/ecss.1993.1031, 1993.

Birks, H. H., Gulliksen, S., Haflidason, H., Mangerud, J., and Possnert, G.: New radio-carbon dates from the Vedde ash and Saksunarvatn ash western Norway, Quaternary Research, 127, 119-127, https://doi.org/10.1006/qres.1996.0014, 1996.

Björck, S., Ingólfsson, Ó., Haflidason, H., Hallsdóttir, M., and Anderson, N. J.: Lake Torfadalsvatn: a high resolution record of the North Atlantic ash zone I and the last glacial-interglacial environmental changes in Iceland, Boreas, 21, 15-22, https://doi.org/10.1111/j.1502-3885.1992.tb00009.x, 1992.

Blaauw, M., and Christen, J. A.: Flexible paleoclimate age-depth models using an autoregressive gamma process, Bayesian Analysis, 6, 457–474, http://doi.org/10.1214/11-BA618, 2011.

Blaauw, M., Christen, J. A., Bennett, K. D., and Reimer, P. J.: Double the dates and go for Bayes – Impacts of model choice, dating density and quality on chronologies, Quaternary Science Reviews, 188, 58-66, https://doi.org/10.1016/j.quascirev.2018.03.032, 2018.

Blair, C. L., Geirsdóttir, Á., and Miller, G. H.: A high-resolution multi-proxy lake record of Holocene environmental change in southern Iceland, Journal of Quaternary Science, 30, 281-292, https://doi.org/10.1002/jqs.2780, 2015.

Boygle, J.: Variability of tephra in lake and catchment sediments, Svínavatn, Iceland, Global and Planetary Change, 21, 129-149, https://doi.org/10.1016/S0921-8181(99)00011-9, 1999.

Bradley, L.-A. and Stafford, T. W.: Comparison of manual and automated pretreatment methods for AMS radiocarbon dating of plant fossils, Radiocarbon, 36, 399–405, https://doi.org/10.1017/S0033822200014570, 1994.

Bronk Ramsey, C.: Bayesian analysis of radiocarbon dates, Radiocarbon, 51, 337-360, https://doi.org/10.1017/S0033822200033865, 2009.

Cabedo-Sanz, P., Belt, S. T., Jennings, A. E., Andrews, J. T., and Geirsdóttir, Á.: Variability in drift ice export from the Arctic Ocean to the North Icelandic Shelf over the last 8000 years: A multi-proxy evaluation, Quaternary Science Reviews, 146, 99–115, https://doi.org/10.1016/j.quascirev.2016.06.012, 2016.

Caseldine, C., Geirsdóttir, Á., and Langdon, P. G.: Efstadalsvatn – a multi-proxy study of a Holocene lacustrine sequence from NW Iceland, Journal of Paleolimnology, 30, 55-73, https://doi.org/10.1023/A:1024781918181, 2003.

Caseldine, C., Langdon, P., and Holmes, N.: Early Holocene climate variability and the timing and extent of the Holocene thermal maximum (HTM) in northern Iceland, Quaternary Science Reviews, 25, 2314-2331, https://doi.org/10.1016/j.quascirev.2006.02.003, 2006.

Conley D. J. and Schelske, C. L.: Biogenic Silica. Track Environmental Change Using Lake Sediments 3, 281–293, 2001.

Curtin, L., D'Andrea, W. J., Balascio, N. L., Shirazi, S., Shapiro, B., de Wet, G. A., and Bradley, R. S., Bakke, J.: Sedimentary DNA and molecular evidence for early human occupation of the Faroe Islands, Communications Earth & Environment, 2, 253, https://doi.org/10.1038/s43247-021-00318-0, 2021.

D'Anjou, R. M., Bradley, R. S., Balascio, N. L., and Finkelstein, D. B.: Climate impacts on human settlement and agricultural activities in northern Norway revealed through sediment biogeochemistry, Proceedings of the National Academy of Sciences, 109, 20332–20337, https://doi.org/10.1073/pnas.1212730109, 2012.

Davies, S. M., Albert, P. G., Bourne, A. J., Owen, S., Svensson, A., Bolton, M. S. M., Cook, E., Jensen, B. J. L., Jones, G., Ponomareva, V. V., and Suzuki, T.: Exploiting the Greenland volcanic ash repository to date caldera-forming eruptions and widespread isochrons during the Holocene, Quaternary Science Reviews, 334, 108707.

De Senerpont Domis, L. N., Mooij, W. M., and Huisman, J.: Climate-induced shifts in an experimental phytoplankton community: A mechanistic approach, Hydrobiologia, 584, 403–413, https://doi.org/10.1007/s10750-007-0609-6, 2007.

DI Diplomatarium Islandicum): Íslenzkt Fornbréfasafn III. Íslenzka Bókmenntafélagið, Kaupmannahöfn (Copenhagen), 1857-1986.

Dugmore, A. J., and Buckland, P. C.: Tephrochronology and late Holocene soil erosion in south Iceland. In: Maizels, Judith K., Caseldine, Christopher (Eds.), Environmental Change in Iceland Past and Present. Dordrecht, the Netherlands: Kluwer, pp. 147-161, 1991.

Dugmore, A. J., and Erskine, C. C.: Local and regional patterns of soil erosion in southern Iceland, Münchener Geographische Abhandlungen, 2, 63-79, 1994.

Dugmore, A. J., Cook, G. T., Shore, J. S., Newton, A. J., Edwards, K. J., and Larsen, G.: Radiocarbon dating tephra layers from Britain and Iceland, Radiocarbon, 37, 379-388, https://doi.org/10.1017/S003382220003085X, 1995.

Eddudóttir, S. D., Erlendsson, E., and Gísladóttir, G.: Life on the periphery is tough: Vegetation in Northwest Iceland and its responses to early-Holocene warmth and later climate fluctuations, The Holocene, 25, 1437-1453, https://doi.org/10.1177/0959683615585839, 2015.

Eddudóttir, S. D., Erlendsson, E., and Gísladóttir, G.: Effects of the Hekla 4 tephra on vegetation in northwest Iceland, Vegetation History and Archaeobotany, 26, 389-402, https://doi.org/10.1007/s00334-017-0603-5, 2017.

Eddudóttir, S.D., Erlendsson, E., Gísladóttir, G.: An Icelandic terrestrial record of North Atlantic cooling c. 8800-8100 cal. yr BP, Quaternary Science Reviews, 197, 246-256, https://doi.org/10.1016/j.quascirev.2018.07.017, 2018.

Eddudóttir, S. D., Erlendsson, E., Tinganelli, L., and Gísladóttir, G.: Climate change and human impact in a sensitive ecosystem: the Holocene environment of the Northwest Icelandic highland margin, Boreas, 45, 715-728, https://doi.org/10.1111/bor.12184, 2016.

Egan, J., Allott, T. E. H., and Blackford, J. J.: Diatom-inferred aquatic impacts of the mid-Holocene eruption of Mount Mazama, Oregon, USA, Quaternary Research, 91, 163-178, https://doi.org/10.1017/qua.2018.73, 2019.

Finkel, Z. V., Matheson, K. A., Regan, K. S., and Irwin, A. J.: Genotypic and phenotypic variation in diatom silicification under paleo-oceanographic conditions, Geobiology, 8, 433–445, https://doi.org/10.1111/j.1472-4669.2010.00250.x, 2010.

Fisher, R. V., and Schmincke, H.-U.: Pyroclastic Rocks. Springer Verlag, Berlin-Heidelberg, 472 pages, 1984.

Florian, C. R.: Multi-proxy Reconstructions of Holocene Environmental Change and Catchment Biogeochemistry Using Algal Pigments and Stable Isotopes Preserved in Lake Sediment from Baffin Island and Iceland. PhD thesis, University of Colorado Boulder and University of Iceland, 2016.

Flowers, G. E., Björnsson, H., Geirsdóttir, Á., Miller, G. H., Black, J. L., and Clarke, G. K. C.: Holocene climate conditions and glacier variation in central Iceland from physical modelling and empirical evidence, Quaternary Science Reviews, 27, 797-813, https://doi.org/10.1016/j.quascirev.2007.12.004, 2008.

Gathorne-Hardy, F. J., Erlendsson, E., Langdon, P. G., and Edwards, K. J.: Lake sediment evidence for late Holocene climate change and landscape erosion in western Iceland, Journal of Paleolimnology, 42, 413-426, https://doi.org/10.1007/s10933-008-9285-4, 2009.

Geirsdóttir, Á., Harning, D. J., Miller, G. H., Andrews, J. T., Zhong, Y., and Caseldine, C.: Holocene history of landscape instability in Iceland: Can we deconvolve the impacts of climate, volcanism and human activity?, Quaternary Science Reviews, 249, 106633, https://doi.org/10.1016/j.quascirev.2020.106633, 2020.

Geirsdóttir, Á., Miller, G. H., Andrews, J. T., Harning, D. J., Anderson, L. S., Florian, C., Larsen, D. J., and Thordarson, T.: The onset of Neoglaciation in Iceland and the 4.2 ka event, Climate of the Past, 15, 25-40, https://doi.org/10.5194/cp-15-25-2019, 2019.

Geirsdóttir, Á., Miller, G. H., Harning, D. J., Hannesdóttir, H., Thordarson, T., and Jónsdóttir, I.: Evidence for recurrent outburst floods and active volcanism in Icelandic lacustrine settings during dynamic Younger Dryas-Early Holocene deglaciation, Journal of Quaternary Research, 37, 1006-1023, https://doi.org/10.1002/jqs.3344, 2022.

Geirsdóttir, Á., Miller, G. H., Larsen, D. J., and Ólafsdóttir, S.: Abrupt Holocene climate transitions in the northern North Atlantic recorded by synchronized lacustrine records in Iceland, Quaternary Science Reviews, 70, 48-62, https://doi.org/10.1016/j.quascirev.2013.03.010, 2013.

Geirsdóttir, Á., Miller, G. H., Thordarson, T., Ólafsdóttir, K. B.: A 2000 year record of climate variations reconstructed from Haukadalsvatn, West Iceland, Journal of Paleolimnology, 41, 95-115, https://doi.org/10.1007/s10933-008-9253-z, 2009.

Gerrard, J.: An assessment of some of the factors involved in recent landscape change in Iceland. In: Maizels, J. K., and Caseldine, C. (Eds.), Environmental Change in Iceland Past and Present. Dordrecht, the Netherlands: Kluwer, pp. 237-253, 1991.

Grönvold, K., Óksarsson, N., Johnsen, S.J., Clausen, H. B., Hammer, C. U., Bond, C., and Bard, E.: Ash layers from Iceland in the Greenland GRIP ice core correlated with oceanic and land sediments, Earth and Planetary Science Letters, 135, 149-155, https://doi.org/10.1016/0012-821X(95)00145-3, 1995.

Gudmundsdóttir, E. R., Larsen, G., Björck, S., Ingólfsson, Ó., and Striberger, J.: A new high-resolution Holocene tephra stratigraphy in eastern Iceland: improving the Icelandic and North Atlantic tephrochronology, Quaternary Science Reviews, 150, 234-249, https://doi.org/10.1016/j.quascirev.2016.08.011, 2016.

Gudmundsdóttir, E. R., Larsen, G., and Eiríksson, J.: Two new Icelandic tephra markers: the Hekla Ö tephra layer, 6060 cal. yr BP, and Hekla DH tephra layer, ~6650 cal. yr BP. Land-sea correlation of mid-Holocene tephra markers, The Holocene, 21, 629–639, https://doi.org/10.1177/0959683610391313, 2011.

Gudmundsdóttir, E. R., Schomacker, A., Brynjólfsson, S., Ingólfsson, Ó., and Larsen, N. K.: Holocene tephrostratigraphy in Vestfirðir, NW, Iceland, Journal of Quaternary Science, 33, 827-839, https://doi.org/10.1002/jqs.3063, 2018.

Hagstofa Íslands: Talnagrunnur, https://px.hagstofa.is/pxen/pxweb/en/, 2024.

Hallsdóttir, M.: Pollen analytical studies of human influence on vegetation in relation to the Landn?am tephra layer in southwest Iceland, Lundqua Thesis 18, 45, 1987.

Hallsdóttir, M.: On the pre-settlement history of Icelandic vegetation, Icelandic Agricultural Sciences, 9, 17-29, 1995.

Hallsdóttir, M., and Caseldine, C.J.: The Holocene vegetation history of Iceland, state-of- the-art and future. In: Caseldine, C., Russell, A., Hardardóttir, J., and Knudsen, O. (eds.) Iceland-Modern Processes and Past Environments, 5, 319, 2005.

Hanna, E., Jónsson, T., and Box, J. E.: An analysis of Icelandic climate since the nineteenth century, International Journal of Climatology, 24, 1193-1210, https://doi.org/10.1002/joc.1051, 2004.

Hannesdóttir, H., Björnsson, H., Pálsson, F., Aðalgeirsdóttir, G., and Guðmundsson, S.: Variations of southeast Vatnajökull ice cap (Iceland) 1650-1900 and reconstruction of the glacier surface geometry at the Little Ice Age maximum, Geografiska Annaler: Series A Physical Geography, 97, 237-264, https://doi.org/10.1111/geoa.12064, 2015.

Hannesdóttir, H., Sigurðsson, O., Þrastarson, R. H., Guðmundsson, S., Belart, J. M. C., Pálsson, F., Magnússon, E., Víkingsson, S., Kaldal, I., and Jóhannesson, T.: A national inventory and variations in glacier extent in Iceland from the Little Ice Age maximum to 2019, Jökull, 70, 1-34, https://doi.org/10.33799/jokull2020.70.001, 2020.

Harðarson, B. S., Fitton, J. G., and Hjartarson, Á.: Tertiary volcanism in Iceland, Jökull, 58, 161-178, http://doi.org/10.33799/jokull208.58.161, 2008.

Harning, D. J., Curtin, L., Geirsdóttir, Á., D'Andrea, W. J., Miller, G. H., and Sepúlveda, J.: Lipid biomarkers quantify Holocene summer temperature and ice cap sensitivity in Icelandic lakes, Geophysical Research Letters, 47, e2019GL085728, https://doi.org/10.1029/2019GL085728, 2020.

Harning, D. J., Geirsdóttir, Á., Miller, G. H., and Anderson, L. S.: Episodic expansion of Drangajökull, Vestfirðir, Iceland over the last 3 ka culminating in its maximum dimension during the Little Ice Age, Quaternary Science Reviews, 152, 118-131, https://doi.org/10.1016/j.quascirev.2016.10.001, 2016a.

Harning, D. J., Geirsdóttir, Á., Miller, G. H., and Zalzal, K.: Early Holocene deglaciation of Drangajökull, Vestfirðir, Iceland, Quaternary Science Reviews, 153, 192-198, https://doi.org/10.1016/j.quascirev.2016.09.030, 2016b.

Harning, D. J., Geirsdóttir, Á., Miller, G. H.: Punctuated Holocene climate of Vestfirðir, Iceland, linked to internal/external variables and oceanographic conditions, Quaternary Science Reviews, 189, 31-42, https://doi.org/10.1016/j.quascirev.2018.04.009, 2018a.

Harning, D. J., Jennings, A. E., Köseoğlu, D., Belt, S. T., Geirsdóttir, Á., and Sepúlveda, J.: Response of biological productivity to North Atlantic marine front migration during the Holocene, Climate of the Past, 17, 379-396, https://doi.org/10.5194/cp-17-379-2021, 2021.

Harning, D. J., Sacco, S., Anamthawat-Jónsson, K., Ardenghi, N., Thordarson, T., Raberg, R. H., Sepúlveda, J., Geirsdóttir, Á., Shapiro, B., Miller, G. H.: Delayed postglacial colonization of *Betula* in Iceland and the circum North Atlantic, eLife, 12, 1-23, https://doi.org/10.7554/eLife.87749.3, 2023.

Harning, D. J., Thordarson, T., Geirsdóttir, Á., Miller, G. H., and Florian, C. R.: Repeated Early Holocene eruptions of Katla, Iceland, limit the temporal resolution of the Vedde Ash, Bulletin of Volcanology, 86, 2, https://doi.org/10.1007/s00445-023-01690-9, 2024.

Harning, D. J., Thordarson, T., Geirsdóttir, Á., Miller, G. H., and Ólafsdóttir, S.: Marker tephra in Haukadalsvatn lake sediment: A key to the Holocene tephra stratigraphy of Northwest Iceland, Quaternary Science Reviews, 219, 154-170, https://doi.org/10.1016/j.quascirev.2019.07.019, 2019.

Harning, D. J., Thordarson, T., Geirsdóttir, Á., and Zalzal, K.: Provenance, stratigraphy and chronology of Holocene tephra from Vestfirðir, Iceland, Quaternary Geochronology, 46, 59-76, https://doi.org/10.1016/j.quageo.2018.03.007, 2018b.

Holmes, N., Langdon, P. G., Caseldine, C. J., Wastegård, S., Leng, M. J., Croudace, I. W., and Davies, S. M.: Climatic variability during the last millennium in Western Iceland from lake sediment records, The Holocene, 26, 756–771, https://doi.org/10.1177/0959683615618260, 2016.

Janebo, M. H., Thordarson, T., Houghton, B. F., Bonadonna, C., Larsen, G., and Carey, R. J.: Dispersal of key subplinian-Plinian tephras from Hekla volcano, Iceland: implications for eruption source parameters, Bulletin of Volcanology, 78, 1-16, https://doi.org/10.1007/s00445-016-1059-7, 2016.

Jennings, A. E., Andrews, J. T., Pearce, C., Wilson, L., Ólafsdóttir, S.: Detrital carbonate peaks on the Labrador shelf, a 13-7 ka template for freshwater forcing from the Hudson Strait outlet of the Laurentide Ice Sheet into the subpolar gyre, Quaternary Science Reviews, 107, 62-80, https://doi.org/10.1016/j.quascirev.2014.10.022, 2015.

Jennings, A. E., Thordarson, T., Zalzal, K., Stoner, J., Hayward, C., Geirsdóttir, Á., and Miller, G. H.: Holocene tephra from Iceland and Alaska in SE Greenland Shelf Sediments. In: Austin, W.E.N., Abbott, P.M., Davies, S.M., Pearce, N.J.G., and Wastegård, S. (eds) *Marine Tephrochronology*. Geological Society, London, Special Publications, 398, 2014.

Jóhannsdóttir, G. E.: Mid-Holocene to late glacial tephrochronology in west Iceland as revealed in three lacustrine environments. MS thesis, University of Iceland, 2007.

Kluger, M. O., Lowe, D. J., Moon, V. G., Chaneva, J., Johnston, R., Villamor, P., Ilanko, T., Melchert, R. A., Orense, R. P., Loame, R. C., and Ross, N.: Seismically-induced down-saggin structures in tephra layers (tephra-seismites) preserved in lakes since 17.5 cal ka, Hamilton lowlands, New Zealand, Sedimentary Geology, 445, 106327, https://doi.org/10.1016/j.sedgeo.2022.106327, 2023.

Kristjánsdóttir, G. B., Moros, M., Andrews, J. T., and Jennings, A. E.: Holocene Mg/Ca, alkenones, and light stable isotope measurements on the outer North Iceland shelf (MD99–2269): A comparison with other multi-proxy data and sub-division of the Holocene, The Holocene, 26, 55–62, https://doi.org/10.1177/0959683616652703, 2017.

Kristjánsdóttir, G. B., Stoner, J. S., Jennings, A. E., Andrews, J. T., and Grönvold, K.: Geochemistry of Holocene cryptotephras from the North Iceland Shelf (MD99-2269): intercalibration with radiocarbon and palaeomagnetic chronostratigraphies, The Holocene 17, 155-176, https://doi.org/10.1177/0959683607075829, 2007.

Lacasse, C.: Influence of climate variability on the atmospheric transport of Icelandic tephra in the subpolar North Atlantic, Global Planetary Change, 29, 31-55, https://doi.org/10.1016/S0921-8181(01)00099-6, 2001.

Langdon, P. G., and Barber, K. E.: New Holocene tephras and a proxy climate record from a blanket mire in northern Skye, Scotland, Journal of Quaternary Science, 16, 753-759, https://doi.org/10.1002/jqs.655, 2001.

Langdon, P. G., Leng, M. J., Holmes, N., and Caseldine, C. J.: Lacustrine evidence of early-Holocene environmental change in northern Iceland: a multiproxy palaeoecology and stable isotope study, The Holocene, 20, 205-214, https://doi.org/10.1177/0959683609354301, 2010.

Larsen, D. J., Miller, G. H., Geirsdóttir, Á., and Ólafsdóttir, S.: Non-linear Holocene climate evolution in the North Atlantic: a high-resolution, multi-proxy record of glacier activity and environmental change from Hvítárvatn, central Iceland, Quaternary Science Reviews, 39, 14-25, https://doi.org/10.1016/j.quascirev.2012.02.006, 2012.

Larsen, D. J., Miller, G. H., Geirsdóttir, Á., and Thordarson, T.: A 3000-year varved recoed of glacier activity and climate change form the proglacial lake Hvítárvatn, Iceland, Quaternary Science Reviews, 30, 2715-2731, https://doi.org/10.1016/j.quascirev.2011.05.026, 2011.

Larsen, G.: Gjóskulagid úr Heklugosinu 1158 (The tephra layer from the 1158 AD eruption of Hekla). Jardfrædafélag Islands, Vorrádstefna, Yfirlit og Ágrip. Geoscience Society of Iceland, Reykjavík: 25–27, 1992.

Larsen, G., Dugmore, A. J., and Newton, A. J.: Geochemistry of historical-age silicic tephras in Iceland, The Holocene, 9, 463-471, https://doi.org/10.1191/095968399669624108, 1999.

Larsen, G., and Eiríksson, J.: Holocene tephra archives and tephrochronology in Iceland – a brief overview, Jökull, 58, 229-250, http://doi.org/10.33799/jokull2008.58.229, 2008.

Larsen, G., Eiríksson, J., Knudsen, K. L., and Heinemeier, J.: Correlation of late Holocene terrestrial and marine tephra markers, north Iceland: implications for reservoir age changes, Polar Research, 21, 283-290, https://doi.org/10.3402/polar.v21i2.6489, 2002.

Larsen, G., Newton, A. J., Dugmore, A. J., Vilmundardóttir, E. G.: Geochemistry, dispersal, volumes and chronology of Holocene silicic tephra layers from the Katla volcanic system, Iceland, Journal of Quaternary Science, 16, 119-132, https://doi.org/10.1002/jqs.587, 2001.

Larsen, G., Róbertsdóttir, B. G., Óladóttir, B. A., and Eiríksson, J.: A shift in eruption mode of Hekla volcano, Iceland, 3000 years ago: two-coloured Hekla tephra series, characteristics, dispersal and age, Journal of Quaternary Science, 35, 143-154, https://doi.org/10.1002/jqs.3164, 2020.

Larsen, G., and Thórarinsson, S.: H-4 and other acid Hekla tephra layers, Jökull, 27, 27-46, 1977.

Lavaud, J., Rousseau, B., van Gorkom, H. J., and Etienne, A.-L: Influence of the diadinoxanthin pool size on photoprotection in the marine planktonic diatom *Phaeodactylum tricornutum*, Plant Physiology, 129, 1398–1406, https://doi.org/10.1104/pp.002014, 2002.

Lawson, I. T., Gathorne-Hardy, F. J., Church, M. J., Newton, A. J., Edwards, K. J., Dugmore, A. J., and Einarsson, Á.: Environmental impacts of the Norse settlement: Palaeoenvironmental data from Mývatnssveit, northern Iceland, Boreas, 36,1–19, https://doi.org/10.1111/j.1502-3885.2007.tb01176.x, 2007.

Lawson, I. T., Swindles, G. T., Plunkett, G., and Greenberg, D.: The spatial distribution of Holocene cryptotephras in north-west Europe since 7 ka: implications for understanding ash fall events from Icelandic eruptions, Quaternary Science Reviews, 41, 57-66l, https://doi.org/10.1016/j.quascirev.2012.02.018, 2012.

Leavitt, P. R., and Hodgson, D. A.: Sedimentary pigments. In: Smol, J. P., H. J. B. Birks and W. M. Last (eds.), Tracking Environmental Change using Lake Sediments. Volume 3: Terrestrial, Algal and Siliceous Indicators. Kluwer Academic Publishers, Dordrecht. The Netherlands, 295-325, 2001.

Lowe, D. J.: Tephrochronology and its application: A review, Quaternary Geochronology, 6, 107-153, https://doi.org/10.1016/j.quageo.2010.08.003, 2011.

Mangerud, J., Furnes, H., and Jóhansen, J.: A 9000-year-old ash bed on the Faroe Islands, Quaternary Research, 26, 262-265, https://doi.org/10.1016/0033-5894(86)90109-2, 1986.

Mangerud, J., Lie, S.E., Furnes, H., Kristiansen, I. L., and Lømo, L.: A Younger Dryas Ash bed in Western Norway, and its possible correlations with tephra in cores from the Norwegian Sea and the North Atlantic, Quaternary Research, 21, 85-104, https://doi.org/10.1016/0033-5894(84)90092-9, 1984.

Marshall, J., Kushnir, Y., Battisti, D., Chang, P., Czaja, A., Dickson, R., Hurrell, J., McCartney, M., Saravanan, R., and Visbeck, M.: North Atlantic climate variability: phenomena, impacts and mechanisms, International Journal of Climatology, 21, 1863-1898, https://doi.org/10.1002/joc.693, 2001.

McMurdie, P. J., and Holmes, S.: phyloseq: An R package for reproducible interactive analysis and graphics of microbiome census data, PLoS ONE 8, e61217, http://dx.plos.org/10.1371/journal.pone.0061217, 2013.

Möckel, S. C., Erlendsson, E., Prater, I., and Gísladóttir, G.: Tephra deposits and carbon dynamics in peatlands of a volcanic region – lessons from the Hekla 4 eruption, Land Degradation and Development, 32, 654-669, https://doi.org/10.1002/ldr.3733, 2021.

Moossen, H., Bendle, J., Seki, O., Quillmann, U., and Kawamura, K.: North Atlantic Holocene climate evolution recorded by high-resolution terrestrial and marine biomarker records, Quaternary Science Reviews, 129, 111–127, https://doi.org/10.1016/j.quascirev.2015.10.013, 2015.

Óladóttir, B. A., Larsen, G., Thordarson, T., and Sigmarsson, O: The Katla volcano S-Iceland: Holocene tephra stratigraphy and eruption frequency, Jökull, 55, 53-74, http://doi.org/10.33799/jokull2005.55.053, 2005.

Óladóttir, B. A., Thordarson, T., Larsen, G., and Sigmarsson, O.: Survival of the Mýrdalsjökull ice cap through the Holocene thermal maximum: evidence from sulfur contents in Katla tephra layers (Iceland) from the last ~8400 years, Annals of Glaciology, 45, 183-188, https://doi.org/10.3189/172756407782282516, 2007.

Óladóttir, B. A., Larsen, G., and Sigmarsson, O.: Holocene volcanic activity at Grímsvötn, Bárdarbunga and Kverkfjöll subglacial centres beneath Vatnajökull, Iceland, Bulletin of Volcanology, 73, 1187-1208, https://doi.org/10.1007/s00445-011-0461-4, 2011.

Óladóttir, B. A., Thordarson, T., Geirsdóttir, Á., Jóhannsdóttir, G. E., and Mangerud, J.: The Saksunarvatn Ash and the G10ka series tephra. Review and current state of knowledge, Quaternary Geochronology, 56, 101041, https://doi.org/10.1016/j.quageo.2019.101041, 2020.

Ólafsdóttir, S., Geirsdóttir, Á., Miller, G. H., Stoner, J. S., and Channell, J. E. T.: Synchronizing Holocene lacustrine and marine sediment records using paleomagnetic secular variation, Geology, 41, 535-538, https://doi.org/10.1130/G33946.1, 2013.

Paerl, H. W., and Paul, V. J.: Climate change: Links to global expansion of harmful cyanobacteria, Water Research, 46, 1349-1363, https://doi.org/10.1016/j.watres.2011.08.002, 2012.

Patton, H., Hubbard, A., Bradwell, T., and Schomacker, A.: The configuration, sensitivity and rapid retreat of the Late Weichselian Icelandic ice sheet, Earth-Science Reviews, 166, 223-245, https://doi.org/10.1016/j.earscirev.2017.02.001, 2017.

Pilcher, J. R., Hall, V. A., and McCormac, F. G.: Dates of Holocene Icelandic volcanic eruptions from tephra layers in Irish peats, The Holocene, 5, 103-110, https://doi.org/10.1177/095968369500500111, 1995.

Pilcher, J. R., Hall, V. A., and McCormac, F. G.: An outline tephrochronology for the Holocene of the north of Ireland, Journal of Quaternary Science, 11, 485-494, https://doi.org/10.1002/(SICI)1099-1417(199611/12)11:6<485::AID-JQS266>3.0.CO;2-T, 1996.

Quillmann, U., Marchitto, T. M., Jennings, A. E., Andrews, J. T., and Friestad, B. F.: Cooling and freshening at 8.2 ka on the NW Iceland Shelf recorded in paired δ ^{18}O and Mg/Ca measurements of the benthic foraminifer *Cibicides lobatulus*, Quaternary Research, 78, 528-539, https://doi.org/10.1016/j.yqres.2012.08.003, 2012.

Rasmussen, S. O., Andersen, K. K., Svensson, A. M., Steffensen, J. P., Vinther, B. M., Clausen, H. B., Siggaard-Andersen, M.-L., Johnsen, S. J., Larsen, L. B., Dahl-Jensen, D., Bigler, M., Röthlisberger, R., Fischer, H., Goto-Azuma, K., Hansson, M. E., and Ruth, U.: A new Greenland ice core chronology for the last glacial termination, Journal of Geophysical Research, 111, 1-16, https://doi.org/10.1029/2005JD006079, 2006.

R Core Team: R: A language and environment for statistical computing. Vienna, Austria: R Foundation for Statistical Computing, https://www.R-project.org/, 2021.

Reimer, P. J., Austin, W. E. N., Bard, E., Bayliss, A., Blackwell, P. G., Bronk Ramsey, C., Butzin, M., Cheng, H., Edwards, R. L., Friedrich, M., Grootes, P. M., Guilderson, T. P., Hajdas, I., Heaton, T. J., Hogg, A. G., Hughen, K. A., Kromer, B., Manning, S. W., Muscheler, R., Palmer, J. G., Pearson, C., van der Plicht, J., Reimer, R. W., Richards, D. A., Scott, E. M., Southon, J. R., Turney, C. S. M., Wacker, L., Adolphi, F., Büntgen, U., Capano, M., Fahrni, S. M., Fogtmann-Schulz, A., Friedrich, R., Köhler, P., Kudsk, S., Miyake, F., Olsen, J., Reinig, F., Sakamoto, M., Sookdeo, A., and Talamo, S.: The IntCal20 northern hemisphere radiocarbon age calibration curve (0-55 cal kBP), Radiocarbon, 62, 725-757, https://doi.org/10.1017/RDC.2020.41, 2020.

Richter, N., Russell, J. M., Garfinkel, J., and Huang, Y.: Winter-spring warming in the North Atlantic during the last 2000 years: evidence from southwest Iceland, Climate of the Past, 17, 1363-1383, https://doi.org/10.5194/cp-17-1363-2021, 2020.

Rohling, E. J., and Pälike, H.: Centennial-scale climate cooling with a sudden cold event around 8,200 years ago, Nature, 434, 975-979, https://doi.org/10.1038/nature03421, 2005.

Rousseau, V., Leynaert, A., Daoud, N., and Lancelot, C.: Diatom succession, silicification and silicic acid availability in Belgian coastal waters (Southern North Sea), Marine Ecology Progress Series, 236, 61–73, http://doi.org/meps236061, 2002.

Rundgren, M.: Biostratigraphic evidence of the Allerød-Younger Dryas-Preboreal Oscillation in Northern Iceland, Quaternary Research, 44, 405-416, https://doi.org/10.1006/qres.1995.1085, 1995.

Rundgren, M.: Early Holocene vegetation of northern Iceland: pollen and plant macrofossil evidence from the Skagi peninsula, The Holocene, 5, 553-564, https://doi.org/10.1191/095968398669995117, 1998.

Rundgren, M., and Ingólfsson, Ó.: Plant survival in Iceland during periods of glaciation?, Journal of Biogeography, 26, 387-396, https://doi.org/10.1046/j.1365-2699.1999.00296.x, 1999.

Rundgren, M., Ingólfsson, Ó., Björck, S., Jiang, H., and Haflidason, H.: Dynamic sea-level change during the last deglaciation of northern Iceland, Boreas, 26, 201-215, https://doi.org/10.1111/j.1502-3885.1997.tb00852.x, 1997.

Simkin, A. J., Kapoor, L., Doss, C. G. P., Hofmann, T. A., Lawson, T., and Ramamoorthy, S.: The role of photosynthesis related pigments in light harvesting, photoprotection and enhancment of photosynthetic yield in planta, Photosynthesis Research, 152, 23-42, https://doi.org/10.1007/s11120-021-00892-6, 2022.

Smith, K. P.: Landnam: The settlement of Iceland in archaeological and historical perspective, World Archaeology, 26, 319-347, https://doi.org/10.1080/00438243.1995.9980280, 1995.

Smith, V. H.: Nutrient dependence of primary productivity in lakes, Limnology and Oceanography, 24, 1051–1064, https://doi.org/10.4319/lo.1979.24.6.1051, 1979.

Smol, J. P., and Cumming, B. F.: Tracking long-term changes in climate using algal indicators in lake sediments, Journal of Phycology, 1011, 986–1011, https://doi.org/10.1046/j.1529-8817.2000.00049.x, 2000.

Stoner, J. S., Channell, J. E. T., Mazaud, A., Strano, S. E., Xuan, C.: The influence of high-latitude flux lobes on the Holocene paleomagnetic record of IODP Site U1305 and the northern North Atlantic, Geochemistry, Geophysics, Geosystems, 14, 4623-4646, https://doi.org/10.1002/ggge.20272, 2013.

Stoner, J. S., Jennings, A., Kristjánsdóttir, G. B., Dunhill, G., Andrews, J. T., and Hardardóttir, J.: A paleomagnetic approach toward refining Holocene radiocarbon-based chronologies: Paleoceanographic records from the north Iceland (MD99-2269) and east Greenland (MD99-2322) margins, Paleoceanography, 22, 1-23, https://doi.org/10.1029/2006PA001285, 2007.

Storm, G.: Annales Reseniani. Islandske Annaler: indtil 1578. Kristjanía: Norsk historisk kildeskriftfond, 27, 1977a.

Storm, G.: Flatbøgens Annaler Islandske Annaler: indtil 1578. Kristjanía: Norsk historisk kildeskriftfond, 534, 1977b.

Storm, G.: Skálholts-Annaler Islandske Annaler: indtil 1578. Kristjanía: Norsk historisk kildeskriftfond, 193, 1977c.

Stramski, D., Sciandra, A., and Claustre, H.: Effects of temperature, nitrogen, and light limitation on the optical properties of the marine diatom *Thalassiosira pseudonana*, Limnology and Oceanography, 47, 392–403, https://doi.org/10.4319/lo.2002.47.2.0392, 2002.

Streeter, R., Dugmore, A. J., Lawson, I. T., Erlendsson, E., and Edwards, K. J.: The onset of the palaeoanthropocene in Iceland: changes in complex natural systems, The Holocene, 25, 1662-1675, https://doi.org/10.1177/0959683615594468, 2015.

Striberger, J., Björck, S., Holmgren, S., and Hamerlík, L.: The sediments of Lake Lögurinn e a unique proxy record of Holocene glacial meltwater variability in eastern Iceland, Quaternary Science Reviews 38, 76-88, https://doi.org/10.1016/j.quascirev.2012.02.001, 2012.

Skrzypek, G., Paul, D., and Wojtun, B.: Stable isotope composition of plants and peat from Arctic mire and geothermal area in Iceland, Polar Research, 29, 365-376, 2008.

Telford, R. J., Barker, P., Metcalfe, S., and Newton, A.: Lacustrine responses to tephra deposition: examples from Mexico, Quaternary Science Reviews, 23, 23-24, https://doi.org/10.1016/j.quascirev.2004.03.014, 2004.

Thórarinsson, S.: Tefrokronoliska studier pa Island (Tephrochronological studies in Iceland), Geogr. Ann. 26, 1-217, 1944.

Tierney, J. E., Poulsen, C. J., Montañez, I. P., Bhattacharya, T., Feng, R., Ford, H. L., Hönisch, B., Inglis, G. N., Petersen, S. V., Sagoo, N., Tabor, C. R., Thirumalai, K., Zhu, J., Burls, N. J., Foster, G. L., Goddéris, Y., Huber, B. T., Ivany, L. C., Turner, S. K., Lunt, D. J., McElwain, J. C., Mills, B. J. W., Otto-Bliesner, B. L., Ridgwell, A., and Zhang, Y. G.: Past climates inform our future, Science, 370, 680, http://doi.org/10.1126/science.aay3701, 2020.

Thórarinsson, S.: Tefrokronoliska studier pa Island (Tephrochronological studies in Iceland), Geografiska Annaler, 26, 1–217, 1944.

Thórarinsson, S.: Uppblástur á Íslandi í ljósi öskulaga-rannsókna, Ársrit Skógræktarfélag Íslands, Reykjavík, 17-54, 1961.

Deleted: Sveinbjörnsdóttir, Á. E., Heinemeier, J., Kristensen, P., Rud, N., Geirsdóttir, Á., and Harðardóttir, J.: 14C AMS dating of Icelandic lake sediments, Radiocarbon, 40, 865-872, https://doi.org/10.1017/S003382220001883X, 1998.¶

Thórarinsson, S.: The eruptions of Hekla in historical times: a tephrochronological study. In: Einarsson, T., Kjartansson, G., Thorarinsson, S. (eds) *The eruption of Hekla 1947-1948*. Societas Scientiarum Islandica, Reykjavik, 1-177, 1967.

Thordarson, T., and Larsen, G.: Volcanism in Iceland in historical time: volcano types, eruption styles and eruptive history, Journal of Geodynamics, 43, 118–152, https://doi.org/10.1016/j.jog.2006.09.005, 2007.

Thordarson, T., and Höskuldsson, Á.: Postglacial volcanism in Iceland, Jökull, 58, 197-228, http://doi.org/10.33799/jokull2008.58.197, 2008.

Thordarson, T., Self, S., Óskarsson, N., and Hulsebosch, T.: Sulphur, chlorine, and fluorine degassing and atmospheric loading by the 1783-1784 AD Laki (Skaftár Fires) eruption in Iceland, Bulletin of Volcanology, 58, 205-225, http://doi.org/10.1007/s004450050136, 1996.

Timms, R. G. O., Matthews, I. P., Palmer, A. P., and Candy, I.: Toward a tephrostratigraphic framework for the British Isles: A Last Glacial to Interglacial Transition (LGIT c. 16-8 ka) case study from Crudale Meadow, Orkney, Quaternary Geochronology, 46, 28-44, https://doi.org/10.1016/j.quageo.2018.03.008, 2018.

Timms, R. G. O., Matthews, I. P., Palmer, A. P., Candy, I., and Abel, L.: A high-resolution tephrostratigraphy from Quoyloo Meadow, Orkney, Scotland: Implications for the tephrostratigraphy of NW Europe during the Last Glacial-Interglacial Transition, Quaternary Geochronology, 40, 67-81, https://doi.org/10.1016/j.quageo.2016.06.004, 2017.

Tinganelli, L., Erlendsson, E., Eddudóttir, S. D., and Gísladóttir, G.: Impacts of climate, tephra, and land use upon Holocene landscape stability in Northwest Iceland, Geomorphology, 322, 117-131, https://doi.org/10.1016/j.geomorph.2018.08.025, 2018.

van den Bogaard, C., Dorfler, W., Sandgren, P., and Schmincke, H.-U.: Correlating the Holocene records: Icelandic Tephra found in Schleswig-Holstein (Northern Germany), Naturwissenschaften, 81, 554-556, https://doi.org/10.1007/BF01140005, 1994.

van den Bogaard, C., Dorfler, W., Glos, R., Nadeau, M.-J., Grootes, P. M., and Erlenkeuser, H.: Two tephra layers bracketing late Holocene paleoecological changes in northern Germany, Quaternary Research, 57, 314-324, https://doi.org/10.1006/qres.2002.2325, 2002.

Vésteinsson, O., and McGovern, T.: The peopling of Iceland, Norwegian Archaeological Review, 45, 206-218, https://doi.org/10.1080/00293652.2012.721792, 2012.

Vogel, H., Rósen, P., Wagner, B., Melles, M., and Persson, P.: Fourier transform infrared spectroscopy, a new cost-effective tool for quantitative analysis of biogeochemical properties in long sediment records, Journal of Paleolimnology, 40, 689-702, https://doi.org/10.1007/s10933-008-9193-7, 2008.

Walker, G. P. L., and Croasdale, R.: Characteristics of some basaltic pyroclasts, Bulletin of Volcanology, 35, 303-317, https://doi.org/10.1007/BF02596957, 1972.

Wang, Y., and Wooller, M.: The stable isotopic (C and N) composition of modern plants and lichens from northern Iceland: with ecological and paleoenvironmental implications, Jökull, 56, 27-38, http:doi.org/10.33799/jokull2006.56.027, 2006.

Wastegård, S., Björck, S., Grauert, M., and Hannon, G. E.: The Mjáuvøtn tephra and other Holocene tephra horizons from the Faroe Islands: a link between the Icelandic source region, the Nordic Seas, and the European continent, The Holocene, 11, 101-109, https://doi.org/10.1191/095968301668079904, 2001.

Wastegård, S., Rundgren, M., Schoning, K., Andersson, S., Björck, S., Borgmark, A., and Possnert, G.: Age, geochemistry and distribution of the mid-Holocene Hekla-S/Kebister tephra, The Holocene, 18, 539-549, https://doi.org/10.1177/0959683608089208, 2008.

Wastegård, S., Gudmundsdóttir, E. R., Lind, E. M., Timms, R. G. O., Björck, S., Hannon, G. E., Olsen, J., and Rundgren, M.: Towards a Holocene tephrochronology for the Faroe Islands, North Atlantic, Quaternary Science Reviews, 195, 195-214, https://doi.org/10.1016/j.quascirev.2018.07.024, 2018.

Wunsch, C.: Meridional heat flux of the north Atlantic Ocean, Proceedings of the National Academy of Sciences, 77, 5043-5047, https://doi.org/10.1073/pnas.77.9.5043, 1980.

Xiao, X., Zhao, M., Knudsen, K.L., Sha, L., Eiríksson, J., Gudmundsdóttir, E., Jiang, H., and Guo, Z.: Deglacial and Holocene sea-ice variability north of Iceland and response to ocean circulation changes, Earth and Planetary Science Letters, 472, 14-24, https://doi.org/10.1016/j.epsl.2017.05.006, 2017.

Page 16: [1] Deleted **David John Harning** **6/21/24 3:59:00 PM**

Supporting Information for

High-resolution Holocene record based on detailed tephrochronology from Torfdalsvatn, north Iceland, reveals natural and anthropogenic impacts on terrestrial and aquatic environments

David J. Harning[1,2], Christopher R. Florian[1,2,3], Áslaug Geirsdóttir[2], Thor Thordarson[2], Gifford H. Miller[1], Yarrow Axford[4], Sædís Ólafsdóttir[5]

[1] Institute of Arctic and Alpine Research, University of Colorado, Boulder, CO
[2] Faculty of Earth Sciences, University of Iceland, Reykjavík, Iceland
[3] National Ecological Observatory Network, Battelle, Boulder, CO
[4] Department of Earth and Planetary Sciences, Northwestern University, Evanston, IL
[5] Reykjavík Energy, Bæjarháls 1, 110 Reykavík

Please see the Supporting Data (SD) for accompanying tables (SDT#) and figures (SDF#) referred to in this text.

SDT1: Tephra compositional data from sediment cores 2012NC (this study), 2012BC (Harning et al., 2024) and 2004NC (this study).

SDT2: Number and frequency of eruptive events in Torfdalsvatn as recorded by tephra layer composition.

SDT3: Bulk geochemical and algal pigment proxy data.

Deleted: ¶

1. *Tephra layers descriptions*

Hekla 1766 (12-TORF-1A-15): At 15 cm depth in 2012NC is a 0.1-cm thick layer of greyish black fine to medium ash, with diverse tephra grains in their attribute and chemical composition. The characteristic grain types are icelandite and rhyolite pumices and shards with minor abundance of basaltic grains (SDT1). Of the 86 grains analyzed, 76 grains (88%) have composition conforming with origin from the Hekla volcanic system (SDT1 and SDF1). This grain population ranges from alkali basalt (*n*=5, 6%) to icelandite (*n*=38, 44%) to rhyolite (*n*=33, 38%), where the latter two compositions dominate the population.

The intermediate Hekla population defines a tight compositional cluster, and on some elemental plots defines two distinct clusters that best match tephra composition from the Hekla 1766 eruption (SDF1). Other icelandite historic Hekla tephra layers, such as Hekla 1206, 1510, 1597, 1845 and 1947, can be ruled out as a source based on their southerly tephra dispersal (Thorarinsson, 1958). Others can be eliminated based on their chemical composition, namely the basaltic icelandite tephras from the Hekla 1970, 1980, 1991 and 2000 events and the dacite of Hekla 1300 and 1158 (SDF1). The tephra from the Hekla 1693 eruption has similar dispersal and composition (e.g., Thorarinsson, 1967; Janebo et al., 2016). However, the 12-TORF-1A-15 icelandite component exhibits a better fit to Hekla 1766 (SDF1). This is one of the larger intermediate Hekla eruption in historical time (VEI 4) that featured an explosive sub-Plinian phase that lasted for 5 to 6 hours on 5 April 1766 CE (Thorarinsson, 1967) with a northward tephra dispersal in the direction of Torfdalsvatn (Janebo et al., 2016).

The rhyolite component, not present in the reference data set obtained from proximal to medial lapilli size Hekla 1766 tephra samples (Harning et al., 2018, 2019), is comprised of two distinct compositional populations. The more abundant low silica population has composition that resembles Hekla 1104 tephra deposits. The high silica population is a minor component and has composition similar to Hekla 4 tephra deposits (SDF1). It is difficult to reconcile that the rhyolitic component is derived from local reworking of Hekla 4 and Hekla 1104 Hekla tephra layers via erosion of the soil cover around Torfdalsvatn, because 1) these compositional groups are in different proportions (0.15 vs 0.85) while the thickness of the layers is roughly the same in local soil sections (Möckel et al., 2021), and 2) of the pristine nature of the grains. It is more likely that this component originated at the source vents. The distance from Hekla to Torfdalsvatn is just over 230 km and the thickness of the 12-TORF-1A-15 tephra layer in the lake is 0.1 cm, matching well with the mapped isopach thickness (Janebo et al., 2016). Consequently, it is logical to assume that tephra from only the most intense initial explosive phase reached Torfdalsvatn. In this regard, it is important to note that 1) the eruption's climax is reached at the very beginning and then intensity drops off rapidly (e.g., Thordarson and Larsen, 2007), and 2) the magma erupted in silicic and intermediate Hekla eruptions are typically compositionally zoned, spanning the felsic realm with the most silicic component erupted first (e.g., Sigmarsson et al., 1992; Sverrisdóttir, 2007; Meara et al., 2020). Alternatively, it may represent Hekla 1104 and Hekla 4 tephra incorporated into the erupting mixture as the magma was opening its path towards the surface at the beginning of the eruption. In any case, we interpret this tephra to be a previously undocumented rhyolitic component of the Hekla 1766 eruption.

The remaining ten grains exhibit tholeiite basalt compositions consistent with the Grímsvötn (n=8, 9%) and possibly Askja volcanic systems (n=2, 2%; SDF1) and may represent tephra produced by eruptions at these volcanic centers in this timeframe.

Hekla 1300 (12-TORF-1A-66): At 66 cm depth in 2012NC is a 0.1-cm thick, greyish white tephra of fine to medium ash. Tephra grains feature diverse attributes and chemical compositions, although the characteristic grain types are rhyolite pumices, with minor abundances of intermediate and basaltic grains (SDT1). Of the 69 grains analyzed, 43 grains (62%) are silicic, where 40 (58%) have Hekla affinities; 38 (55%) are low-silica rhyolite and two are high-silica rhyolite (SDF2). The low silica component falls within the rhyolite compositional fields for Hekla 1104 and Hekla 1300 and the high silica components matches well with the high-silica tail of the Hekla 1300 field (SDF2). The high-silica rhyolite has Hekla 4-like composition. Three rhyolite grains have a mildly alkalic compositions with affinities towards the Katla system, except they feature much higher TiO_2 content (SDF2). Components of Hekla 1300 dacite (n=3), icelandite (n=3) and alkali basalt (n=3) are also present. The remaining 17 grains are of tholeiite basalt compositions, where 13 grains have Grímsvötn (n=13) and 4 grains have Veiðivötn-Bárðarbunga system compositions (SDF2). As the western side of the 0.1 cm isopach of the Hekla 1300 tephra layer is just south of Torfdalsvatn (Thorarinsson, 1967; Janebo et al., 2016), it is likely that only the most evolved tephra from the most intense part of the initial explosive phase from this eruption reached the lake. Hence, the 12-TORF-1A-66 tephra layer is taken here to represent the Hekla 1300 event. In addition, the tholeiite basalt component may represent tephra from roughly concurrent eruptions within the Grímsvötn and Veiðivötn-Bárðarbunga volcanic systems, as several such events are known to have taken place within ± 70 years of 1300 CE (e.g., Óladóttir et al., 2011).

Hekla 1104 (04-TORF-01, A-1, 90-92, 102-103; 12-TORF-2A-1N-01A-80,5, 84.4): This is a greyish white tephra, which is present in 2004NC over 15.4 cm interval (88.1 to 103.5 cm depth) as three distinct and separate layers/wedges connected by mm-thick, irregular light-colored stringers (Fig. S1). In 2012NC it is present as two distinct layers at depths of 80.5 cm (0.1 cm) and 84.5 cm (0.7 cm). This tephra layer is found in a previously published record from Torfdalsvatn (Alsos et al., 2021), where the stratigraphy is also discontinuous with stringers below and above the main tephra layer horizon (Bender, 2020). The chemical composition of these tephra horizons is identical in all instances, even in the minor components (STD1 and SDF3). Hence, we take this to represent a single layer, which was subsequently deformed to produce the observed features (see main text Section 4.2.3 for Discussion). As a result, we do not explicitly include this tephra layer in the age model.

This horizon is dominantly comprised of rhyolite tephra grains, with minor icelandite and alkalic basalt tephra grains that are mixed with juvenile crystals and minor lithics (SPF3). Of the 222 grains analyzed, 168 (74%) are of rhyolite pumices that not only have affinities to the Hekla volcanic system but also match the composition of the rhyolitic component of Hekla 1104 (SPF3). A total of 14 grains (6%) feature intermediate and 21 grains (9%) have alkali basalt composition consistent with the Hekla volcanic system (SPF3). These compositional results, along with the mapped dispersal thickness (Thorarinsson, 1967; Janebo et al., 2016), strongly suggest that this tephra represents fallout from the largest historical Hekla eruption, Hekla 1104 (VEI 4-5, e.g., Larsen et al., 1999). The residual sulfur in the degassed rhyolite tephra population (SDT1) indicates extended degassing upon eruption, consistent with the notion that Hekla 1104 was a dry magmatic Plinian eruption (e.g., Janebo et al., 2016). Conversely, the residual sulfur in the degassed alkali basalt component of the tephra (SDT1) indicates about 60% degassing during the eruption, suggesting involvement of external water in the explosive activity that produced the basalt tephra (e.g., Thordarson et al., 2001). The remaining 22 grains are tholeiitic basalt of the Grímsvötn (n=10) and Veiðivötn-Barðárbunga (n=12) volcanic systems (SPF3).

C-990 (12-TORF-1A-104, mix of tephra layers): The sample at 104 cm depth in 2012NC is a cryptotephra and has a modeled age of 990 ± 80 cal a BP (960 CE). Of the 46 grains analyzed, 12 (28%) are tholeiitic basalt with composition indicating origin within the Veiðivötn-Barðárbunga volcanic system, whereas 15 (37%) are tholeiite basalt of the Grímsvötn volcanic system (SDF4). In addition, there are 5 (11%) alkalic basalt grains of the Katla volcanic system, matching best with the Eldgjá 934-9 CE compositional field. Grains of rhyolite composition are 10 (24%) and are identical to that of Hekla 1104 (SDT1 and SDF4). This grain population represents an evenly weighted mixture of tephra layers from four different volcanic systems. Hence, we interpret this to be a mixture of tephra layers from the period around 960 CE. As this horizon includes Hekla 1104 grains, it is possible that the mixing event that produced it is related to the event that broke up the Hekla 1104 tephra layer.

C-1180 (12-TORF-1B-9, *mix of tephra layers):* The sample at 125 cm depth in 2012NC is a cryptotephra and has a modeled age of 1180 ± 70 cal a BP (770 CE). Of the 37 grains analyzed, 20 (54%) exhibit alkalic basalt compositions consistent with the Katla volcanic system, whereas 15 (41%) exhibit tholeiitic basalt compositions consistent with Grímsvötn volcanic system (SDT1 and SDF5). In addition, there are two rhyolitic pumice grains with composition matching the Hekla 4 marker tephra layer, but likely reflect reworked material due to their low abundance. The dominant basaltic composition suggests that this horizon is comprised of tephra fallout from two separate eruptions originating from the Grímsvötn and Katla volcanic systems around 1180 cal a BP. Similar to C-990, it is possible that it was disturbed during the unknown event that broke up the Hekla 1104 tephra layer.

Katla 1220 (12-TORF-1B-15): A 1-cm thick, black layer of fine to medium ash with diffuse upper and lower contacts is located at 131 cm depth in 2012NC and has a modeled age of 1220 ± 50 cal a BP (730 CE). Of the 55 grains analyzed, 49 (89%) exhibit alkalic basalt composition consistent with the Katla volcanic system (SDF6). The remaining 6 grains reflect minor contamination from other systems including Grímsvötn/Kverkfjöll (n=3) and Veiðivötn-Bárðarbunga (n=2) due to their low abundance (SDT1 and SDF6).

Katla 1270 (12-TORF-1B-26.5): A 2-cm thick, black layer of fine to medium ash is located at 142.5 cm depth in 2012NC and has a modeled age of 1270 ± 40 cal a BP (680 CE). Of the 33 grains analyzed, 29 (88%) exhibit alkalic basalt composition consistent with the Katla volcanic system (SDT1 and SDF7). The remaining 4 grains reflect minor contamination from other systems including Grímsvötn (n=3) and Hekla (n=1).

C-1850 (12-TORF-1B-86, mix of Katla and Grímsvötn layers): The sample at 202 cm depth in 2012NC is a cryptotephra and has a modeled age of 1850 ± 50 cal a BP. Of the 36 grains analyzed, 20 (56%) exhibit alkalic basalt compositions of the Katla volcanic system and 10 (28%) exhibit tholeiitic basalt compositions consistent with the Grímsvötn volcanic system (SDT1 and SDF8). The remaining grains reveal dacitic to rhyolitic composition that fall into the domains of the Hekla or the Katla volcanic system (SD1 and SDF8). The dominance of basalt tephra grains and lack of a clear stratigraphical horizon suggests that this horizon may be a disturbed mixture of tephra fallout from separate Katla and Grímsvötn eruptions around 1850 cal a BP.

Katla/Grímsvötn 1990 (12-TORF-1B-103): A 0.4-cm thick, black layer of fine to medium ash is located at 219 cm depth in 2012NC and has a modeled age of 1990 ± 140 cal a BP. Of the 32 grains, 21 (66%) are alkalic basalt (SDF9) and one is dacite (SDT1 and SDF9). Their composition is consistent with origin within the Katla volcanic system. The remaining 11 (34%) grains are tholeiite basalt indicating origin at Grímsvötn (n=8) and Veiðivötn-Barðárbunga (n=3) volcanic systems (SDT1 and SDF9). The composition of this layer suggests concurrent tephra fall

from two to three Katla and Grímsvötn (and possibly Bárðarbunga-Veiðivötn) eruptions around 1990 cal a BP.

C-2320 (12-TORF-1B-141, mix of tephra layers): The sample at 257 cm depth in 2012NC is a cryptotephra and has a modeled age of 2320 ± 70 cal a BP. Of the 39 grains analyzed, 17 (44%) are tholeiite basalt originating at the Veiðivötn-Barðárbunga volcanic system, whereas seven (18%) are consistent with the Grímsvötn volcanic system (SDF10). In addition, seven (18%) alkali basalt grains from the Katla volcanic system and three (8%) dacitic grains plus two (5%) rhyolitic grains, both from the Hekla volcanic system (SDT1 and SDF10). The cryptotephra nature of this horizon and dominance of basaltic tephra from Veiðivötn-Barðárbunga, Grímsvötn and Katla suggest it is a disturbed mixture of tephra fall from three closely spaced eruptions around 2320 cal a BP.

Hekla C? (12-TORF01, A-2-47.5): A distinct 0.5-cm thick, grayish brown tephra horizon situated at 197.2 m on the 2004NC core (anticipated at ~340 cm in 2012NC but not identified) and has a modeled age of 2800 ± 80 cal a BP. It features rhyolite, dacite, icelandite and alkali basalt and tholeiite basalt grains. Of the 19 grains analyzed, 12 (63%) have composition with distinct Hekla affinities (SDT1 and SDF11), spanning the range from alkali basalt to rhyolite but dominated by icelandite grains (SDF11). It is possible that this tephra horizon represents the eastern edge of the Hekla C tephra fall (2800 cal a BP, Larsen et al., 2020), although origin via reworking of the underlying Hekla 3 tephra cannot be ruled out, especially since the icelandite component in our samples show stronger affinity with the intermediate component of Hekla 3 rather than Hekla C (SDF11). The remaining seven grains are tholeiite basalt with composition indicating origin within the Grímsvötn volcanic system (SDF11). This may imply that the Hekla C tephra fall coincided with deposition from an explosive eruption at the Grímsvötn volcano.

Hekla 3 (04-TORFA2, 53.5): A 2-cm thick, grayish white tephra is located at 202.2 cm depth in 2004NC and anticipated at ~349 cm in 2012NC but not identified (SDT1 and SDF12). Of the 47 measured tephra grains, 9 (19%) are rhyolite, 30 (64%) have dacite to icelandite composition and two (4%) alkali basalt tephra grains all of which exhibit affinity with the Hekla volcanic system (SDT1 and SDF11). In terms of chemical composition, these components fit well with the compositional trend defined by the Hekla 3 tephra layer (SDF11). Along with its stratigraphic position, these results verify that this is the Hekla 3 marker layer (Larsen and Thorarinsson, 1977; Meara et al., 2020), which has a calibrated C^{14} age of 3060 ± 30 cal a BP (Dugmore et al., 1995) and identified in a previous record from Torfdalsvatn (Alsos et al., 2021). The residual sulfur in the degassed alkali basalt tephra population (SDT1) indicates that the magma lost >70% of its volatiles upon eruption, consistent with the notion that Hekla 3 was a dry magmatic Plinian eruption (e.g., Larsen and Thorarinsson, 1977). The remaining six (13%) tephra grains are tholeiite basalt of the Grímsvötn volcanic system and their residual sulfur is indicative of phreatomagmatic origin (SDT1 and SDF11).

Hekla 4 (12-TORF-2A-118): A 1.3-cm thick, grayish white tephra is located at 391 cm depth in 2012NC and at 226.8 cm depth in 2004NC, both as salt and pepper tephra horizons (i.e., light and dark grains). Of the 86 grains analyzed, 81 (94%) are rhyolite (n=68), icelandite (n=2) and alkali basalt (n=11) with composition of the Hekla volcanic system (SDT1 and SDF12). The stratigraphic position and the diagnostic high-silica rhyolite composition verifies this as the Hekla 4 marker tephra (Larsen and Thorarinsson, 1977; Meara et al., 2020) that has a calibrated C^{14} age of 4260 ± 10 cal a BP in Icelandic and British Isle peat sequences (Dugmore et al., 1995) and identified in a previous record from Torfdalsvatn (Alsos et al., 2021). The five (6%) remaining tholeiite basalt tephra grains have composition that is consistent with the Grímsvötn volcanic

system. Humic acid extracted from bulk sediments in 2004NC at depth of 227.5 cm immediately below Hekla 4 produced an age of 4030 ± 50 cal a BP (Axford et al., 2007) consistent with previously published Hekla 4 ages. However, due to some irregularities and possible deformation observed in the layer in both the 2004NC core and from a previously published record (Bender, 2020), we do not include this tephra layer in the age model.

Hekla 4270 (12-TORF-2B-03): The sample at 397 cm depth in 2012NC is a cryptotephra and has a modeled age of 4270 ± 180 cal a BP. Of the 37 tephra grains analyzed, 29 (78%) are evolved alkalic basalt (MgO range 4.4 to 5.76 wt. %). While the biplots cannot effectively distinguish between Katla or Hekla origin, the overall variability seems to favor the Hekla volcanic system (SDF13). Moreover, the two rhyolite tephra grains also have composition consistent with the Hekla volcanic system (SDF13, Meara et al., 2020). The remaining six tholeiite basalt grains have composition suggestive of origin from within the Grímsvötn volcanic system (SDF13).

Hekla 5100 (04-TORFA2, 112): A 0.8-cm thick, light grey tephra is located at 261.5cm depth in 2004NC and anticipated at ~450 cm in 2012NC core, but not detected during sampling (SDT1 and SDF12). It has a modeled age of ~5100 cal a BP. A strongly bimodal composition is reflected in the 28 analyzed grains, where 16 (57%) are rhyolite and 12 (43%) are alkali basalt. Both components have clear affinity to the Hekla volcanic system, the basalt features the classic Hekla compositional variability, while the silicic part exhibits resemblance to Hekla 4 but is distinctly different from Hekla 5 in its composition (SDT1 and SDF14). The residual sulfur in the degassed rhyolite tephra population (SDT1) is consistent with full degassing upon eruption, thus, implying a dry magmatic explosive eruption. The residual sulfur in the degassed alkali basalt component of this tephra (SDT1) indicates 65-70% degassing upon eruption, also indicating a magmatic eruption or at best a very minor involvement of external water. This is a previously unidentified bimodal Hekla tephra layer and has the potential of becoming a useful marker tephra in the Middle Holocene.

Askja 5700 (04-TORF-A2, 143.5): A 0.1-cm thick, dark colored tephra is located at 293.1 cm depth in 2004NC, equivalent to ~505 cm in 2012NC (SDT1 and SDF12) and has a modeled age ~5700 cal a BP. This is a tholeiitic basalt tephra of uniform composition (n=19; SDT1 and SDF15) and is one of two olivine tholeiite tephra layers identified in the Torfdalsvatn record. Its composition indicates origin from within the Bárðarbunga-Veiðivötn-Askja-Krafla (VAK) sector of the Northern Volcanic Zone and has relatively high sulfur content, suggesting that degassing upon eruption was arrested prematurely via quenching with external water.

Kverkfjöll/Katla 5850 (*12-TORF-2B-118):* A 0.1-cm thick, black layer of fine ash is located at 512 cm depth in 2012NC (SDT1 and SDF16) and has a modeled age of 5850 ± 200 cal a BP. Of the 14 grains analyzed, 10 (71%) feature a tholeiitic basalt composition indicative of origin within the Kverkfjöll volcanic system (SDF16). Several Kverkfjöll tephra layers are identified in soil sections around the Vatnajökull ice cap in the time interval between 6500 and 5500 cal a BP and dated via sediment accumulation rates (Óladóttir et al., 2011). Although one of these is likely the source event for the basalt component of this layer, direct correlation is not currently possible due to multiple correlations possibilities and the uncertainty of soil section tephra age estimates. Four remaining tephra grains are rhyolitic and have composition indicating origin within the Katla volcanic system (Larsen et al., 2001). The stratigraphical position and age of the Holocene SILK (silicic Katla) tephra layer series is well-established and the closest layers in age to TORF-2B-118 are SILK-A1 (~5000 cal a BP) and SILK-A7 (~6200 cal a BP) (Larsen et al., 2001). In addition, another SILK tephra layer (6750 cal a BP) has been identified in the Hvítárvatn lake sediment record (Jóhannsdóttir, 2007). Of these, correlation with the SILK-A7

seems most plausible, however, correlation is not currently possible due to the uncertainty of soil section tephra age estimates. Alternatively, TORF-2B-118 may reflect a previously unidentified Middle Holocene SILK layer.

Katla 6500 (*12-TORF-2C-8/04TORF-A3-20.5):* A 0.4 to 1.1-cm thick, black layer of medium to coarse ash is located at 557 cm depth in 2012NC and at 318.7 cm depth in 2004NC, and has a modeled age of 6490 ± 130 cal a BP. All 64 grains analyzed are alkalic basalt that generally occupy the compositional fields of the Katla system on bi-elemental plots (SDT1 and SDF17). Residual sulfur content of this tephra is low and indicative of a dry magmatic eruption (see main text Section 5.1.3). The youngest tephra layer described by Björck et al. (1992), labelled Tv-5, has similar composition and thickness to the 12-TORF-2C-8. The same can be said about the tephra layer, termed "Katla S" (SDF17), in lake sediment from Barðalækjartjörn, ~75 km south of Torfdalsvatn (Eddudóttir et al., 2016). Katla S has been ^{14}C dated using adjacent Betula (6661 to 6501 cal a BP) and Salix twigs (6679 to 6529 cal a BP, Eddudóttir et al., 2015, 2016). Given the overlap of ages derived for Tv-5 in Torfdalsvatn and Katla S in Barðalækjartjörn, in addition to compositional similarity, we suggest these tephra layers were generated from the same Katla eruption. We note that another Katla tephra layer, termed Katla EG, has recently been described with an age of 6240 cal a BP in the lakes Bæjarvötn and Haukadalsvatn (Fig. 1), as well as on the southeast Greenland shelf (Jennings et al., 2014; Harning et al., 2018, 2019). However, small but distinct compositional differences (SDF17) and the modeled age difference indicate that these were generated by tephra fall from two separate eruptions at Katla.

Grímsvötn/Katla 8500 (04-TORF-01-A-3-54.5): A 0.1 to 0.2-cm thick, black layer of fine to medium ash is located at 353 cm depth in 2004NC and has a modeled age of ~8500 cal a BP. Of the 19 grains analyzed, 11 (58%) are tholeiite basalt with distinct Grímsvötn volcanic system affinities and their residual sulfur values are indicative of arrested degassing due to interaction with external water, consistent with origin from a subglacial eruption (SDT1 and SDF18). The remaining 8 (42%) tephra grains exhibit alkali basalt composition that sit within the Hekla basalt compositional field and at the boundary of the Katla basalt field (SDT1 and SDF18). However, the residual sulfur content of this tephra makes Katla origin more viable (see main text Section 5.1.3).

Grímsvötn? 9260 (12-TORF-2D-34): A 0.3-cm thick, black layer of fine to medium ash is located at 730 cm depth in 2012NC (Table 1) and has a modeled age of 9260 ± 300 cal a BP. This layer features pristine and vesicular, basaltic sideromelane grains and a lesser amount of poorly to non-vesicular black basalt grains and minor grey microcrystalline grains. All 19 analyzed tephra grains are tholeiite basalt and the composition of 18 (95%) grains, although variable and dispersed, shows some affinity with the Grímsvötn volcanic system (SDT1 and SDF19).

G10ka Series 9410 to 10400 (12-TORF-2D-38 to -85 and 04-Torf01-A3-105 to -140): The G10ka Series in 2012NC core is represented by sequence of five closely spaced, black tephra layers of fine to medium ash in the depth interval of 734-749 cm and a 26 cm-thick black tephra horizon, extending from 756 to 782 cm depth. The five layers range in thickness from 0.5 to 1.1 cm, each separated by 3-4 cm of lake sediments, while the 26 cm-thick horizon is comprised of alternating beds of very fine gray and coarse black ash (SDF-A). In core 2004NC, it is represented by a 0.3 cm thick tephra layer at 438.3 cm depth and an overlying 26.7 cm thick horizon at depth of 403.9 to 430.6 cm, comprised of mm-dm thick black and brownish black sub-horizons of tephra separated by mm to cm thick packages of organic sediment. Like 2012NC, the 2004NC tephra unit is distinctly bedded with alternating beds of very fine gray and coarse black ash (SDF-A). The modeled age range represented by the G10ka Series horizon in 2012NC is 9410 to 10400 cal a BP.

This estimate is underpinned by two humic acid dates from 2004NC at 432 cm depth (in between the G10ka Series 26.7 cm-thick horizon and 0.3 cm layer at 438.3 cm depth) and at 369 cm depth (i.e., 34.9 cm above the G10ka Series tephra), giving calibrated ages of 10240 ± 10 cal a BP and 9510 ± 20 cal a BP, respectively (SDF-A, Axford et al., 2007). Furthermore, based on chemical composition, total thickness and rhythmic bedding, this unit is correlated with the Tv-4 tephra as originally identified in Torfdalsvatn by Björck et al. (1992). The G10ka Series tephra horizons as well as individual layers were sampled every cm in the 26-cm thick horizon in core 2012NC. In total 46 samples were collected and 44 were analyzed for their chemical composition and described and examined for their physical components (SDT1 and SDF-A).

Of the 672 grains analyzed from these horizons, 660 (98 %) are tholeiite basalt of remarkably uniform composition with distinct affiliation to the Grímsvötn volcanic system, thus confirming a G10ka Series origin (SDT1 and SDF20-21). The remaining 12 grains are tholeiite basalt *(n=2)* from the Bárðarbunga-Veiðivötn system and alkali basalt *(n=10)* from Hekla and/or Katla volcanic systems. Via analysis of the appearance, components, and chemical composition, we have identified 12 separate tephra fall events within the G10ka Series tephra in Torfdalsvatn. In addition, the residual sulfur in the degassed basalt tephra, as measured in a select subpopulation of the samples (SDT1), shows that these Grímsvötn magmas released between 35-50% of the volatiles upon eruption, indicating that these tephra falls were produced by phreatomagmatic eruptions (e.g., Thordarson et al., 1996). These 13 events are briefly described below in chronological order from oldest to youngest.

Samples 12-TORF-2D-85 and -84, representing the lowest 2 cm of the 26 cm-thick G10ka Series tephra horizon at 780 to 782 cm depth in core 2012NC, are comprised of medium to coarse ash containing distinguishing sideromelane grains, including achneliths and fragments of golden pumice. This along with a distinctly broader compositional range compared to the tephra above (i.e., 12-TORF-2D-83 and -79; SDF21) as well as more abundant diatom mud clumps and round clastic sediment grains in 12-TORF-2D-84, are taken to indicate that this is the first tephra fall event recorded in Torfdalsvatn (i.e., G10ka Series event #1). In terms of componentry and chemical composition, the 12-TORF-2D-85 and -84 level correlates with the basal layer of the G10ka series in the 2004NC core (i.e., sample 04-TORF-A3, 140; SDF21). The level represented by samples 12-TORF-2D-83 and -82 (778 to 780 cm depth) is also medium to coarse ash and contains relatively high abundance of silvery grey microcrystalline and black opaque tephra grains and is devoid of diatom mud. This evidence, along with significantly tighter compositional range (SDF21), are taken to indicate a new tephra fall event (i.e., G10ka Series event #2). The level represented by samples TORF-2D-81 to -78 (i.e., 778 to 775 cm depth) is made up of very fine to fine ash. In the lower 2 cm it contains a significant portion of open-framework frothy (i.e., reticulite-like = >90% vesicularity) sideromelane grains featuring very delicate protrusions. This grain type feature less strongly in the upper 2 cm of this level, which is typified by upward increase in the diatom mud component along with appearance of diatoms. Although this level has similar composition 12-TORF-2D-83 and -82 (SDF21), the abrupt shift to a more dominant sideromelane clast populations at 778 cm-depth along with increased sediment contribution at 777-775 cm, supports the notion that this interval represents a separate tephra fall (i.e., G10ka Series event #3). The level represented by 12-TORF-2D-77 to -73 at 775 to 770 cm depth, has a lower part comprised of medium ash (TORF-2D-77 and -76) and an upper part of very fine to fine ash (12-TORF-2D-75 to -73). The medium ash in the lowest 2 cm is devoid of diatom mud and contains reticulite-like grains in moderate abundance, indicating it represents the onset of a new tephra fall. The overlying 3 cm of very fine to fine ash are as follows: 12-TORF-2D-75 characterized by poorly

vesicular black glass and grey microlite-rich grains, containing relatively high abundance of diatom mud and may represent the tapering out phase of G10ka Series event #4. TORF-2D-74 is, again, typified by golden pumice and reticulite-like grains, although mixed in with some diatom mud. 12-TORF-2D-73 is typified by abundant fines that are a mixture of diatom mud and granulated highly vesicular grains. Hence, samples 12-TORF-2D-74 to -73 (i.e., 771 to 769 cm depth) is taken to represent tephra fall G10ka Series event #5 in the Torfdalsvatn record. In this context, it is noteworthy that 12-TORF-2D-78 and -77 correlate, in terms of chemical composition and physical characteristics, well with samples 04TORF-A3, 130 and 131 from the base of the 26.7 cm-thick tephra horizon in the 2004NC core. The significance of this correlation is the C^{14} age determination of 10240 ± 10 cal a BP in core 2004NC (Axford et al., 2007), thus providing an internal age control for the 2012NC horizon (SDF-A). G10ka Series event #6 corresponds to the level represented by samples 12-TORF-2D-72 to -68 is comprised of fine ash with a slight overall fining upwards and contain abundant golden pumice fragments and reticulite-like grains, whereas diatom mud is absent. G10ka Series vent #7 is represented by samples TORF-2D-67 to -63, which range from black medium ash (TORF-2D-67) to grey fine ash (TORF-2D-66 to -63). TORF-2D-67 is clean tephra comprised of golden pumice fragments and reticulate-like sideromelane glass grains in addition to black opaque, greyish black microcrystalline grains, and a minor plagioclase component. In contrast, TORF-2D-66 to -63 also feature white diatom mud, which may represent the tail-end of the fallout as well as redeposition of the tephra after reworking at the land surface. G10ka Series event #8 of the G10ka Series record in Torfdalsvatn is cm represented by samples 12-TORF-2D-62 to -60 from the top 3 cm (depth of 759-756 cm) of the 26 cm -thick tephra horizon in core 2012NC. It is comprised of fine to medium ash with similar grain morphology and composition as the underlying G10ka Series event #7 deposit. However, G10ka Series event #8 is devoid of white diatom mud, indicating pristine tephra fall.

G10ka Series events #9-13 are present in core 2012NC as a series of five 0.5 to 1.1 cm-thick, closely spaced Grímsvötn system tephra layer of fine to medium ash. These layers are in the depth interval of 749-734 cm depth and are separated by 3-4 cm of lake sediments. These five layers correlate with the upper part of the 26.7 cm-thick horizon in 2004NC core (SDF-A and SDT1). Their modeled age spans the range of 9410 to 9960 cal a BP and overlap significantly with the published age range of ~10,625 ± 50 to 9590 ± 315 cal a BP for the G10ka Series elsewhere (Óladóttir et al., 2020).

Hekla 10550 (12-TORF-2D-106): A 0.3-cm thick, black layer of fine to medium ash is located at 802 cm depth in 2012NC (SDT1) and has a modeled age of 10550 ± 150 cal a BP. Of the 28 grains analyzed, 22 (79%) are alkali basalt from the Hekla volcanic system (Fig. 11). The remaining six grains are tholeiite basalt, four from the Grímsvötn volcanic system and two from an unknown source. This layer is taken to represent a basaltic tephra fallout from the Hekla volcanic system with a minor contribution from a Grímsvötn system eruption that took place at a similar time. Note that Hekla 10550 is older than the two andesitic Hekla layers identified in Bæjarvötn (~9600 and 9400 cal a BP, Harning et al., 2018).

I-THOL-I? (TORF-2D-108): A 0.3-cm thick, black layer of fine to medium ash is located at 804 cm depth in 2012NC (SDT1) and has a modeled age of 10560 ± 150 cal a BP. Of 30 tephra grains analyzed, 25 are rather primitive tholeiite basalt (MgO = 8.4 ± 0.26 wt %) that appears be derived from the VAK sector of the Northern Volcanic Zone (NVZ) and most likely from within the Askja volcanic system, possibly the Gígöldur eruption. The remaining five grains are also tholeiite basalt but from the Grímsvötn volcanic system (Fig. 11). This layer is a basaltic tephra fallout distinctly primitive composition from an unknown explosive eruption within the NVZ, with

an indication of contribution from an explosive eruption at the Grímsvötn system of similar age. It has similar chemical attributes to the Tv-3 tephra previously identified in Torfdalsvatn (Björck et al., 1992) and in the lake Bæjarvötn (Harning et al., 2018) support a correlation to the I-THOL-I marker tephra layer of the North Atlantic Ash Zone I (Kvamme et al., 1989). We also note here that Tv-3 likely correlates to the KOL1-2269 tephra identified in marine sediment core MD99-2269 on the North Iceland Shelf (10570 ± 106 cal a BP, Kristjánsdóttir et al., 2007).

Kverkfjöll 10630 (12-TORF-2D-116.5): A 0.3-cm thick, black layer of fine to medium ash is located at 812.5 cm depth in 2012NC (Table 1 and SDT1) and has a modeled age of 10630 ± 150 cal a BP. Of the 35 grains analyzed, 33 grains define three distinctive compositional groups particularly in terms of TiO_2, FeO and MgO wt%. Seven of the 33 grains are alkali basalt from the Katla volcanic system, six tholeiite basalt from the Bárðarbunga-Veiðivötn system and 17 grains are tholeiite basalt with composition that makes the Kverkfjöll the most likely source system (). We take this layer to represent basaltic tephra fallout from Kverkfjöll volcanic system eruption. The minor components suggest that tephra fall from explosive eruptions within the Katla and Bárðarbunga-Veiðivötn systems took place at the similar time.

Please see Harning et al. (2024) for detailed descriptions of the oldest four tephra layers from sediment core 2012BC: Katla 11,170, Katla 11,295, Katla 11,315 (Tv-2), and Hekla 11,390 (Tv-1).

2. Tephra stratigraphy implications

Excluding the 26 cm-thick horizon within the G10ka Series, the average tephra horizon thickness is 0.7 ± 0.5 cm (total range <0.1 to 2 cm), implying that the source eruptions were of subplinian to Plinian/phreatoplinian intensities (Thordarson and Larsen, 2007; Thordarson and Höskuldsson, 2008), activity that is taken to typify explosive eruptions producing magmas of silicic and intermediate compositions (e.g., Walker, 1973). Yet over 65% (>80% if we include the 26 cm thick G10ka horizon) of the events recorded in the Holocene sediment record from Torfdalsvatn are mafic (i.e., basaltic), including two of primitive magma composition (7.42 ± 0.14 and 8.39 ± 0.26 wt. % MgO, respectively). Furthermore, the thicknesses of individual basalt layers within G10ka Series range from 0.5 to 1.1 cm and up to 3 cm if we include data from the 26 cm thick G10ka series horizon. In addition, the number of Hekla and Katla basalt tephra events in the record are close to that of Hekla and Katla silicic to intermediate events. Collectively, this demonstrates not only that basaltic explosive events can be as powerful and widely dispersed as their silicic and intermediate counterparts in Iceland, but they also have the capacity to be valuable as stratigraphic markers in distal sediment records. Finally, Grímsvötn, Hekla and Katla are the most common sources, consistent with them being three of the most active volcanic systems in Iceland (Thordarson and Larsen, 2007; Thordarson and Höskuldsson, 2008). However, the high frequency of tephra fall from Grímsvötn is principally a consequence of the G10ka Series eruption episode in the Early Holocene, between ~10400 and 9400 cal a BP.

2.1. G10ka Series Tephra

The Saksunarvatn Ash has been one of the most widely applied tephra markers sourced from Iceland in Northern Hemisphere tephra stratigraphies (Mangerud et al., 1986; Merkt et al., 1993; Björck et al., 1992; Grönvold et al., 1995; Birks et al., 1996). However, evidence in Iceland and abroad demonstrates that as many as seven compositionally indistinguishable Saksunarvatn-like tephra layers (i.e., G10ka Series tephra) were deposited between 10400 and 9900 cal a BP, with

no more than five reported in superposition (Jóhannsdóttir, 2007; Jennings et al., 2014; Kristjánsdóttir et al., 2017; Harning et al., 2018b, 2019; Wastegård et al., 2018; Timms et al., 2019; Óladóttir et al., 2020). Although Greenland ice core records date one layer of the G10ka Series tephra to 10,300 ± 90 cal a BP (Rasmussen et al., 2006), ^{14}C-based age estimates on the G10ka Series elsewhere range from 10,625 ± 50 to 9590 ± 315 cal a BP (Óladóttir et al., 2020), which supports successive Grímsvötn eruptions rather than a single event.

In Torfdalsvatn, we correlate 13 layers to the G10ka Series tephra based on Grímsvötn composition (Fig. S2) and modeled ages (10,400 to 9410 cal a BP) that overlap with ^{14}C-based age estimates elsewhere (10,625 ± 50 to 9590 ± 315 cal a BP, Óladóttir et al., 2020). Of these 13 total layers, the 26 cm thick unit in 2012NC reflects eight separate tephra layers based on distinct variations in grain size, sedimentology and morphology. The remaining five G10ka Series tephra layers are located immediately above the 26 cm thick unit and are each separated by organic sediment. Although Björck et al. (1992) attribute their 22 cm thick „Saksunarvatn Ash“ to a single event, the authors do describe a rhythmic tephra unit, which was later proposed to be partially comprised of reworked tephra (upper 10 cm) from catchment erosion based on the incorporation of pollen (Rundgren, 1998). However, in addition to the detailed grain morphology and compositions, each of the high-resolution samples (every cm) retains delicate protrusions that would not survive aeolian or fluvial erosion, supporting the interpretation that the entire 26 cm thick sequence is comprised of multiple, primary tephra deposits. In the lake Bæjarvötn, NW Iceland (Fig. 1), a similar conclusion is also supported by the presence of at least two G10ka Series tephra layers that are separated by tephra from the Veiðivötn-Bárðarbunga volcanic system (Harning et al., 2018). Despite our high-resolution sampling strategy throughout the 26 cm thick unit in Torfdalsvatn, we find no evidence that tephra from Veiðivötn-Bárðarbunga tephra or elsewhere is interbedded. However, the lowermost sample tephra layer in Torfdalsvatn (TORF-2D-53) does feature a more clustered composition compared to the subsequent G10ka Series layers (Fig. 7), which may aid in future correlations. Given the lack of firmer age control on individual layers as well as the compositional indistinctions on the subsequent G10ka Series layers, it remains difficult to correlate Torfdalsvatn sequence to other sites in Iceland where multiple G10ka Series layers have been identified, such as southern (Geirsdóttir et al., 2022) western (Jóhannsdóttir, 2007; Harning et al., 2019) and northwestern lake sediments (Harning et al., 2018). In addition, it still remains unclear how the G10ka Series tephra layers found in Iceland correlate to the Saksunarvatn Ash layers found in Greenland and the Faroe Islands (e.g., Óladóttir et al., 2020), but it is the focus of ongoing research.

2.2. Middle and Late Holocene tephra stratigraphy

Given the presumed distribution of several key marker tephra layers over Torfdalsvatn, it is surprising that they were not found in our records. These marker tephra include the widely distributed and rhyolitic Hekla 5 tephra (~7075 cal a BP, Meara et al., 2020), a local but distinctly intermediate Katla tephra layer found in Barðalækjartjörn (Fig. 1A main text), termed HUN (5530 ± 60 cal a BP, Eddudóttir et al., 2016), and the trachydacitic to rhyolitic Snæfellsjökull-1 tephra (1820 ± 90 cal a BP, Larsen et al., 2002) that has been found across western and northern Iceland (Larsen et al., 2002; Gudmundsdóttir et al., 2012, 2018; Harning et al., 2018, 2019). Although these tephra layers were not present in our Torfdalsvatn sediment cores, some such as Hekla 5 have been found in nearby Barðalækjartjörn (Eddudóttir et al., 2016). Given the known distribution, distinct compositional characteristics, and relatively firm age control of these tephra

layers, it is conceivable that these could become useful marker layers in north Iceland with additional sediment records from nearby lakes.

Notable Middle Holocene tephra layers in Torfdalsvatn derive from the Katla, Kverkfjöll, Askja and Hekla volcanic systems (Table 2, main text). One of the thickest is the Katla 6500 tephra layer (1.1 cm thick, TORF-2C-6), which correlates with the previously termed Tv-5 tephra in prior Torfdalsvatn studies (Fig. S3B, Björck et al., 1992). In lake sediment from Barðalækjartjörn, ~75 km south of Torfdalsvatn (Fig. 1A, main text), a compositionally similar tephra layer has been termed Katla S (Fig. S3B, Eddudóttir et al., 2016), which was ^{14}C-dated using adjacent Betula (6661 to 6501 cal a BP) and Salix twigs (6679 to 6529 cal a BP, Eddudóttir et al., 2015, 2016). Given the overlap of ages derived for Katla 6500 in Torfdalsvatn and Katla S in Barðalækjartjörn, in addition to compositional similarity, we suggest these tephra layers were generated from the same Katla eruption. Additional distinct tephra layers in the Middle Holocene include the olivine tholeiitic basalt Askja 5700, the bimodal Hekla 5100, and a rhyolitic Hekla layer (Hekla 4270, TORF-2B-03) that precedes the Hekla 4 marker tephra layer (TORF-2A-118, Fig. S3). Given the lack of current correlations in other nearby Icelandic sediment records, these layers likely reflect the product of narrow dispersals from their respective sources.

The two uppermost Late Holocene Hekla tephra layers (Hekla 1300 and 1766) are well-known to feature dacitic or andesitic compositions (Thórarinsson, 1967). However, in addition to the dacitic and andesitic tephra grains, each of these tephra layers also contained substantial proportions of high-SiO_2 and low-SiO_2 rhyolitic glass consistent with Hekla 4 and Hekla 3/Hekla 1104 compositions, respectively (TORF-1A-66 and TORF-1A-80.5, respectively, Fig. S1). It is difficult to reconcile that these are derived from local reworking of Hekla 4 and Hekla 3/Hekla 1104 tephra via erosion of the soil cover around Torfdalsvatn because: (1) the proportion of high and low-SiO_2 rhyolitic grains are substantially different, whereas Hekla 4 and 3 are close to each other in local soil profiles and have roughly the same thickness (Möckel et al., 2021) and (2) the pristine nature of these grains that suggests no post-depositional reworking. For Hekla 1300, since Torfdalsvatn is at its western margin of dispersal (Thórarinsson, 1967; Janebo et al., 2016), it is possible that the most intense part of the initial phase was directed more to the north resulting in the dominantly rhyolitic tephra that we observe (Fig. S1). For Hekla 1766, although the initial rhyolitic phase was about 2-3 times less intense than that of Hekla 1300 (Janebo et al., 2016), our data suggests that Torfdalsvatn also saw tephra fall from this initial explosive phase resulting in its rhyolitic as well as intermediate character (Fig. S1). However, it is also possible that the Hekla 1104-like rhyolitic components reflect material incorporated from units within the Hekla volcanic system during the latter two volcanic eruptions. On the other hand, it is unlikely that the Hekla 4-like component could have been incorporated in a similar fashion as the Hekla 4 eruption and its high-SiO_2 magma predates the presumed construction of the modern Hekla edifice (~3000 cal a BP, e.g., Jóhannesson and Einarsson, 1992; Larsen et al., 2020). Although more work is needed to better establish the origins and dispersal limits for the rhyolitic components of Hekla 1300 and 1766 that we observe in Torfdalsvatn, our datasets suggest that rhyolitic tephra from Hekla were generated more frequently during the last millennium than currently established.

3. Residual sulfur content as indication for phreatomagmatic eruptions

In this study, the residual sulfur content was measured in a selected suite of samples (bold font, Table 2, main text) to assess whether the events that produced those tephra layers involved interaction with external water upon eruption. Evidence of such interaction is an indicator of wet

vent environment and thus a proxy for eruptions from within glaciers or through standing body of water (lake or the sea).

During the Early Holocene, recent syntheses show that the Icelandic Ice Sheet retreated from a shallow marine shelf position at ~12,000 cal a BP to the central highlands, when catastrophic drainage of previously ice dammed lakes occurred, between 10,700 and 10,400 cal a BP (Geirsdóttir et al., 2022). The Early Holocene Hekla 11390 basalt tephra has residual sulfur contents showing that the magma lost >70% of its volatiles upon eruption, indicating that this tephra was produced by a dry magmatic eruption (e.g., Thordarson et al., 1996, 2001). This is consistent with a rapid northeastward retreat of the Icelandic Ice Sheet from its position at the Búði moraine complex southwest of Hekla (e.g., Geirsdóttir et al., 2022). Around the same time, the Early Holocene Katla 11,315 and 11,170 tephra layers are typified by residual sulfur indicating about 55% loss of their volatiles upon eruption, suggesting that these tephra layers were produced by wet phreatomagmatic eruptions (e.g., Thordarson et al., 2001). While this may indicate that the Katla volcano was either still covered by the retreating Icelandic Ice Sheet or its caldera was filled with a lake when the eruptions occurred, recent glacier modeling and reconstructions suggest ice sheet cover was more likely (Anderson et al., 2019; Geirsdóttir et al., 2022).

The G10ka Series (10400 to 9410 cal a BP) has residual sulfur showing that these Grímsvötn magmas released between 35-50% of the volatiles upon eruption, implying that these tephra falls were produced by wet phreatomagmatic eruptions (e.g., Thordarson et al., 1996) and most likely from vents within the Vatnajökull glacier during the Early Holocene. These observations are consistent with a recent Holocene glacier model that simulates the presence of Vatnajökull's northern sector, which overlies the Grímsvötn volcanic system's central volcanos, at this time (Anderson et al., 2019). The Grímsvötn/Katla 8500 tephra layer is comprised of tephra fall from two eruptions, a tholeiite basalt from the Grímsvötn volcanic system and alkali basalt from either the Katla or Hekla system. The Grímsvötn portion has residual sulfur values indicative of arrested degassing due to interaction with external water, consistent with origin from a subglacial volcanic eruption. This is also consistent with the glacial model that simulates the persistence of Vatnajökull's northern sector to ~8000 cal a BP, although the timing also depends on glacial isostatic adjustment and precipitation changes, neither of which are well-constrained (Anderson et al., 2019). The alkali basalt portion of the 8500 cal a BP tephra layer has a composition that on bi-element plots sits within the Hekla basalt compositional field and at the boundary of the Katla basalt field but has residual sulfur contents indicative of arrested degassing via interaction with external water. This makes Katla origin a more viable eruption source given that the Katla central volcano likely had some ice cover at this time, albeit smaller than today (Anderson et al., 2019), while the Hekla volcanic system was likely ice-free.

During the Holocene Thermal Maximum (HTM, ~7900 to 5500 cal a BP, Geirsdóttir et al., 2020), warmer than present summer temperatures (Harning et al., 2020) resulted in the significant retreat or disappearance of residual ice caps in Iceland (Larsen et al., 2012; Harning et al., 2016; Geirsdóttir et al., 2019). However, discrepancies exist regarding the HTM persistence of some, including Mýrdalsjökull, the ice cap that today covers Katla. For instance, HTM ice cap presence has been suggested based on sulfur content of other Katla tephra layers over the last 8400 years (Óladóttir et al., 2007). On the other hand, surface mass balance–equilibrium line altitude glacier models suggests the persistence of HTM ice is highly unlikely (Anderson et al., 2019). Sulfur analysis of the Katla 6500 tephra layer features a low and tightly clustered residual sulfur content indicating degree of degassing exceeding 70%, which is typical for dry magmatic basalt eruptions (e.g., Thordarson et al., 2003). Hence, while we cannot draw conclusions about the entirety of the

HTM, the Katla 6500 tephra sulfur content as well as several other Katla tephra layers' sulfur content in this time frame (Óladóttir et al., 2007) indicate that Katla's caldera was at least periodically free of ice and water during the HTM.

Askja 5700 has composition that is consistent with origin within the Bárðarbunga-Veiðivötn-Askja-Krafla (VAK) sector of the Northern Volcanic Zone. For magma of this composition (SDT1), un-degassed values are typically between 1100-1300 ppm S and fully degassed values between 300-400 ppm S (e.g., Thordarson et al., 2003). The measured residual sulfur in this tephra is ~800 ppm on average (SDT1) and thus suggestive of quenching-induced arrest of degassing due to interaction with external water (e.g., Thordarson et al., 1996, 2001). At the time of the eruption the Krafla volcanic system is ice-free and its main phreatomagmatic constructs (i.e., the ~10000 cal a BP Lúdent and ~2500 cal a BP Hverfjall tuff cones) are either much too old or young to be considered likely sources for this tephra layer (Sæmundsson, 1991). Of these three systems, the only one likely to have featured a glacier at this time is the Veiðivötn-Bárðarbunga volcanic system (Anderson et al., 2019). In the pre-Hekla 4 time, the caldera of the Askja volcano did not contain the lavas that fill it to the brim today. It also featured a major episode of phreatomagmatic volcanism during this time that produced the NE- and SW tuff cone complexes (Hartley et al., 2013, 2016). Hence, it is reasonable that the Askja central volcano featured a caldera lake at this time. Although the layer's major element composition is such that our bi-element discrimination plots do not clearly discriminate between the two systems, the overall trend does lean towards Askja origin (SDF15). In addition, the glass composition of the tephra from the NE- and SW tuff cone complexes (Hartley, 2012; Hartley et al., 2013) exhibits similarities to this tephra layer. Hence, we propose that this olivine tholeiite tephra was produced by phreatomagmatic eruption at the Askja central volcano at about 5700 years ago.

Hekla 1104 reveals residual sulfur contents in the degassed rhyolite tephra population (see SDT1) that is indicative of extended degassing upon eruption and consistent with the notion that Hekla 1104 is a dry, magmatic Plinian eruption (e.g., Janebo et al., 2016). Conversely, the residual sulfur in the degassed alkali basalt component of the tephra (SDT1) indicates about 60% degassing upon eruption, suggesting involvement of external water in the explosive activity that produced the basalt tephra (e.g., Thordarson et al., 2001). These contrasting results indicate either that 1) the basalt component is from an older tephra formation that was produced by phreatomagmatic eruption and accidentally incorporated into the silicic tephra of Hekla 1104 during the eruption or 2) it originated from a separate, but simultaneously active, Hekla system vent where the basaltic magma interacted with external water.

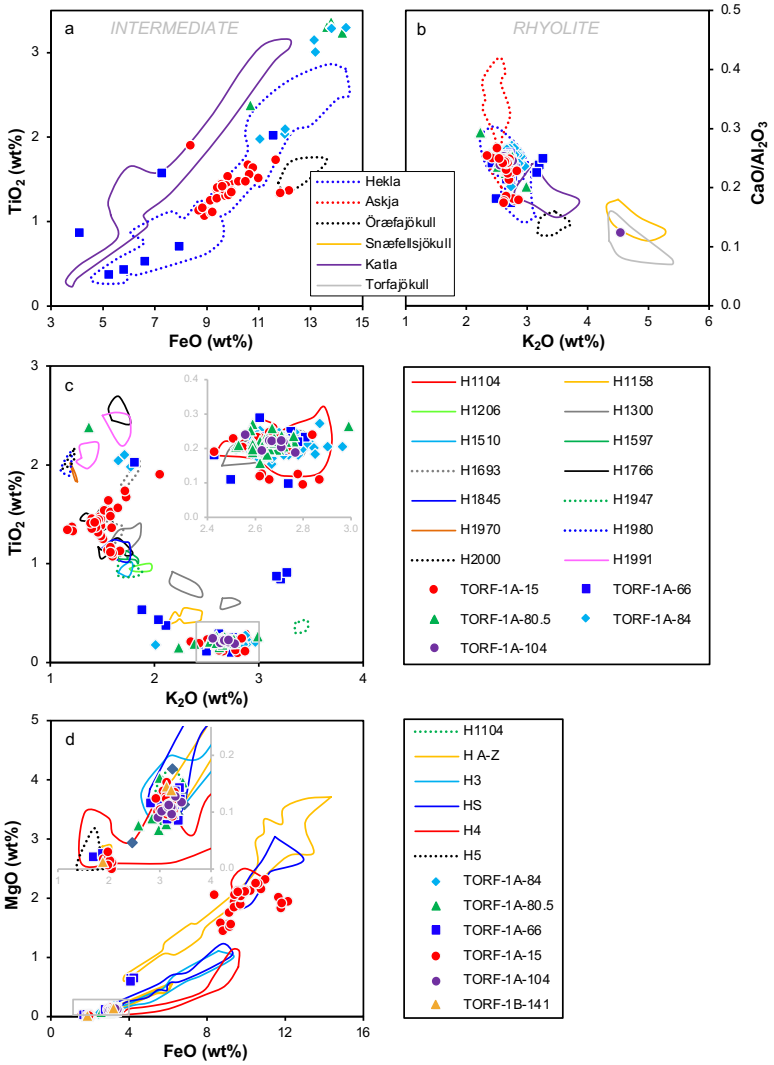

Figure S1*: Late Holocene Hekla rhyolite tephra layer compostions from core 2012NC in comparison to known Hekla eruptions. See Supporting Data for source references.*

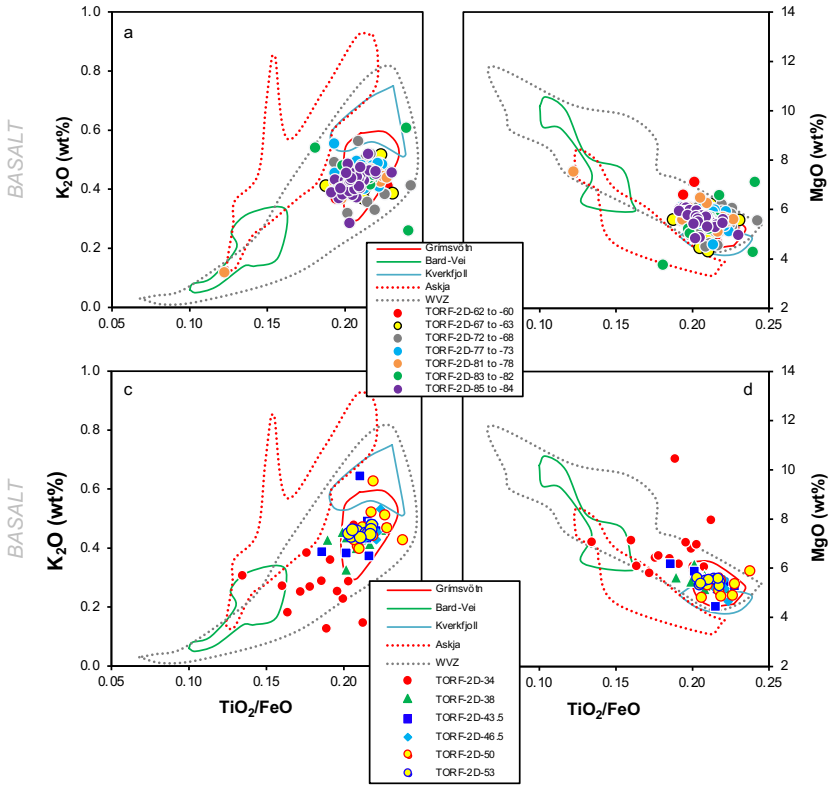

Figure S2*: G10ka Series compositions from core 2012 NC in comparison to volcanic source fields. See Supporting Data for source references.*

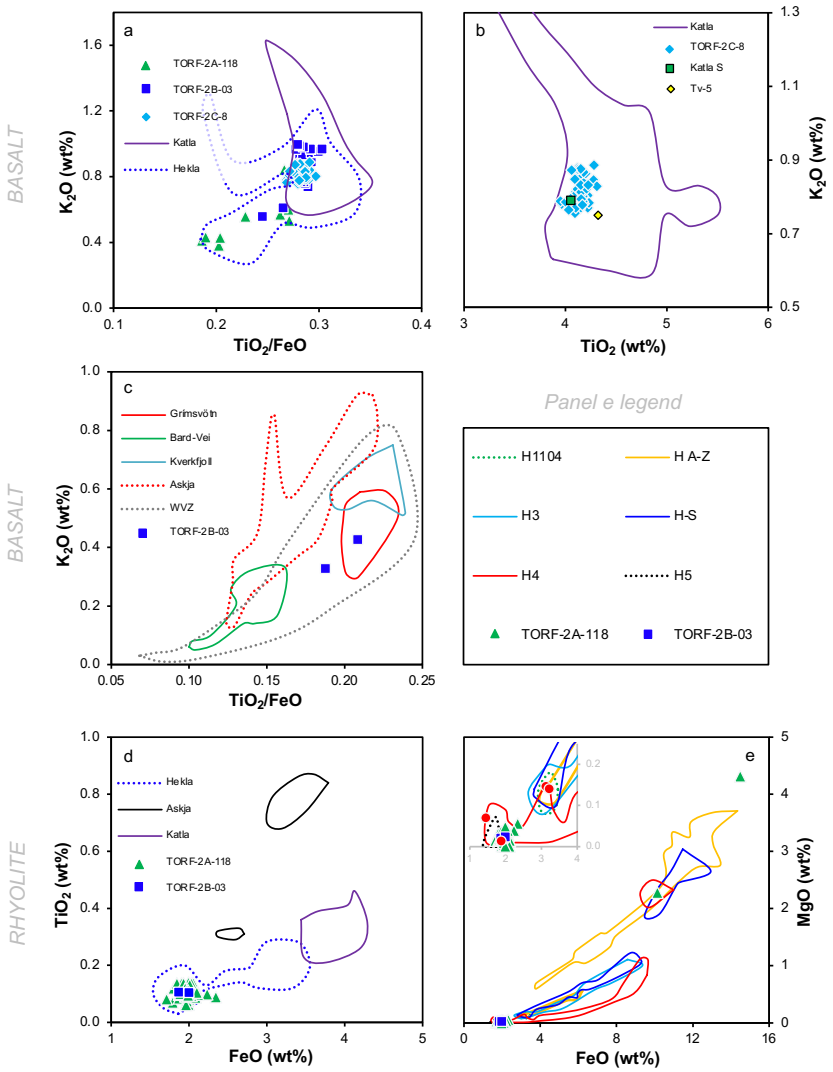

Figure S3: *Notable Middle Holocene tephra layers compositions from core 2012NC in comparison to fields of volcanic sources and known eruptions. See Supporting Data for source references.*

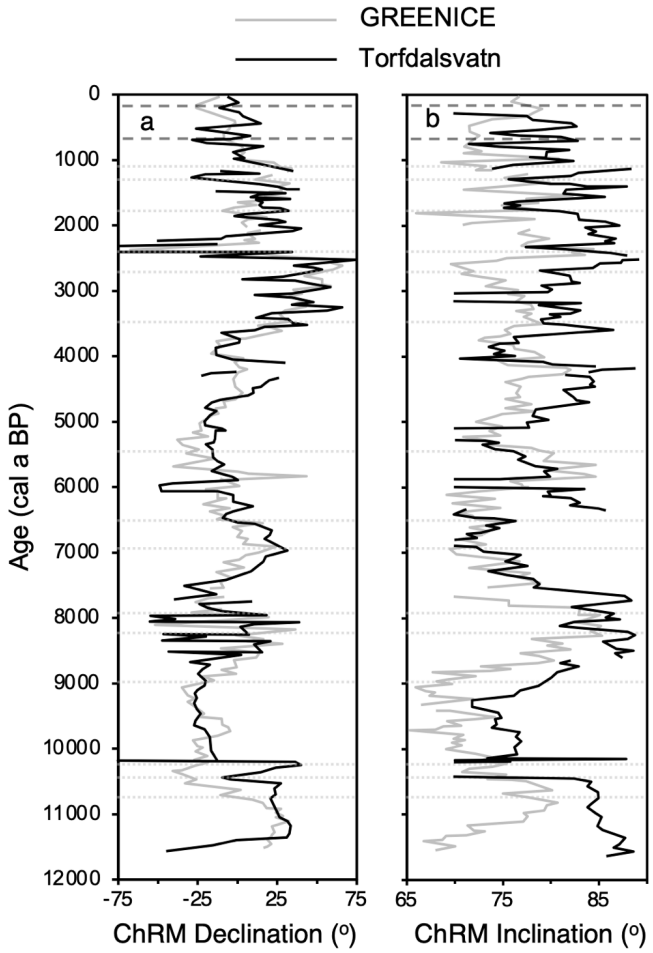

***Figure S4**: PSV data from core 2012NC (black) compared to the master GREENICE record (gray) in terms of a) declination and b) inclination. Marker tephra layers used in the PSV synchronization are shown with dark gray dashed lines and PSV tie points used in the age model are shown with light gray dotted lines.*

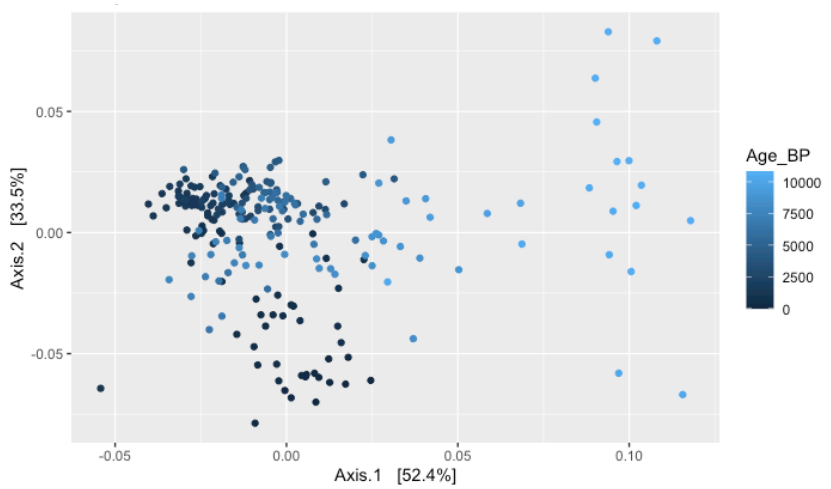

***Figure S5**: Biplot of PCoA axis 1 and 2 results for Torfdalsvatn bulk geochemistry proxies. Data points are colored according to the modeled age, where darker blue is closer to present (0 BP).*

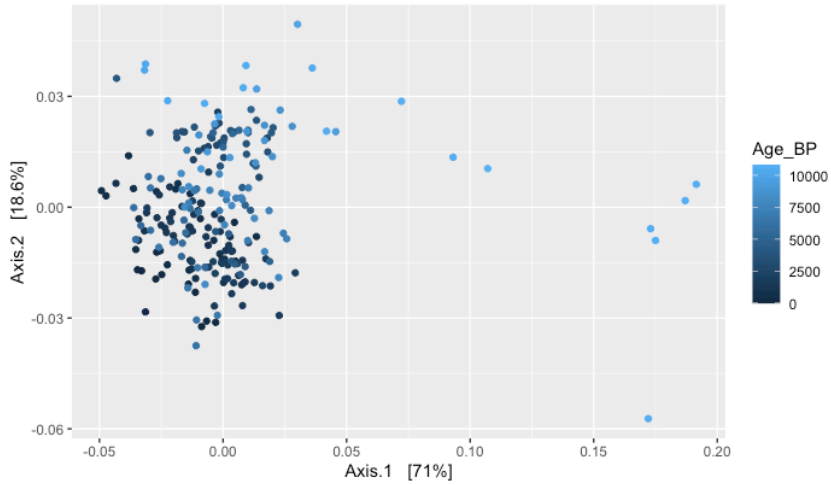

***Figure S6**: Biplot of PCoA axis 1 and 2 results for Torfdalsvatn algal pigment proxies. Data points are colored according to the modeled age, where darker blue is closer to present (0 BP).*

References

Alsos, I. G., Lammers, Y., Kjellman, S. E., Merkel, M. K. F., Bender, E. M., Rouillard, A., Erlendsson, E., Guðmundsdóttir, E. R., Benediktsson, I. Ö., Farnsworth, W. F., Brynjólfsson, S., Gísladóttir, G., Eddudóttir, S. D., and Schomacker A.: Ancient sedimentary DNA shows rapid post-glacial colonisation of Iceland followed by relatively stable vegetation until the Norse settlement (Landnám) AD 870. Quaternary Science Reviews, 259, 106903, 2021.

Anderson, L. S., Geirsdóttir, Á., Flowers, G. E., Wickert, A. D., Aðalgeirsdóttir, G. Th., and Thorsteinsson, T.: Controls on the lifespans of Icelandic ice caps. Earth and Planetary Science Letters, 527, 115780, 2019.

Axford, Y., Miller, G. H., Geirsdóttir, Á., and Langdon, P.: Holocene temperature history of northern Iceland inferred from subfossil midges. Quat. Sci. Rev., 26, 3344-3358, 2007.

Bender, E. M.: Late Quaternary tephra stratigraphy and paleoenvironmental reconstruction based on lake sediments from North and Northeast Iceland. MS thesis, UiT The Arctic University of Norway, 2020.

Birks, H. H., Gulliksen, S., Haflidason, H., Mangerud, J., and Possnert, G.: New radio-carbon dates from the Vedde ash and Saksunarvatn ash western Norway. Quaternary Research, 127, 119-127, 1996.

Björck, S., Ingólfsson, Ó., Haflidason, H., Hallsdóttir, M., and Anderson, N. J.: Lake Torfadalsvatn: a high resolution record of the North Atlantic ash zone I and the last glacial-interglacial environmental changes in Iceland. Boreas, 21, 15-22, 1992.

Dugmore, A. J., Cook, G. T., Shore, J. S., Newton, A. J., Edwards, K. J., and Larsen, G.: Radiocarbon dating tephra layers from Britain and Iceland. Radiocarbon, 37, 379-388, 1995.

Eddudóttir, S. D., Erlendsson, E., and Gísladóttir, G.: Life on the periphery is tough: Vegetation in Northwest Iceland and its responses to early-Holocene warmth and later climate fluctuations. Holocene, 25, 1437-1453, 2015.

Eddudóttir, S. D., Erlendsson, E., Tinganelli, L., and Gísladóttir, G.: Climate change and human impact in a sensitive ecosystem: the Holocene environment of the Northwest Icelandic highland margin. Boreas, 45, 715-728, 2016.

Geirsdóttir, Á., Harning, D. J., Miller, G. H., Andrews, J. T., Zhong, Y., and Caseldine, C.: Holocene history of landscape instability in Iceland: Can we deconvolve the impacts of climate, volcanism and human activity? Quaternary Science Reviews, 249, 106633, 2020.

Geirsdóttir, Á., Miller, G. H., Andrews, J. T., Harning, D. J., Anderson, L. S., Florian, C., Larsen, D. J., and Thordarson, T.: The onset of Neoglaciation in Iceland and the 4.2 ka event. Climate of the Past, 15, 25-40, 2019.

Geirsdóttir, Á., Miller, G. H., Harning, D. J., Hannesdóttir, H., Thordarson, T., and Jónsdóttir, I.: Evidence for recurrent outburst floods and active volcanism in Icelandic lacustrine settings during dynamic Younger Dryas-Early Holocene deglaciation. Journal of Quaternary Research, 37, 1006-1023, 2022.

Gudmundsdóttir, E. R., Larsen, G., and Eiríksson, J.: Tephra stratigraphy on the North Icelandic Shelf: extending tephrochronology into marine sediments off North Iceland, Boreas, 41, 719-734, 2012.

Gudmundsdóttir, E. R., Schomacker, A., Brynjólfsson, S., Ingólfsson, Ó., and Larsen, N. K.: Holocene tephrostratigraphy in Vestfirðir, NW, Iceland. Journal of Quaternary Science, 33, 827-839, 2018.

Grönvold, K., Óksarsson, N., Johnsen, S.J., Clausen, H. B., Hammer, C. U., Bond, C., and Bard, E.: Ash layers from Iceland in the Greenland GRIP ice core correlated with oceanic and land sediments. Earth and Planetary Science Letters, 135, 149-155, 1995.

Harning, D. J., Curtin, L., Geirsdóttir, Á., D'Andrea, W. J., Miller, G. H., and Sepúlveda, J.: Lipid biomarkers quantify Holocene summer temperature and ice cap sensitivity in Icelandic lakes. Geophysical Research Letters, 47, e2019GL085728, 2020.

Harning, D. J., Geirsdóttir, Á., Miller, G. H., and Zalzal, K.: Early Holocene deglaciation of Drangajökull, Vestfirðir, Iceland. Quaternary Science Reviews, 153, 192-198, 2016.

Harning, D. J., Thordarson, T., Geirsdóttir, Á., Miller, G. H., and Florian, C. R.: Repeated Early Holocene eruptions of Katla, Iceland, limit the temporal resolution of the Vedde Ash, Bulletin of Volcanology, 86, 2, 2024.

Harning, D. J., Thordarson, T., Geirsdóttir, Á., Miller, G. H., and Ólafsdóttir, S.: Marker tephra in Haukadalsvatn lake sediment: A key to the Holocene tephra stratigraphy of Northwest Iceland. Quat. Sci. Rev., 219, 154-170, 2019.

Harning, D. J., Thordarson, T., Geirsdóttir, Á., and Zalzal, K.: Provenance, stratigraphy and chronology of Holocene tephra from Vestfirðir, Iceland. Quat. Geochronol., 46, 59-76, 2018.

Hartley, M. E.: Postglacial volcanism and magmatism on the Askja volcanic system, North Iceland. PhD thesis, University of Edinburgh, 2012.

Hartley, M. E., Thordarson, T., and de Joux, A.: Postglacial eruptive history of the Askja region, North Iceland. Bulletin of Volcanology, 78, 2016.

Hartley, M. E., and Thordarson, T.: The 1874-76 volcano-tectonic episode at Askja, North Iceland: lateral flow revisited. Geochemistry, Geophysics, Geosystems, 14, 2286-2309, 2013.

Janebo, M. H., Thordarson, T., Houghton, B. F., Bonadonna, C., Larsen, G., and Carey, R. J.: Dispersal of key subplinian-Plinian tephras from Hekla volcano, Iceland: implications for eruption source parameters. Bull. Volcanol., 78, 1-16, 2016.

Jennings, A. E., Thordarson, T., Zalzal, K., Stoner, J., Hayward, C., Geirsdóttir, Á., and Miller, G. H.: Holocene tephra from Iceland and Alaska in SE Greenland Shelf Sediments. In: Austin, W.E.N., Abbott, P.M., Davies, S.M., Pearce, N.J.G., and Wastegård, S. (eds) *Marine Tephrochronology*. Geological Society, London, Special Publications, 398, 2014.

Jóhannesson, H., and Einarsson, S.: Hekla, fjall med fortíd. Náttúrufrædingurinn, 61, 177–191, 1992.

Jóhannsdóttir, G. E.: Mid-Holocene to late glacial tephrochronology in west Iceland as revealed in three lacustrine environments. MS thesis, University of Iceland, 2007.

Kristjánsdóttir, G. B., Stoner, J. S., Jennings, A. E., Andrews, J. T., and Grönvold, K.: Geochemistry of Holocene cryptotephras from the North Iceland Shelf (MD99-2269): intercalibration with radiocarbon and palaeomagnetic chronostratigraphies. Holocene 17, 155-176, 2007.

Kvamme, T., Mangerud, J., Furnes, H., and Ruddiman, W. F.: Geochemistry of Pleistocene ash zones in cores from the North Atlantic. Norsk Geologisk Tidsskrift, 69, 251–272, 1989.

Larsen, D. J., Miller, G. H., Geirsdóttir, Á., and Ólafsdóttir, S.: Non-linear Holocene climate evolution in the North Atlantic: a high-resolution, multi-proxy record of glacier activity and environmental change from Hvítárvatn, central Iceland. Quaternary Science Reviews, 39, 14-25, 2012.

Larsen, G., Dugmore, A. J., and Newton, A. J.: Geochemistry of historical-age silicic tephras in Iceland. Holocene, 9, 463-471, 1999.

Larsen, G., Eiríksson, J., Knudsen, K. L., and Heinemeier, J.: Correlation of late Holocene terrestrial and marine tephra markers, north Iceland: implications for reservoir age changes. Polar Research, 21, 283-290, 2002.

Larsen, G., Newton, A. J., Dugmore, A. J., Vilmundardóttir, E. G.: Geochemistry, dispersal, volumes and chronology of Holocene silicic tephra layers from the Katla volcanic system, Iceland. J. Quat. Sci., 16, 119-132, 2001.

Larsen, G., Róbertsdóttir, B. G., Óladóttir, B. A., and Eiríksson, J.: A shift in eruption mode of Hekla volcano, Iceland, 3000 years ago: two-coloured Hekla tephra series, characteristics, dispersal and age. J. Quat. Sci., 35, 143-154, 2020.

Larsen, G., and Thórarinsson, S.: H-4 and other acid Hekla tephra layers. Jökull, 27, 27-46, 1977.

Mangerud, J., Furnes, H., and Jóhansen, J.: A 9000-year-old ash bed on the Faroe Islands. Quaternary Research, 26, 262-265, 1986.

Meara, R. H., Thordarson, T., Pearce, N. J. G., Hayward, C., and Larsen, G.: A catalogue of major and trace element data for Icelandic Holocene Silicic tephra layers. J. Quat. Sci., 35, 122-142, 2020.

Merkt, J., Müller, H., Knabe, W., Müller, P., and Weiser, T.: The early Holocene Saksunarvatn tephra found in lake sediments in NW Germany. Boreas, 22, 93-100, 1993.

Möckel, S. C., Erlendsson, E., Prater, I., and Gísladóttir, G.: Tephra deposits and carbon dynamics in peatlands of a volcanic region – lessons from the Hekla 4 eruption. Land Degrad. Dev., 32, 654-669, 2021.

Óladóttir, B. A., Larsen, G., and Sigmarsson, O.: Holocene volcanic activity at Grímsvötn, Bárdarbunga and Kverkfjöll subglacial centres beneath Vatnajökull, Iceland. Bull. Volcanol., 73, 1187-1208, 2011.

Óladóttir, B. A., Thordarson, T., Geirsdóttir, Á., Jóhannsdóttir, G. E., and Mangerud, J.: The Saksunarvatn Ash and the G10ka series tephra. Review and current state of knowledge. Quat. Geochron., 56, 101041, 2020.

Óladóttir, B. A., Thordarson, T., Larsen, G., and Sigmarsson, O.: Survival of the Mýrdalsjökull ice cap through the Holocene thermal maximum: evidence from sulfur contents in Katla tephra layers (Iceland) from the last ~8400 years. Ann. Glaciol., 45, 183-188, 2007.

Rasmussen, S. O., Andersen, K. K., Svensson, A. M., Steffensen, J. P., Vinther, B. M., Clausen, H. B., Siggaard-Andersen, M.-L., Johnsen, S. J., Larsen, L. B., Dahl-Jensen, D., Bigler, M., Röthlisberger, R., Fischer, H., Goto-Azuma, K., Hansson, M. E., and Ruth, U.: A new Greenland ice core chronology for the last glacial termination. Journal of Geophysical Research, 111, 1-16, 2006.

Rundgren, M.: Early Holocene vegetation of northern Iceland: pollen and plant macrofossil evidence from the Skagi peninsula. The Holocene, 5, 553-564, 1998.

Sæmundsson, K.: Jarðfræði Kröflukerfisins (Geology of the Krafla volcanic system). In: Gardarsson, A. and Á. Einarsson eds. *Náttúra Mývatns*, Hið íslenska náttúrufræðifélag, Reykjavík, 25–95, 1991.

Sigmarsson, O., Condomines, M., and Fourcade, S.: A detailed Th, Sr and O isotope study of Hekla: differentiation processes in an Icelandic Volcano. Contrib. to Mineral. Petrol., 112, 20–34, 1992.

Sverrisdóttir, G.: Hybrid magma generation preceding Plinian silicic eruptions at Hekla, Iceland: evidence from mineralogy and chemistry of two zoned deposits. Geological Magazine, 144, 643–659, 2007.

Thorarinsson, S.: The Öræfajökull eruption of 1362. Acta Nat. Islandica II, 1–99, 1958.

Thorarinsson, S.: The eruptions of Hekla in historical times: a tephrochronological study. In: Einarsson, T., Kjartansson, G., Thorarinsson, S. (eds) *The eruption of Hekla 1947-1948*. Societas Scientiarum Islandica, Reykjavik, 1-177, 1967.

Thordarson, T., and Höskuldsson, Á.: Postglacial volcanism in Iceland. Jökull, 58, 197-228, 2008.

Thordarson, T., Miller, D. J., Larsen, G., Self, S., and Sigurdsson, H.: New estimates of sulfur degassing and atmospheric mass-loading by the 934a.d. Eldgjá eruption, Iceland. J. Volcanol. Geotherm. Res., 108, 33–54, 2001.

Thordarson, T., and Larsen, G.: Volcanism in Iceland in historical time: volcano types, eruption styles and eruptive history. J. Geodyn., 43, 118–152, 2007.

Thordarson, T., Self, S., Miller, D. J., Larsen, G., Vilmundardóttir, E.G.: Sulphur release from flood lava eruptions in the Veidivötn, Grímsvötn and Katla volcanic systems, Iceland. In: C. Oppenheimer, D.M. Pyle, and J. Barclay (Editors), *Volcanic Degassing*. Geol. Soc. London, Spec. Publ. **213**, 103-121, 2003.

Thordarson, T., Self, S., Óskarsson, N., and Hulsebosch, T.: Sulphur, chlorine, and fluorine degassing and atmospheric loading by the 1783-1784 AD Laki (Skaftár Fires) eruption in Iceland. Bull. Volcanol., 58, 205-225, 1996.

Thordarson, T., Miller, D. J., Larsen, G., Self, S., and Sigurdsson, H.: New estimates of sulfur degassing and atmospheric mass-loading by the 934a.d. Eldgjá eruption, Iceland. Journal of Volcanology and Geothermal Research, 108, 33–54, 2001.

Timms, R. G. O., Matthews, I. P., Lowe, J. J., Palmer, A. P., Weston, D. J., MacLeod, A., Blockley, S. P. E.: Establishing tephrostratigraphic frameworks to air the study of abrupt climatic and glacial transitions: a case study of the Last Glacial-Interglacial Transition in the British Isles (c. 16-8 ka BP). Earth-Science Reviews, 192, 34-64, 2019.

Walker, G. L.: Explosive volcanic eruptions—a new classification scheme. Geol Rundsch, 62, 431–446, 1973.

Wastegård, S., Gudmundsdóttir, E. R., Lind, E. M., Timms, R. G. O., Björck, S., Hannon, G. E., Olsen, J., and Rundgren, M.: Towards a Holocene tephrochronology for the Faroe Island, North Atlantic, Quaternary Science Reviews, 195, 195-214, 2018.